TECHNISCHE UNIVERSITÄT MÜNCHEN

FAKULTÄT FÜR MEDIZIN

Functional characterization and pathophysiological evaluation of the *Olfactomedin-like 2B* gene

Tanja Angelika Plötz

Vollständiger Abdruck der von der Fakultät für Medizin der Technischen Universität München zur Erlangung des akademischen Grades eines

Doktors der Naturwissenschaften (Dr. rer. nat.)

genehmigten Dissertation.

Vorsitzender: Prof. Dr. Radu Roland Rad

Prüfer der Dissertation:

1. Priv.-Doz. Dr. Arne Pfeufer
2. Prof. Dr. Hans-Werner Mewes

Die Dissertation wurde am 20.07.2020 bei der Technischen Universität München eingereicht und durch die Fakultät für Medizin am 16.03.2021 angenommen.

TABLE OF CONTENT

Table of Content **2**

Abbreviations **5**

I. Abstract **8**

Zusammenfassung **9**

II. Introduction **10**

1. Cardiomyopathies and Arrhythmias 10
2. Genome-wide Association Studies 15
3. GWAS for Cardiomyopathies 16
4. The Olfactomedins 20
5. Aims of the Study 22

III. Material and Methods **23**

1. Material 23
1.1. Cohorts 23
1.2. Molecular Biology 23
1.3. Cell Culture 25
1.4. Human Heart Tissue 26
1.5. Antibodies 26
1.6. Laboratory Chemicals and Reagents 28
1.7. Kits 30
1.8. Consumables 31
1.9. Technical Devices 31
2. Methods 33
2.1. Molecular Biology 33
2.1.1. Molecular Cloning 33
2.1.2. RNA Isolation, Purification and Reverse Transcription including qPCR 34
2.2. Cell Culture 35
2.2.1. Growth and Maintenance of HEK293 Cells 35

2.2.2. Transient Transfection and Lysis of HEK293 Cells 36
2.2.3. Cryo-stocks 37
2.3. Protein Preparation 37
2.3.1. Isolation of Protein from HEK293 Cells 37
2.3.2. Isolation of Protein from Human Heart Tissue 37
2.3.3. Isolation of Protein from Human Whole Blood 38
2.3.4. Protein Purification by FLAG Tag 38
2.3.5. Protein Purification by Protein G Conjugated Sepharose Beads 39
2.3.6. Protein Purification by Compat-Able™ Protein Assay 39
2.3.7. Protein Quantitation by BCA 39
2.4. Protein Analysis 39
2.4.1. Sodium Dodecyl Sulphate-polyacrylamide Gel Electrophoresis 39
2.4.2. Western Blot Analysis 39
2.4.3. Colloidal Coomassie Staining 40
2.4.4. Mass Spectrometry 40
2.5. Immunoassays 41
2.5.1. Dot Blot Analysis 41
2.5.2. Enzyme-linked Immunosorbent Assay 41

IV. Results 43

1. Characterization of the OLFML2B Protein 43
1.1. Validation of Monoclonal Antibodies 43
1.2. Intracellular Presence of Wildtype and 23 Mutant Proteins 44
1.3. In-silico Modelling of the Structure 45
1.4. Structural Changes 46
1.5. Secretional Behaviour 47
1.6. Dominant Effect 49
1.7. Temperature-Dependent Secretion 50
2. Detection of OLFML2B in Human Heart Tissue 53
3. Proteomics of OLFML2B by LC-MSMS 54
4. Tenascin C as Interaction Partner of OLFML2B 56

5. Establishment of two Sandwich ELISAs for Soluble OLFML2B 57

V. Discussion 59

1. Characterization of the OLFML2B Protein 59
2. Interaction Partners of the OLFML2B Protein 64
3. Generation of a Biomarker Assay to Detect Circulating OLFML2B Protein 66
4. Conclusion 69

VI. References 70

VII. List of Figures 84

VIII. List of Tables 87

IX. Acknowledgements 89

ABBREVIATIONS

aa	Amino acid
ab	Antibody
AF	Atrial fibrillation
ARIC	Atherosclerosis Risk in Communities
BCA	Bicinchoninic acid
bp	Base pair
BrS	Brugada syndrome
BSA	Bovine serum albumin
C-terminus	Carboxy-terminus
$CaCl_2$	Calcium chloride
CAD	Coronary artery disease
CPVT	Catecholaminergic polymorphic ventricular tachycardia
DCM	Dilated cardiomyopathy
ddH_2O	Double distilled water
DMEM	Dulbecco's modified eagle medium
DNA	Deoxyribonucleic acid
ECG	Electrocardiogram
ECL	Enhanced chemiluminescence
ECM	Extracellular matrix
EDTA	Ethylenediaminetetraacetic acid
ELISA	Enzyme-linked immunosorbent assay
ER	Endoplasmic reticulum
ExAC	Exome aggregation consortium
FBS	Fetal bovine serum
GAPDH	Glycerinaldehyd-3-phosphat-Dehydrogenase
GenNOVA	Genetic Epidemiology Network of Atherosclerosis
GLDN	Gliomedin
gnomAD	Genome Aggregation Database
GWAS	Genome-wide association study

GxE	Gene - environment interaction
HEPES	4-(2-hydroxyethyl)-1-piperazineethanesulfonic acid
HEK	Human embryonic kidney
HNR	Heinz Nixdorf Recall Study
HPLC	High-performance liquid chromatography
HRP	Horse radish peroxidase
IP	Immunoprecipitation
IgG	Immunoglobulin G
IVF	Idiopathic ventricular fibrillation
kb	Kilobase
KORA	Kooperative Gesundheitsforschung in der Region Augsburg
LB	Lysogeny broth
LC	Liquid chromatography
LD	Linkage disequilibrium
LOF	Loss-of-function
LQTS	Long-QT syndrome
M	Molar
MAF	Minor allele frequency
MES	2-(N-morpholino)ethanesulfonic acid
$MgCl_2$	Magnesium chloride
MS	Mass spectrometry
MS/MS	Tandem mass spectrometry
MYOC	Myocilin
N-terminus	Amino-terminus
NHGRI	National Human Genome Research Institute
NOS1AP	Nitric oxide synthase 1 adaptor protein
NP-40	Nonident-40
OD	Optical density
OLFM1	Olfactomedin 1
OLFM2	Olfactomedin 2

OLFM3	Olfactomedin 3
OLFM4	Olfactomedin 4
OLFML1	Olfactomedin-like 1
OLFML2A	Olfactomedin-like 2A
OLFML2B	Olfactomedin-like 2B
OLFML3	Olfactomedin-like 3
PAGE	Polyacrylamide gel electrophoresis
PBS	Phosphate buffered saline
PCR	Polymerase chain reaction
POAG	Primary open angle glaucoma
PPI	Protein-protein interaction
PVDF	Polyvinylidene difluoride
qPCR	Quantitative PCR
QTc_RAS	QT interval corrected for heart rate, age and sex
QTSCD study	Study about QT interval and sudden cardiac death
RNA	Ribonucleic acid
RT	Room temperature
SardiNIA	Sardinian population cohort
SCD	Sudden cardiac death
SDS	Sodium dodecyl sulphate
SIDS	Sudden infant death syndrome
SN	Supernatant
SNP	Single nucleotide polymorphism
SQTS	Short-QT syndrome
TBS/ T	Tris-buffered saline/ with Tween20
TMB	3,3',5,5'-Tetramethylbenzidin
TNC	Tenascin C
Tris	Tris(hydroxymethyl)aminomethane
WHO	World Health Organization
Wt	Wildtype

I. ABSTRACT

Impaired cardiac repolarization can induce life-threatening ventricular arrhythmias and sudden death. While extreme repolarization disturbances occur in the rare monogenic short- and long-QT syndromes, common genetic, non-genetic and exogenous factors such as changes in body temperature are known to potentially trigger arrhythmias in the general population. Genome-wide association studies have mapped the strongest common genetic modifier of QT interval in the *NOS1AP-OLFML2B* genomic region in 1q23.3. This study investigated the contribution of the olfactomedin-like 2B protein (OLFML2B) to the cardiac repolarization process.

As mutations in the olfactomedin paralog myocilin cause disease by impairing protein secretion, wildtype OLFML2B and 23 missense variants were characterized for their temperature dependent secretional behaviour. Monoallelic mutations were identified in patients with atrial (AF) and ventricular arrhythmias (LQT), as well as dilated cardiomyopathy (DCM) and sudden infant death syndrome (SIDS) while three common OLFML2B variants were also analysed. Upon recombinant expression in HEK293 cells, cytosolic OLFML2B levels were indistinguishable, but levels of secreted protein varied strongly by temperature and variant. Combined analysis illustrated that protein secretion correlated highly with population allele frequency and temperature: Poorly secreted variants were rare at the population level and originated exclusively from patients with SIDS, AF or LQT. These findings suggest a role for OLFML2B in fever-triggered impaired cardiac repolarization and for rare *OLFML2B* mutations predisposing to repolarization induced arrhythmia and sudden cardiac death.

Additional evidence for the pathogenicity of OLFML2B is indicated by the pronounced dominant effect of the mutated OLFML2B protein on the wildtype. Consequently, in a heterozygous genotype the wildtype allele is incapable of rescuing the non-secretion caused by the mutant allele, especially since the effect does not seem to depend on protein concentration. This loss-of-function phenotype provides a plausible explanation for the lethal course of all investigated SIDS cases holding an OLFML2B mutation.

The detection of OLFML2B in human heart tissue not only by itself but also simultaneously with its interaction partner Tenascin C (TNC) identified by mass spectrometric analysis illustrates another piece of understanding the overall mode of action: TNC was demonstrated to be abundantly available during embryonic development but only marginally in adults except for phases with high mechanical stress. This puts TNC, a protein that has been shown to impair the inactivation of sodium channels, in context with cardiac injuries pointing to a pathophysiological mechanism to influence the QT interval and thereby repolarization of the heart.

ZUSAMMENFASSUNG

Die Störung kardialer Repolarisation kann zu lebensbedrohlichen ventrikulären Arrhythmien und zum plötzlichen Herztod führen. Während bei seltenen monogenen Short- und Long-QT-Syndromen extreme Repolarisationsstörungen auftreten, können auch häufige genetische, nicht-genetische und exogene Faktoren wie Veränderungen der Körpertemperatur Arrhythmien in der Bevölkerung auslösen. Genomweite Assoziationsstudien haben den stärksten genomischen Modifier des QT-Intervalls in der Region 1q23.3 der Gene *NOS1AP-OLFML2B* lokalisiert. In dieser Arbeit wurde der Beitrag des Proteins Olfactomedin-like 2B (OLFML2B) zur kardialen Repolarisation untersucht.

Da Mutationen im Paralog Myocilin aufgrund verminderter Proteinsekretion Krankheiten verursachen, ist das temperaturabhängige Sekretionsverhalten von Wildtyp-OLFML2B und 23 Missense-Varianten charakterisiert worden. Monoallelische Mutationen konnten bei Patienten mit atrialer (AF) und ventrikulärer Arrhythmie (LQT), dilatativer Kardiomyopathie (DCM) und plötzlichem Kindstod (SIDS) identifiziert werden; zusätzlich zu diesen Mutationen wurden drei häufige OLFML2B-Varianten untersucht. Während die zytosolischen Proteinkonzentrationen keine Unterschiede zeigten, variierten die Werte für sekretiertes OLFML2B je nach Temperatur und Proteinvariante erheblich. Kombinierte Analysen ließen auf eine starke Korrelation der Proteinsekretion mit der Temperatur und der Allelfrequenz in der Population schließen: Schlecht sekretierende Varianten kamen selten auf der Bevölkerungsebene vor und stammten ausschließlich von Patienten mit SIDS, AF oder LQT. Diese Ergebnisse deuten auf eine Rolle von OLFML2B bei fieberbedingten kardialen Repolarisationsstörungen und seltenen *OLFML2B*-Mutationen hin, welche zu ventrikulären Arrhythmien und plötzlichem Herztod führen können.

Einen weiteren Hinweis auf die Pathogenität von OLFML2B liefert der ausgeprägte dominante Effekt des mutierten OLFML2B-Proteins auf den Wildtyp. Dadurch wird im heterozygoten Genotyp ein Ausgleich der durch das mutierte Allel verursachten Nicht-Sekretion durch das Wildtyp-Allel verhindert, zumal der Effekt nicht von der Proteinkonzentration abzuhängen scheint. Dieser Loss-of-Function-Phänotyp bietet eine naheliegende Erklärung für den tödlichen Verlauf aller untersuchter SIDS-Fälle, bei denen eine OLFML2B-Mutation nachgewiesen wurde.

Der Nachweis von OLFML2B in menschlichem Herzgewebe, nicht nur isoliert sondern gemeinsam mit seinem durch massenspektrometrische Analysen identifizierten Interaktionspartner Tenascin C (TNC), verdeutlicht die Wirkungsweise: TNC ist während der Embryonalentwicklung im Überfluss vorhanden, bei Erwachsenen jedoch nur geringfügig mit Ausnahme von Phasen mechanischen Stresses. Dies assoziiert TNC, ein Protein das die Inaktivierung von Natriumkanälen beeinträchtigt, mit kardialen Verletzungen und weist auf einen pathophysiologischen Mechanismus hin, der das QT-Intervall und damit die Repolarisation des Herzens beeinflusst.

II. INTRODUCTION

1. CARDIOMYOPATHIES AND ARRHYTHMIAS

Despite a lot of recent progress in our understanding of genetic cardiomyopathies and arrhythmias, cardiac diseases still remain one of the most prevalent causes of premature death in developed societies (Arking et al., 2006; Arking and Sotoodehnia, 2012). About 64% of those deaths are induced by Sudden Cardiac Death (SCD), which is referred to as unexpected, natural death induced by cardiac causes that occurs within one hour of the onset of symptoms (Zipes and Wellens, 1998; Parakh, 2015). In 2008, SCD was affecting about four to five million people each year worldwide (Chugh et al., 2008). The number of deaths increased drastically over the past years with more than seven million lives per year currently (Abhilash and Namboodiri, 2014; Parakh, 2015). The overall age distribution of SCD indicates a distinctive pattern with a bimodal peak: The childhood peak occurs at <1 year and the adult peak between 45 and 75 years of age (Parakh, 2015). With approximately 80% of all cases, coronary artery disease (CAD) and its complications such as acute myocardial infarction are supposed to be the main cause of SCD. Beyond CAD, 10% to 15% of adult SCDs are due a structurally and 5% to 10% due to an electrically abnormal heart (Zipes and Wellens, 1998; Chugh et al., 2000; Huikuri et al., 2001).

A significant fraction of cardiomyopathies and arrhythmias are provoked by monogenic conditions with Mendelian inheritance. These primary electric disorders of the heart predispose to SCD in the absence of concomitant structural abnormalities by modifying the cardiac action potential or intracellular calcium handling (Benito et al., 2009):

- Brugada syndrome (BrS): Imbalance between currents in early phases of repolarization, either by decrease in inward (sodium and calcium) or increase in outward (potassium) currents
- Catecholaminergic polymorphic ventricular tachycardia (CPVT): Delayed afterdepolarization by abnormal release of Ca^{2+} from sarcoplasmic reticulum
- Short-QT syndrome (SQTS): Shortened QT interval by faster repolarization rates and shorter refractory periods
- Long-QT syndrome (LQTS): Prolonged QT interval by either increase in sodium or decrease in potassium currents
- Idiopathic ventricular fibrillation (IVF): All remaining cases without the distinct abnormalities described above (Wever and de Medina, 2004; Garcia-Elias and Benito, 2018)

The long-QT syndrome with an incidence of about 1/2500 people (Schwartz et al., 2009; Parakh, 2015) represents the most common hereditary cause of sudden arrhythmic death (Behr et al., 2008).

The QT interval is measured from the beginning of the QRS complex until the end of the T wave in the electrocardiogram (ECG). Consequently, it describes stages of ventricular depolarization and repolarization mediated by different cardiac ion channels: While the rapid inflow of positively charged ions (sodium and calcium) triggers depolarization, the repolarization is initiated by the outflow of positively charged potassium ions (Al-Khatib et al., 2003).

With retention of the positively charged ions potassium, sodium and calcium inside the cardiomyocytes, the repolarization phase of the cardiac action potential extends. Impaired cardiac repolarization often reveals itself by a prolonged QT interval (Figure 1) in the ECG (Schwartz, 2012). This generates electrical instability and leads to a propensity toward the polymorphic ventricular arrhythmia torsade de pointes followed by ventricular fibrillation. Without immediate defibrillation this can result in SCD (Priori et al., 2001; Roden, 2008).

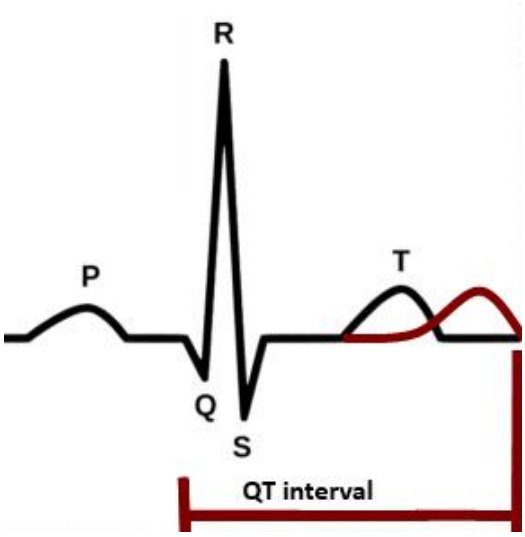

Figure 1: Schematic ECG showing extended QT interval in red.

So far, 15 subtypes of the congenital LQT syndrome have been identified (Table 1).

Table 1: Overview about 15 subtypes of congenital LQTS (adapted from Spears and Gollob, 2015).

LQTS SUBTYPES	GENE	PROTEIN AFFECTED	FUNCTIONAL EFFECT OF MUTATION	FREQUENCY
LQT1	*KCNQ1*	Alpha-subunit of I_{Ks}	Loss-of-function, reduced I_{Ks}	30–35 %
LQT2	*KCNH2*	Alpha-subunit of I_{Kr}	Loss-of-function, reduced I_{Kr}	25–30 %
LQT3	*SCN5A*	Alpha-subunit of I_{Na}	Gain-of-function, increased late I_{Na} inward current	5–10 %
LQT4	*ANK2*	Ankyrin-B; links membrane proteins with underlying cytoskeleton	Loss-of-function, disrupts function of multiple ion channels	<1 %
LQT5	*KCNE1*	Beta-subunit of I_{Ks}	Loss-of-function, reduced I_{Ks}	<1 %

LQTS SUBTYPES	GENE	PROTEIN AFFECTED	FUNCTIONAL EFFECT OF MUTATION	FREQUENCY
LQT6	*KCNE2*	Beta-subunit of I_{Kr}	Loss-of-function, reduced I_{Kr}	<1 %
LQT7	*KCNJ2*	Alpha-subunit of I_{K1}	Loss-of-function, reduced I_{K1}	<1 %
LQT8	*CACNA1c*	Alpha-subunit of I_{CaL}	Gain-of-function, increased I_{CaL}	<1 %
LQT9	*CAV3*	Caveolin-3; a scaffolding protein in caveolae	Increased late I_{Na} inward current	<1 %
LQT10	*SCN4B*	Beta 4-subunit of I_{Na}	Gain-of-function, increased late I_{Na} inward current	<1 %
LQT11	*AKAP9*	A kinase-anchor protein-9; sympathetic I_{Ks} activation	Loss-of-function, reduced I_{Ks}	<1 %
LQT12	*SNTA1*	Alpha1-syntrophin; regulation of I_{Na}	Increased late I_{Na} inward current	<1 %
LQT13	*KCNJ5*	Kir 3.4	Loss-of-function, reduced I_{KACh}	<1 %
LQT14	*CALM1*	Calmodulin-1	Altered calcium signalling	<1 %
LQT15	*CALM2*	Calmodulin-2	Altered calcium signalling	<1 %

Though each of the 15 monogenic subtypes shows a different pathophysiological mechanism, around 90% of all cases undergoing genetic testing and providing a positive result point to one of the three major subtypes of LQT syndrome: LQT1, LQT2 or LQT3 (Wallace et al., 2019).

Besides the hereditary monogenic LQT syndrome, the acquired LQTS occurs with an even higher frequency and is mostly caused by pharmacological therapy with QT-prolonging drugs in hearts susceptible to repolarization prolongation. Significant prolongation of repolarization is mainly detected by clinical diagnostic methods such as anamnesis and subsequent ECG. A QT interval corrected for heart rate is considered normal within a range of 380-440 ms. If the ECG shows a QT interval of ≥440 ms in a male or ≥460 ms in a female, it is interpreted as prolonged (Priori et al., 2001).

Due to the great effort in identifying genes responsible for LQT syndrome, the molecular-based approach for routine diagnosis now has success rates in the magnitude of 80% when screening for a genetic predisposition (Alders et al., 2003 updated 2018), leading to the combination of genetic and clinical methods as preferred approach for the diagnosis of LQTS; however, the success rate of 80% leaves 20% of the affected patients deprived of a potential genetic cause. The percentage of negative genetic testing has been shown to be even greater regarding other cardiac channelopathies, i.e. 40% of patients with CPVT and 80% of patients with SQTS or BrS (Tester and Ackerman, 2011).

Several studies suggest, that intrinsic channelopathies like LQT syndrome, BrS, CPVT and others are not only partly responsible for SCD but in addition account for 5% to 10% of all

SIDS cases as well (Skinner, 2005; Tester and Ackerman, 2005; Hunt and Hauck, 2006). This was first recognized when cases with prolongation of the QT interval in SIDS patients were reported (Border and Benson, 2007) and mutations in the same genes coding for ion channels that cause LQT syndrome were discovered in SIDS (Schwartz et al., 2001; Otagiri et al., 2008). Schwartz et al. (1998) conducted a study from 1976 to 1994, in which ECGs of 33,034 new-borns were screened including follow-up data for one year. 24 out of the neonates died prospectively from SIDS, who showed with 435±45 ms a longer corrected QT interval than the survivors with 400±20 ms. While none of the survivors showed a prolonged QT interval, 12 of the SIDS cases had been measured with ≥440 ms. This increases the risk of SIDS for an infant with prolonged QT interval by the factor 41.3, which is far greater than any other established risk factor for SIDS such as sleeping position and environment, overheating, maternal risk factors and postnatal care (American Academy of Pediatrics, 2016):

- Sleeping position and environment: Prone position has been recognized as a major risk factor for SIDS (Hauck et al., 2002). Since it is easier for the infant to roll to the prone position than on its back, side sleeping is considered just as dangerous (American Academy of Pediatrics, 2005). For both positions, the immediate risk for the infant is based on rebreathing expired gases resulting in hypercapnia and hypoxia. In addition, the use of soft bedding, pillows or soft toys have been strongly associated with an increased risk for SIDS since it can increase the potential of rebreathing and suffocation (Patel et al., 2001; Kanetake et al., 2003). Epidemiologic studies of co-sleeping have shown that it can increase risk factors of SIDS such as rebreathing, head covering, overheating and exposure to tobacco smoke (American Academy of Pediatrics, 2011). Many parents choose to share their bed anyway because it facilitates breastfeeding (Horsley et al., 2007).
- Overheating: There is clear evidence, that risk of SIDS is associated with room temperature and the amount of clothing. This could be due to the higher possibility of asphyxiation when the number of blankets is raised and also correlates with the season of the year since infants wear more clothes during the cold weather (Ponsonby et al., 1992).
- Maternal risk factors: It is quite evident that good pre- and postnatal care can lower the risk of SIDS (Stewart et al., 1995) as it can increase the infant's overall chances of survival. Tobacco smoke, alcohol and other illicit substances are major risk factors for SIDS, irrespective of the exposure taking place during pregnancy or after birth (Gelfer and Tatum, 2014).
- Postnatal care: Breastfeeding is protective against SIDS especially when applied exclusively (Hauck et al., 2011). In addition, routine immunization (Mitchell et al., 1995) and providing a pacifier for sleeping (Hauck et al., 2005) are by now known to not in- but decrease the risk of SIDS.

SIDS is defined as the sudden and unexpected death of an infant before one year of age that cannot be explained after a thorough case investigation including scene examination, autopsy, and review of the clinical history (Willinger et al., 1991). This disease is regarded as multifactorial and its origin described best with the Triple-Risk Hypothesis (Figure 2).

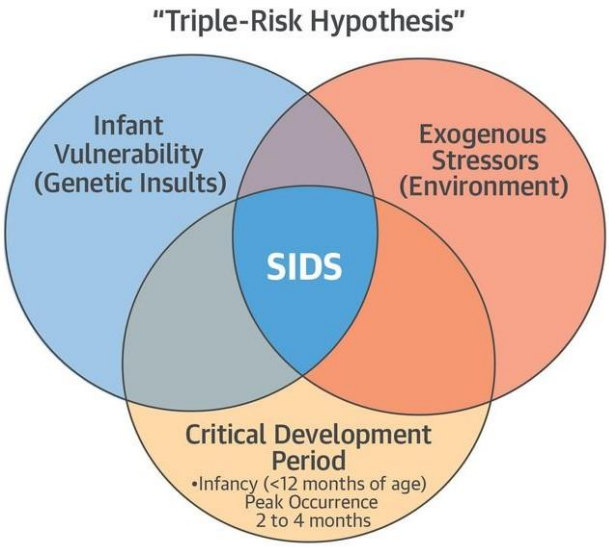

Figure 2: Triple-Risk Hypothesis for SIDS (Tester et al., 2018).

This model of the disease development proposes that three conditions have to be fulfilled in order to provoke SIDS: Dysfunctional or immature cardiorespiratory or arousal systems, external triggers such as prone position and critical period of development, which represents the first year of the infant's life.

After identification of the above risk factors, an organization has been built called Safe to Sleep campaign, formerly known as the Back to Sleep campaign (https://safetosleep.nichd.nih.gov/ website accessed on May 3rd, 2020). The overall goal of this campaign was to inform communities, educating caregivers and health care providers about how to reduce the amount of SIDS cases. Since its beginning in 1994, the SIDS incidence dropped by more than 50% until 2000. Despite the great success of the campaign, the SIDS rate remained constant since then (Trachtenberg et al., 2012).

This may be due to the still unknown pathological mechanism. Recent case-control studies proposed several candidate genes for SIDS, where variants were discovered during post-mortem genetic screening, that were absent in healthy infants and those dying of other causes (Hunt and Hauck, 2006):

- Promoter region of serotonin transporter gene (*5-HTT*)
- Autonomic nervous system development genes (*Phox2a, RET, ECE1, TLX3, EN1*)
- Genes regulating infection and inflammation (*complement C4A/ B*, *Il-10*)

Although a lot of progress has been made in identifying predisposing genetic and environmental factors increasing the probability to these multifactorial and complex disorders, further research is needed to fully understand the relevant interactions.

2. Genome-wide Association Studies

After deeper insight into cardiomyopathies, a significant amount of genetic influence seems undeniable. SCD and SIDS have proven to be mostly not monogenic but multifactorial and complex diseases. Unlike Mendelian disorders, which are characterized by a specific segregation pattern and caused by rare variants with high effect sizes, the different genetic architecture of quantitative traits limits the success in identification of the responsible genetic variant(s) by the otherwise effective linkage analysis.

Genome-wide association studies (GWAS) on the other hand qualify highly for the search of complex disease susceptibility factors. These studies detect association signals between complex traits and chromosomal location that influence the risk of disease by comparing the allele frequency in affected and unaffected individuals across the whole genome (Panoutsopoulou et al., 2013). The way GWAS is set up, it is completely unbiased regarding previous or expected results (Visscher et al., 2012). Several key developments were required for GWAS to achieve reproducible and true results:

1. Advances in high throughput genotyping technologies allowed to assay thousands of common single nucleotide polymorphisms (SNPs) and decreased the per-sample costs (Manolio and Collins, 2009).
2. The HapMap project typed several million SNPs in 270 individuals providing a genome-wide database for human genetic variation patterns to be used in genetic association studies of common diseases (Manolio et al., 2008).
3. The Wellcome Trust Case Control Consortium tested the hypothesis that phenotypes caused by complex traits are due to common variants demonstrating that robust associations between genetic loci and traits can be found and that the ‘common variant hypothesis’ is true (Atanasovska et al., 2015).

GWAS analysis is based on the premise that SNPs within close physical distance are in linkage disequilibrium (LD) with each other. The HapMap project mapped the LD landscape and developed a genome-wide set of tag-SNPs, which are tested by GWAS to identify the LD block with the disease association. However, any LD block only provides information about the haplotype and pinpoints to the genomic region comprehending the causal variant without distinguishing between disease-causing and bystander SNPs (Atanasovska et al., 2015). A thorough functional and mechanistic characterization of the association signal is necessary to verify the correlation between SNP and phenotype.

Welter et al. (2014) published the actual numbers of GWAS data included in the National Human Genome Research Institute (NHGRI) Catalog. It mentions 1,751 publications of 11,912 SNPs claiming to have assayed at least 100,000 SNPs. An update was given by

MacArthur et al. in 2017, stating that the GWAS data set was containing 2,518 publications with 24,218 SNPs in September 2016. Recent GWAS data published on their website (https://www.ebi.ac.uk/gwas website accessed on May 17th, 2020) show analysis of 185,724 SNP-trait associations from 4,545 publications as of May 3rd, 2020. Figure 3 visualizes all associations detected by GWAS mapping SNPs to the cytogenetic band.

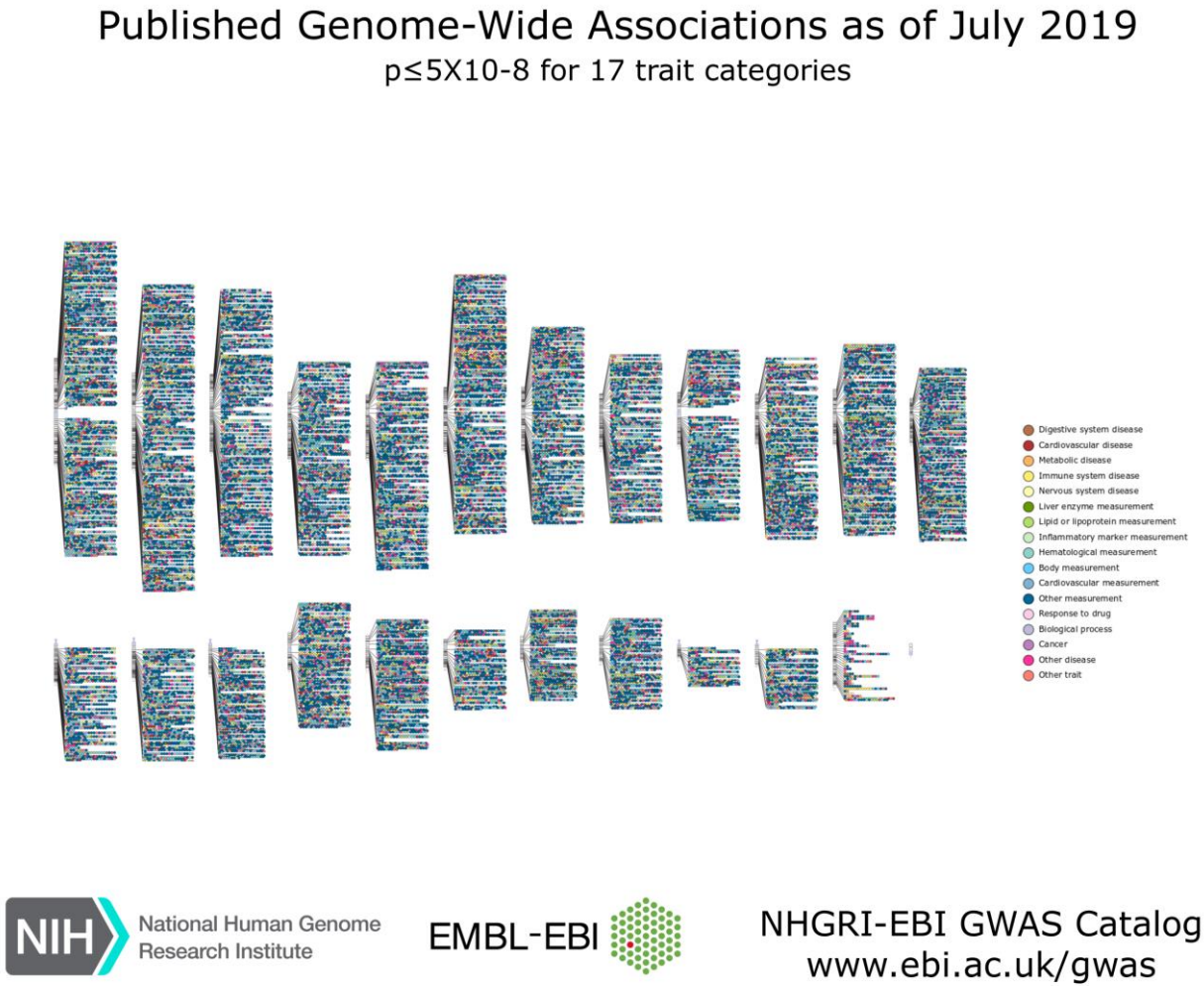

Figure 3: The interactive GWAS diagram visualizes all SNP-trait associations with P < 5.0 x 10^{-8}, mapped to the SNP's cytogenetic band (https://www.ebi.ac.uk/gwas website accessed on May 17th, 2020).

3. GWAS FOR CARDIOMYOPATHIES

The first attempt to identify SNPs associated with the QT interval was performed in 2006 by Arking et al. on large, population-based cohorts. They corrected the QT interval value for the known influencing covariates heart rate, age and sex (QTc_RAS). To minimize false positive findings but maximize power and efficiency of the study, a multiple-stage design approach was conducted including three stages (Figure 4).

- Stage I: Genotyping of 200 females of the KORA S4 survey with extreme QTc_RAS values (QT intervals below the 7.5th percentile or above 92.5th percentile)

- Stage II: Genotyping of 400 additional women having QTc_RAS below the 15th or above the 85th percentile with SNPs that passed stage I
- Stage III: Genotyping of all samples excluding women analysed in stage I and II with SNPs that passed both previous stages

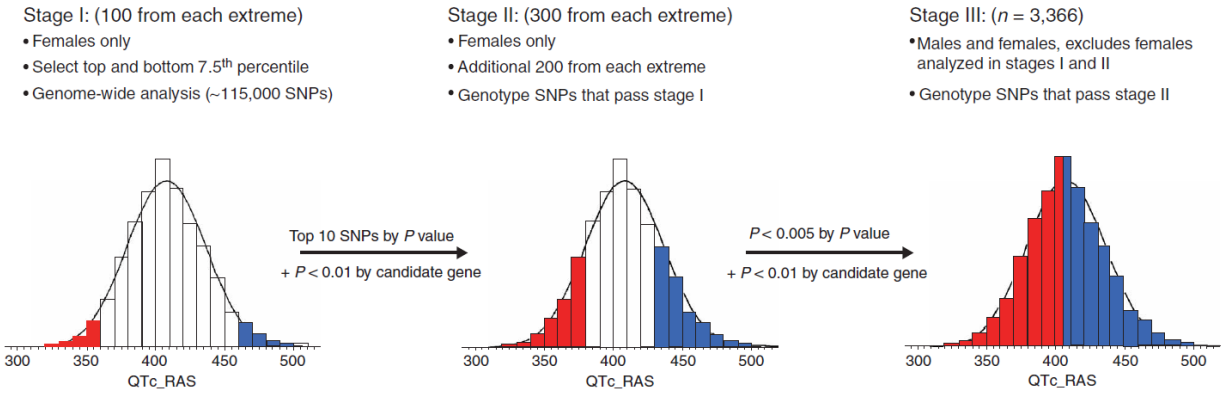

Figure 4: GWAS of QT interval showing the three-stage study design (Arking et al., 2006).

Three loci with nominal significance (P < 0.05) were identified during stage III:

- *NOS1AP* (*Nitric oxide synthase 1 adaptor protein*) on cytoband 1q23.3 with SNP rs10494366 (P < 10^{-7}): coding for the C-terminal PDZ domain ligand to neuronal nitric oxide synthase
- *QTc_5.3* GeneScan prediction (Burge and Karlin, 1997) with SNP rs1559578 (P < 0.004): non-coding
- *CACNA2D1* on cytoband 7q21.11 with SNP rs7341478 (P < 0.024): coding for an L-type voltage-dependent calcium channel regulatory subunit

These results were further validated by genotyping 2,646 samples of the KORA F3 cohort as well as 1,805 participants from the Framingham Heart Study for seven SNPs from stage III. Both independent cohorts were able to replicate the association signal for rs10494366 in *NOS1AP*. After fine-scale association mapping of the *NOS1AP* locus by genotyping 13 SNPs in the 600 stage II samples, the strongest association was found in the 5' upstream region of the *NOS1AP* gene (rs4657139), although there was a very strong association detectable in the entire area between rs10494366 and rs2880058 (Figure 5).

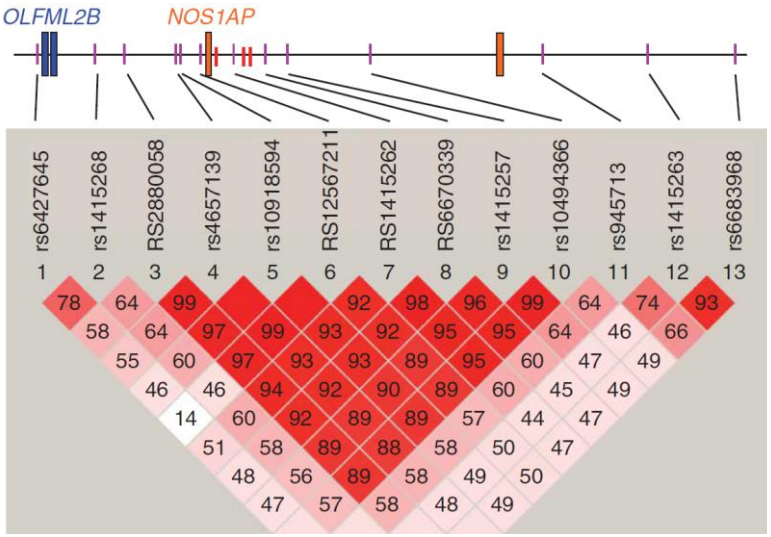

Figure 5: Fine mapping of *NOS1AP* showing LD between SNPs. Each value in the diamonds corresponds to pairwise correlation signals between SNPs, also represented in the shading of the fields. Fields without a number represent a signal of 1. *NOS1AP* exons 1 and 2 are shown in orange (Arking et al., 2006).

The identification of *NOS1AP*, a gene with unknown and unsuspected involvement in the QT interval variation, is supposed to explain 1.5% of the QT variance. This association of *NOS1AP* and QT interval variation was replicated in several more studies (Aarnoudse et al., 2007; Post et al., 2007; Tobin et al., 2008).

These GWASs of the QT interval were followed by a meta-analysis of the combined results by Pfeufer et al. (2009). In this QTSCD study (study about QT interval and sudden cardiac death), the five population-based cohorts ARIC (Atherosclerosis Risk in Communities; Dekker et al., 2004), KORA (Kooperative Gesundheitsforschung in der Region Augsburg; Wichmann et al., 2005), SardiNIA (Sardinian population cohort; Pilia et al., 2006), GenNOVA (Genetic Epidemiology Network of Atherosclerosis; Pattaro et al., 2007) and HNR (Heinz Nixdorf Recall Study; Schmermund et al., 2002) were analysed including a total of 15,847 individuals. They were able to identify ten association signals across the genome (Figure 6).

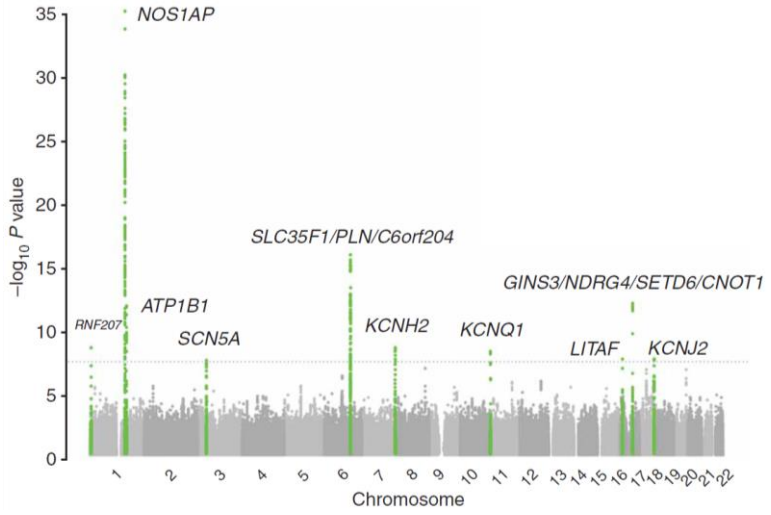

Figure 6: Manhattan Plot of genome-wide association analyses. The threshold for genome-wide significance is marked by the blue dotted line (5×10^{-8}). SNPs within loci exceeding this threshold are highlighted in green (Pfeufer et al., 2009).

Four loci near the monogenic LQT genes *KCNQ1*, *KCNH2*, *SCN5A* and *KCNJ2* as well as two loci near genes with known electrophysiological function *ATP1B1* and *PLN* were identified. In addition, three new loci that map to *RNF207*, *LITAF* and *GINS3-NDRG4-SETD6-CNOT1* were found without an obvious candidate for cardiovascular disease. The strongest main association signal maps to the *NOS1AP* locus, which is consistent with the previous GWAS finding (Arking et al., 2006). This signal derives from SNP rs12143842. A second, independent signal at rs4657178 showed low LD to the main signal. The whole chromosomal region 1q23.3 harbours several variants independently contributing to the overall effect (Figure 7).

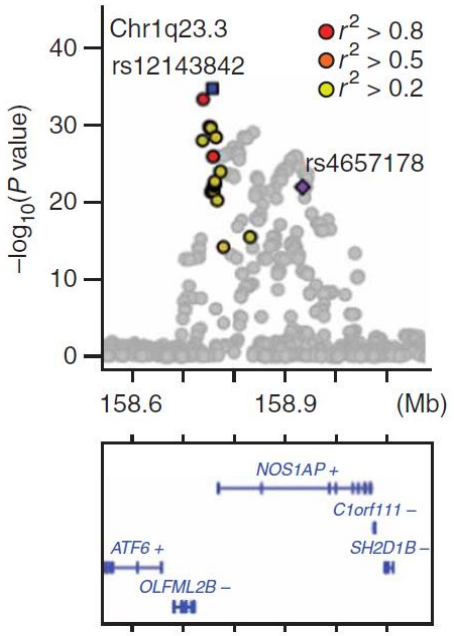

Figure 7: Association results at locus 1q23.3 spanning ± 600 kb around each SNP. The SNPs are coloured according to their LD; the leading variant is highlighted with a blue square, while SNPs representing independent signals from the leading variant are highlighted with a purple diamond. Gene transcripts are annotated in the lower box indicating the direction of transcription by '+' or '-' (Pfeufer et al., 2009).

While some of the SNPs are located within the genetic region of *NOS1AP*, others map to the *Olfactomedin-like 2B* (*OLFML2B*) gene. No coding SNP within *NOS1AP* or *OLFML2B* has been identified to be responsible for this association, pinpointing to a regulatory haplotype effect in the intergenic region. 1.0% of the variation in duration of the QT interval was explained by the *NOS1AP* SNP rs12143842 alone. Inclusion of all nine newly identified main association signals increases this to a rate of 3.3%.

Another study composed of 13,685 individuals with an independent yet similar meta-analysis by the QTGEN consortium (Newton-Cheh et al., 2009) was published at the same time. By comparing the results of the two studies, all association signals found in the QTSCD study were replicated by the QTGEN study.

In conclusion, the genome-wide data collected in these studies suggest a high association of the chromosomal region 1q23.3 with the QT interval and a strong focus on the *NOS1AP* gene.

4. The Olfactomedins

Due to the absence of SIDS cases correlated with mutations in *NOS1AP* and the investigation of this gene by Dr. Chakravarti together with his workgroup at the Johns Hopkins University School of Medicine in Baltimore (Kapoor et al., 2014), this study focused on the *OLFML2B* gene.

OLFML2B belongs to the protein family of ten olfactomedins, which all share an olfactomedin domain at their c-terminal region. This family was discovered during a study for identification of novel proteins involved in olfaction (Anholt et al., 1990). The first glycoprotein found was characterized by Snyder et al. (1991) and named 'olfactomedin'.

Karavanich and Anholt (1998) showed the widespread occurrence of olfactomedins among vertebrates and invertebrates with extensive homologies throughout the protein indicating a function of universal importance. OLFML2A (photomedin-1) and OLFML2B (photomedin-2) were discovered during a search for extracellular matrix (ECM) proteins. The basic domain structure of the proteins (Figure 8) was demonstrated as well as their ability to secrete into the extracellular space, which enables them to bind to the ECM components heparin and chondroitin sulphate-E. They also share the ability to form disulphide-bonded homodimers and oligomers (Furutani et al., 2005).

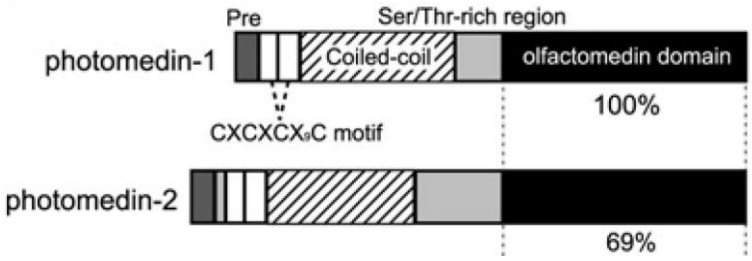

Figure 8: Schematic domain structure showing photomedin-1 (OLFML2A) and photomedin-2 (OLFML2B). Signal sequences (labelled 'Pre') and Ser/Thr-rich regions are shaded dark and light grey respectively; regions containing CXC motifs including $CXCXCX_9C$ motifs are indicated by white boxes, coiled-coil domains by hatched boxes, and olfactomedin domains by black boxes displaying the sequence homologies between photomedin-1 and photomedin-2 below (Furutani et al., 2005).

In contrast to that, the structure of OLFML2B described on UniProt slightly differs: OLFML2B shows an n-terminal signal peptide from amino acid (aa) 1 to 22, coiled-coil sequences from aa 40 to 68 as well as from aa 179 to 213 and ends with the c-terminal olfactomedin domain from aa 493 to 750. Post-translational modifications include O-glycosylation and N-glycosylation (https://www.uniprot.org/uniprot/Q68BL8 website accessed on May 3rd, 2020).

Phylogenetic analyses by Zeng et al. (2005) have categorized proteins containing the conserved olfactomedin domain into seven evolutionary distinct subfamilies. Those families were grouped by similar structural and functional characteristics with focus on the coevolved and interdependent domains. OLFML2A and OLFML2B were classified as members of subfamily IV. Though both proteins show similar expression patterns, OLFML2B

exhibits a broader spectrum of tissue specificity as it was detected in every human tissue but brain, certain cells, oesophagus (mucosa), liver, pancreas and stomach (Figure 9).

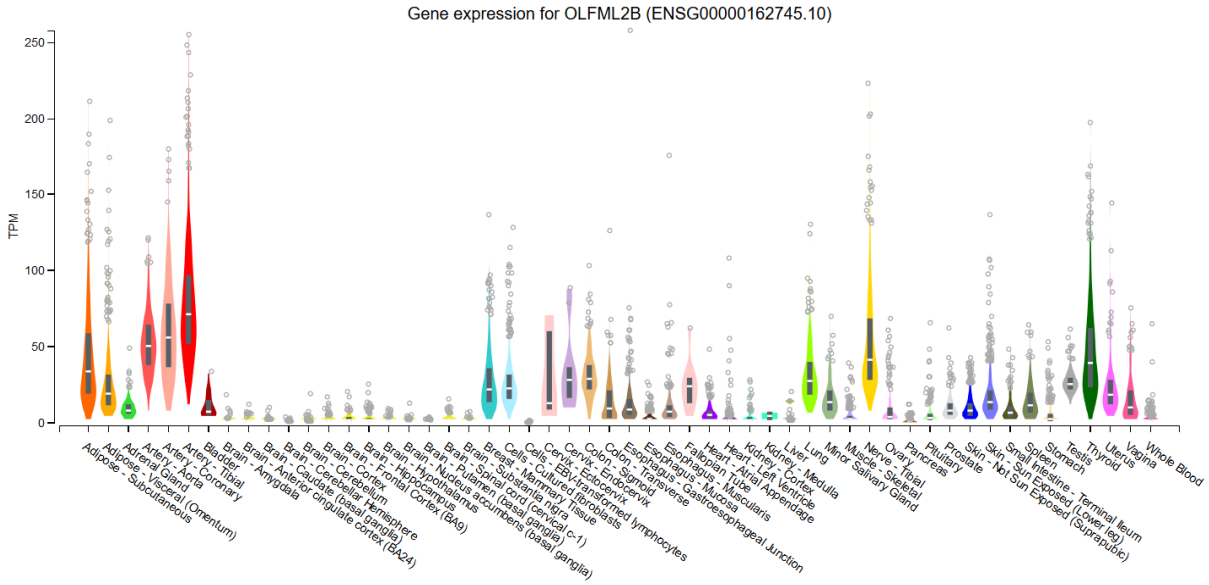

Figure 9: Gene expression of OLFML2B in human tissue (https://gtexportal.org/home/gene/OLFML2B website accessed on May 3rd, 2020).

Nine paralogs of *OLFML2B* have been identified in the human genome. While the four olfactomedins OLFML1, OLFML2A, OLFML2B and OLFML3 were not analysed for their functions yet, six are already identified to correlate with diseases (Table 2).

Table 2: Overview of olfactomedins and their functions.

OLFACTOMEDIN	GENE	AFFECTED PATHWAYS/ PHENOTYPES	DISEASES
GLIOMEDIN	*GLDN*	Nodes of Ranvier formation	Neurologic diseases
MYOCILIN (TIGR)	*MYOC*	Eye determination (ciliary muscle)	Primary open angle glaucoma (POAG)
OLFACTOMEDIN 1 (NOELIN 1, PANCORTIN)	*OLFM1*	Cell proliferation	Lung adenocarcinoma
OLFACTOMEDIN 2 (NOELIN 2)	*OLFM2*	Neuronal differentiation	Open angle glaucoma
OLFACTOMEDIN 3	*OLFM3*	Cell proliferation	Endothelioma
OLFACTOMEDIN 4	*OLFM4*	Cell proliferation	Gastric, colon, breast, lung and pancreatic cancer

Gliomedin is involved in generating and maintaining the clustering of sodium channels at the nodes of Ranvier to ensure the saltatory conduction (Eshed et al., 2007; Feinberg et al., 2010; Eshed-Eisenbach and Peles, 2013; Amor et al., 2014). Node of Ranvier disruption

seems to be the cause of many neurologic diseases (Susuki, 2013). In 1997, Myocilin was first implicated by Stone et al. with primary open angle glaucoma (Adam et al., 1997). Olfactomedin 1 has been linked to lung adenocarcinoma (Wu et al., 2010), Olfactomedin 2 to open angle glaucoma (Funayama et al., 2006) and Olfactomedin 3 to endothelioma (Miljkovic-Licina et al., 2012), whereas Olfactomedin 4 is believed to cause several types of cancer, among them gastric (Oue et al., 2009), colon, breast, lung (Koshida et al., 2007) and pancreatic cancer (Kobayashi et al., 2007).

It appears that olfactomedins play essential roles in development and cell differentiation. Mutations, especially in the evolutionary highly conserved olfactomedin domain, are associated with many common diseases including glaucoma and several types of cancer (Anholt, 2014). Though there has been a lot of progress in identifying and characterizing olfactomedin family members, the physiological function of *OLFML2B* remains elusive.

5. Aims of the Study

The objective of this study was to detect a potential connection between the OLFML2B gene and QT interval prolongation in order to explain one of the causes for atrial (AF) and ventricular arrhythmias (LQT), dilated cardiomyopathy (DCM) and sudden infant death syndrome (SIDS). In detail, the following projects have been conducted:

(1) Detection of OLFML2B in human heart tissue.

(2) Characterization of wildtype and mutant OLFML2B proteins including protein stability and structure as well as secretional status in HEK293 cells.

(3) Cultivation at different temperatures and subsequent analysis of the secretion to elucidate the stability of the protein and the influence of fever and hypothermia.

(4) Co-expression of wildtype and mutant protein to determine a possible dominant effect of OLFML2B.

(5) Detection and characterization of antibody binding sites by LC-MSMS.

(6) Mass spectrometry analyses with synthetic OLFML2B protein for identification of intra- and extracellular protein-protein interaction (PPI) partners and follow-up of most likely PPIs.

(7) Validation of a sandwich ELISA for OLFML2B protein to generate a biomarker that can be used to test serum of affected patients for insufficiency or arrhythmogenic predisposition.

III. MATERIAL AND METHODS

1. MATERIAL

1.1. COHORTS

We investigated individuals with a diverse set of cardiac conditions for mutations in *OLFML2B* including cohorts of patients with long-QT syndrome (LQTS), atrial fibrillation (AF), dilative cardiomyopathy (DCM) and sudden infant death syndrome (SIDS) as well as a control study population (Table 3).

Table 3: Patient and control cohorts.

NUMBER OF INDIVIDUALS	DISEASE	COHORT CENTERS
125	LQTS	Klinikum der Universität München, Großhadern, Université de Nantes and University Medical Center Amsterdam
92	AF	Klinikum der Universität München, Großhadern
94	DCM	Klinikum der Universität München, Großhadern
93	SIDS (all patients died within the first year of life)	German Study on Sudden Infant Death, forensic medicine department of the Ludwig-Maximilians-Universität München and Sheffield Children's Hospital, UK
141,456	Control	Non-Finnish European descent from the ExAC (Exome aggregation consortium; Lek et al., 2016) accessible through the Genome Aggregation Database (gnomAD; https://gnomad.broadinstitute.org/ website accessed on May 5th, 2020)

1.2. MOLECULAR BIOLOGY

The *Escherichia coli* strain XL1-Blue supercompetent cells by Stratagene (La Jolla, USA) and oligonucleotides provided by Metabion (Martinsried, Germany) were used for cloning of *OLFML2B* cDNA (NM_015441.2). To design primers for cDNA amplification, the ExonPrimer software based on Primer3 according to hg18 was applied (Table 4).

Table 4: Nucleotide sequence of primers.

PRIMER	SEQUENCE	APPLICATION
OLFML2B-CDNA-F	5' - CCCCAGCCATTCTCTGAAGG - 3'	qPCR
OLFML2B-CDNA-R	5' - TTCTGCTTGTGGGGACAAGG - 3'	qPCR
GAPDH-CDNA-F	5' - TCCTCTGACTTCAACAGCGA - 3'	qPCR
GAPDH-CDNA-R	5' - GGGTCTTACTCCTTGGAGGC - 3'	qPCR
OLFML2B_SEQ_118_F	5´- tgcggaggacgagactctg - 3´	Sequencing
OLFML2B_SEQ_217_R	5´- agccctcagacazagccttg - 3´	Sequencing

PRIMER	SEQUENCE	APPLICATION
OLFML2B_SEQ_340_F	5´- tgcaagtgtgcctgtgatgc - 3´	Sequencing
OLFML2B_SEQ_389_R	5´- ctcgcaggattgaggg - 3´	Sequencing
OLFML2B_SEQ_704_F	5´- cagcctagcccacccagag - 3´	Sequencing
OLFML2B_SEQ_1077_F	5´- tgtgacaagcgacctgaaca – 3	Sequencing
OLFML2B_SEQ_1487_F	5´- acactctctccacaatcacg - 3´	Sequencing
OLFML2B_SEQ_1945_F	5´- agcaagctcaatgccgc - 3´	Sequencing
OLFML2B_QC_WT_A12S_F	5´ - tgctagttctctacttctctctgattgtggttccg - 3´	Site directed mutagenesis
OLFML2B_QC_WT_A12S_R	5´- cggaaccacaatcagagagaagtagagaactagca - 3`	Site directed mutagenesis
OLFML2B_QC_WT_V15G_F	5´- cttcgctctgattggggttccggcctggg - 3´	Site directed mutagenesis
OLFML2B_QC_WT_V15G_R	5´- cccaggccggaaccccaatcagagcgaag - 3´	Site directed mutagenesis
OLFML2B_QC_WT_R347W_F	5´- gaccagtgtcacctggaggcctgcagc - 3'	Site directed mutagenesis
OLFML2B_QC_WT_R347W_R	5´- gctgcaggcctccaggtgacactggtc - 3´	Site directed mutagenesis
OLFML2B_QC_WT_R353H_F	5´- cctgcagccacccatcagggacacagc - 3´	Site directed mutagenesis
OLFML2B_QC_WT_R353H_R	5´- gctgtgtccctgatgggtggctgcagg - 3´	Site directed mutagenesis
OLFML2B_QC_WT_A436S_F	5´- cccagctcctccgtcagtgtctcccag - 3´	Site directed mutagenesis
OLFML2B_QC_WT_A436S_R	5´- ctgggagacactgacggaggagctggg - 3´	Site directed mutagenesis
OLFML2B_QC_WT_P504L_F	5´- cacaatcacggggctgaccacccagaacac - 3´	Site directed mutagenesis
OLFML2B_QC_WT_P504L_R	5´ - gtgttctgggtggtcagccccgtgattgtg - 3´	Site directed mutagenesis
OLFML2B_QC_WT_G515E_F	5´- catatgggcggaatgaagaggcctggatgaaccaccc - 3´	Site directed mutagenesis
OLFML2B_QC_WT_G515E_R	5´-gggtccttcatccaggcctattcattccacccatatg - 3´	Site directed mutagenesis
OLFML2B_QC_WT_R527Q_F	5´- gaagaggcctggatgatgaaggaccc - 3´	Site directed mutagenesis
OLFML2B_QC_WT_R527Q_R	5´- gggtccttcatcatccagcctcttc - 3´	Site directed mutagenesis
OLFML2B_QC_WT_Y557H_F	5´- cgctggagcaattcccacaagctcccgtaca - 3´	Site directed mutagenesis
OLFML2B_QC_WT_Y557H_R	5´- tgtacgggagcttgtgggaattgctccagcg - 3´	Site directed mutagenesis
OLFML2B_QC_WT_V604M_F	5´- ccatgctgcatgacatggcctacgaggag - 3´	Site directed mutagenesis
OLFML2B_QC_WT_V604M_R	5´- ctcctcgtaggccatgtcatgcagcatgg - 3´	Site directed mutagenesis
OLFML2B_QC_WT_N690S_F	5´- gccgtggacagctacagccagcggaatgccaac - 3´	Site directed mutagenesis
OLFML2B_QC_WT_N690S_R	5´- gttggcattccgctggctgtagctatccacggc - 3´	Site directed mutagenesis

All clones were inserted into the mammalian expression vector pcDNA3.0 by Invitrogen (Carlsbad, USA). The following *OLFML2B* variants were generated as cDNA clones (Table 5).

Table 5: *OLFML2B* cDNA clones (AF: atrial fibrillation, DCM: dilated cardiomyopathy, LQTS: long-QT syndrome, SIDS: sudden infant death syndrome).

PROTEIN VARIANT			ORIGIN FROM PATIENT WITH	CDNA	VECTOR
PROTEIN	CDNA	GENOME (HG19)			
Wildtype		-	Common	*OLFML2B*	pcDNA3.0
A12S	c.34C>A	1-161993187-C-A	DCM	*OLFML2B*	pcDNA3.0
V15G	c.44T>G	1-161993177-A-C	AF	*OLFML2B*	pcDNA3.0
R86W	c.256C>T	1-161989891-G-A	LQT	*OLFML2B*	pcDNA3.0
S113L	c.338C>T	1-161989809-G-A	LQT	*OLFML2B*	pcDNA3.0
T149A	c.445A>G	1-161987291-T-C	LQT	*OLFML2B*	pcDNA3.0
L269P	c.806T>C	1-161970046-A-G	Common	*OLFML2B*	pcDNA3.0
P289L	c.866C>T	1-161969986-G-A	Common	*OLFML2B*	pcDNA3.0
R347W	c.1039G>A	1-161968050-G-A	LQT	*OLFML2B*	pcDNA3.0
R353H	c.1058G>A	1-161968031-C-T	LQT	*OLFML2B*	pcDNA3.0
R367W	c.1099C>T	1-161967990-G-A	AF	*OLFML2B*	pcDNA3.0
S379L	c.1136C>T	1-161967953-G-A	DCM	*OLFML2B*	pcDNA3.0
S384R	c.1152C>G	1-161967937-G-C	LQT	*OLFML2B*	pcDNA3.0
A436S	c.1306G>T	1-161967783-C-A	AF	*OLFML2B*	pcDNA3.0
T456I	c.1367C>T	1-161967722-G-A	DCM	*OLFML2B*	pcDNA3.0
W470R	c.1408T>C	1-161967681-A-G	Common	*OLFML2B*	pcDNA3.0
P504L	c.1512G>T	1-161954734-G-A	SIDS	*OLFML2B*	pcDNA3.0
G515E	c.1544G>A	1-161954701-C-T	SIDS	*OLFML2B*	pcDNA3.0
R527Q	c.1580G>A	1-161954665-C-T	LQT	*OLFML2B*	pcDNA3.0
G536S	c.1606G>A	1-161954639-C-T	SIDS	*OLFML2B*	pcDNA3.0
Y557H	c.1669T>C	1-161954049-A-G	SIDS	*OLFML2B*	pcDNA3.0
V604M	c.1810G>A	1-161953908-C-T	DCM	*OLFML2B*	pcDNA3.0
G674D	c.2021G>A	1-161953697-C-T	SIDS	*OLFML2B*	pcDNA3.0
N690S	c.2069A>G	1-161953649-T-C	AF	*OLFML2B*	pcDNA3.0

1.3. Cell Culture

Human embryonic kidney cells HEK293 were used for cell culture (DSMZ, Braunschweig, Germany).

1.4. Human Heart Tissue

All cardiac tissue used in this study was retrieved from the Klinikum der Universität München, Großhadern.

1.5. Antibodies

The commercial primary antibodies listed in Table 6 were used in various applications in this study.

Table 6: Commercial primary antibodies.

PRIMARY ANTIBODY	SPECIES, CLONALITY	DILUTION	COMPANY
ANTI-FLAG-M2	Mouse, monoclonal	1:1,000	Sigma-Aldrich, St. Louis, MO, USA
ANTI-FLAG-6F7	Rat, monoclonal	1:10	HMGU
ANTI-TENASCIN C (E-9)	Mouse, monoclonal	1:100	Santa Cruz Biotechnology, Dallas, Texas, USA
ANTI-TENASCIN C	Rabbit, polyclonal	0.5 µg/ml	Merck KGaA, Darmstadt, Germany
ANTI-TENASCIN C (4C8mS)	Mouse, monoclonal	1:200-1:1,000	Thermo Fisher Scientific, Waltham, Massachusetts
ANTI-TENASCIN C (BC-24)	Mouse, monoclonal	2-4 µg/ml	Thermo Fisher Scientific, Waltham, Massachusetts

Monoclonal antibodies had previously been generated by peptide vaccination in rat or mouse with the peptide sequences described in Table 7.

Table 7: Peptide sequence of self-generated primary antibodies.

PEPTIDE	PEPTIDE SEQUENCE	AMINO ACID	LENGTH
OLF1	n-TSEPPDAQTVAPAEDETLQNC-c	28 to 48	21 aa
OLF2	n-EDMEEIRTEMNKRGKENC-c	197 to 214	18 aa
FUSION PEPTIDE	GST fused to n-(GS)TTSVSPDPTRESVLQPSPQVPATTVAHTA TQQPAAPAPPAVSPREALMEAMHTVPVPPTTVRTDSLGK(S)-c	397 to 464	68 aa
CDNA	entire OLFML2B	1 to 750	750 aa

All antibodies listed below were available as culture supernatant, purified (Western Blot, Dot blot analysis) and 25% or 50% biotinylated (ELISA). They were raised against the following antigens (Table 8).

Table 8: Self-generated primary hybridoma cell line antibodies.

HYBRIDOMA CELL LINE ANTIBODY	SPECIES, CLONALITY	IGG CLASS	PEPTIDE	DILUTION FOR SDS-PAGE	DILUTION FOR ELISA
7C4	Rat, monoclonal	IgG2a	OLF1	1:10	250ng/ 1:10,000
7B9	Rat, monoclonal	IgG2c	OLF2	1:10	250ng/ 1:10,000
5A5	Rat, monoclonal	IgG2a	OLF2	1:10	250ng/ 1:10,000
6B11	Rat, monoclonal	IgG1	OLF2	1:10	250ng/ 1:10,000
5D8	Rat, monoclonal	IgG2a	cDNA	1:10	250ng/ 1:10,000
6B1	Rat, monoclonal	IgG2a	OLF2	1:10	250ng/ 1:10,000
7E9	Rat, monoclonal	IgG2a	OLF2	1:10	250ng/ 1:10,000
8B10	Rat, monoclonal	IgG2a	cDNA	1:10	250ng/ 1:10,000
2E9	Mouse, monoclonal	IgG1	Fusion Peptide	1:10	250ng/ 1:10,000
7D7	Mouse, monoclonal	IgG1	Fusion Peptide	1:10	250ng/ 1:10,000
1E8	Mouse, monoclonal	IgG2a	Fusion Peptide	1:10	250ng/ 1:10,000
6D1	Mouse, monoclonal	IgG2a	Fusion Peptide	1:10	250ng/ 1:10,000
7A12	Mouse, monoclonal	IgG2a	Fusion Peptide	1:10	250ng/ 1:10,000
4C2	Mouse, monoclonal	IgG2b	Fusion Peptide	1:10	250ng/ 1:10,000

Anti-OLFML2B monoclonal antibodies producing hybridoma cell lines have been provided by HMGU, Institute for Molecular Immunology, Dr. Elisabeth Kremmer.

For detection of the antigen-antibody-complex, a secondary antibody was applied (Table 9).

Table 9: Secondary antibodies.

SECONDARY ANTIBODY	DILUTION	COMPANY
GOAT ANTI-MOUSE HRP	1:20,000	Dianova, Hamburg, Germany
RAT ANTI-MOUSE HRP	1:400	HMGU
RAT ANTI-MOUSE IGG1 HRP	1:1,000	HMGU
RAT ANTI-MOUSE IG2A HRP	1:1,000	HMGU
RAT ANTI-MOUSE IG2B HRP	1:1,000	HMGU
RABBIT ANTI-MOUSE HRP	1:150,000	Dianova, Hamburg, Germany
GOAT ANTI-RAT HRP	1:20,000	Dianova, Hamburg, Germany
MOUSE ANTI-RAT HRP	1:400	HMGU
MOUSE ANTI-RAT IGG1 HRP	1:1,000	HMGU

SECONDARY ANTIBODY	DILUTION	COMPANY
MOUSE ANTI-RAT IG2A HRP	1:1,000	HMGU
MOUSE ANTI-RAT IG2C HRP	1:1,000	HMGU
RABBIT ANTI-RAT	1:20,000	Dianova, Hamburg, Germany
GOAT ANTI-RABBIT	1:100,000	Dianova, Hamburg, Germany
AVIDIN HRP	1:4,000	HMGU

1.6. Laboratory Chemicals and Reagents

The chemicals and reagents listed in Table 10 were used in this study.

Table 10: Chemicals and reagents.

DEVICE	APPLICATION	COMPANY
1-STEP™ ULTRA TMB-ELISA	Dot blot, ELISA	Thermo Fisher Scientific, Waltham, Massachusetts
5% SKIM MILK POWDER	SDS-PAGE, ELISA	Fluka, Sigma-Aldrich, Taufkirchen, Germany
AMERSHAM™ ECL™ PRIME	SDS-PAGE	GE Healthcare, Freiburg, Germany
ANTI-FLAG M2 AFFINITY GEL	Protein purification	Sigma-Aldrich, Taufkirchen, Germany
BORIC ACID	Molecular cloning	Sigma-Aldrich, Taufkirchen, Germany
BSA (BOVINE SERUM ALBUMIN)	Protein purification	Sigma-Aldrich, Taufkirchen, Germany
C0MPLETE TABLETS EASYPACK	Cell culture	Roche Diagnostics GmbH, Mannheim, Germany
COOMASSIE BRILLIANT BLUE G-250 DYE	Mass spectrometry	Thermo Fisher Scientific, Waltham, Massachusetts
DMEM (DULBECCO'S MODIFIED EAGLE MEDIUM – HIGH GLUCOSE)	Cell culture	Gibco, Invitrogen, Carlsbad, USA
DOUBLE DISTILLED WATER (DDH_2O)	SDS-PAGE	Thermo Fisher Scientific, Waltham, Massachusetts
EDTA (ETHYLENEDIAMINETETRAACETIC ACID)	Cell culture	Sigma-Aldrich, Taufkirchen, Germany
FBS (FETAL BOVINE SERUM)	Cell culture	Gibco, Invitrogen, Carlsbad, USA
GENERULER 100 BP DNA LADDER	Agarose gel electrophoresis	Thermo Fisher Scientific, Waltham, Massachusetts
GLYCEROL	Molecular Cloning	Sigma-Aldrich, Taufkirchen, Germany
H_2O	Cell culture	Biochrom, Berlin, Germany

DEVICE	APPLICATION	COMPANY
HEPES BUFFER 1M (4-(2-HYDROXYETHYL)-1-PIPERAZINEETHANESULFONIC ACID)	Protein purification	Biochrom, Berlin, Germany
HIMARK™ PRE-STAINED PROTEIN STANDARD	SDS-PAGE	Thermo Fisher Scientific, Waltham, Massachusetts
HUMAN TENASCIN-C PURIFIED PROTEIN	SDS-PAGE	Merck KGaA, Darmstadt, Germany
LIPOFECTAMINE® LTX & PLUS™ REAGENT	Cell culture	Invitrogen, Carlsbad, USA
L-GLUTAMINE	Cell culture	Gibco, Invitrogen, Carlsbad, USA
MAGICMARK™ XP WESTERN PROTEIN STANDARD	SDS-PAGE	Invitrogen, Carlsbad, USA
MES (2-(N-MORPHOLINO)ETHANESULFONIC ACID)	Cell culture	Carl Roth, Karlsruhe, Germany
NP-40 (NONIDENT-40)	Cell culture	Roche Diagnostics GmbH, Mannheim, Germany
NUPAGE® NOVEX ANTIOXIDANT	SDS-PAGE	Invitrogen, Carlsbad, USA
NUPAGE® NOVEX REDUCING AGENT (10X)	SDS-PAGE	Invitrogen, Carlsbad, USA
NUPAGE® NOVEX LDS (LITHIUM DODECYL SULFATE) SAMPLE BUFFER	SDS-PAGE	Invitrogen, Carlsbad, USA
PBS (PHOSPHATE BUFFERED SALINE)	Cell culture	Gibco, Invitrogen, Carlsbad, USA
PENICILLIN-STREPTOMYCIN	Cell culture	Gibco, Invitrogen, Carlsbad, USA
PHOSSTOP	Cell culture	Roche Diagnostics GmbH, Mannheim, Germany
PONCEAU S SOLUTION	SDS-PAGE	Sigma-Aldrich, Taufkirchen, Germany
PRECISION PLUS PROTEIN STANDARD, UNSTAINED	Mass spectrometry	BioRad, Munich, Germany
PROTEIN G CONJUGATED SEPHAROSE BEADS	Protein purification	Sigma-Aldrich, Taufkirchen, Germany
SODIUM CHLORIDE	Protein isolation	Sigma-Aldrich, Taufkirchen, Germany
SODIUM HYDORXIDE	Protein isolation	Sigma-Aldrich, Taufkirchen, Germany
STRIPPING BUFFER	Protein isolation	CANDOR Bioscience GmbH, Wangen, Germany
SULFURIC ACID	ELISA	Sigma-Aldrich, Taufkirchen, Germany
SUPERSCRIPT III REVERSE TRANSCRIPTASE	RNA reverse transcription	Invitrogen, Carlsbad, USA
TRIS (TRIS(HYDROXYMETHYL) AMINOMETHANE)	Molecular Cloning	Calbiochem, San Diego, USA

DEVICE	APPLICATION	COMPANY
TRIZOL™ REAGENT	RNA isolation	Thermo Fisher Scientific, Waltham, Massachusetts
TRYPSIN	Cell culture	Gibco, Invitrogen, Carlsbad, USA
TURBO™ DNASE	RNA purification	Invitrogen, Carlsbad, USA

1.7. KITS

For better reproducibility and standardization of laboratory work, the molecular biology kits specified in Table 11 were used.

Table 11: Molecular biology kits.

DEVICE	APPLICATION	COMPANY
AMERSHAM ECL PRIME WESTERN BLOTTING DETECTION REAGENT	Western blot	GE Healthcare, Freiburg, Germany
COMPAT-ABLE™ PROTEIN ASSAY PREPARATION REAGENT SET	Protein purification	Thermo Fisher Scientific, Waltham, Massachusetts
ENDOFREE PLASMID MAXI KIT (10)	Plasmid DNA purification	Qiagen, Hilden, Germany
PERFECTPREP PLASMID MINI	Plasmid DNA isolation	Eppendorf, Hamburg, Germany
QIAAMP DNA BLOOD MINI KIT (50)	DNA purification	Qiagen, Hilden, Germany
QIAFILTER PLASMID MIDI KIT (25)	Plasmid DNA purification	Qiagen, Hilden, Germany
QIAQUICK GEL EXTRACTION KIT (50)	DNA purification	Qiagen, Hilden, Germany
QUIKCHANGE II XL SITE-DIRECTED MUTAGENESIS KIT	Site-directed mutagenesis	Agilent, Santa Clara, USA
QUICKLYSE MINIPREP KIT (100)	Plasmid DNA isolation	Qiagen, Hilden, Germany
PIERCE™ BCA PROTEIN ASSAY KIT	Protein concentration	Thermo Fisher Scientific, Waltham, Massachusetts
PROTEOEXTRACT® SUBCELLULAR PROTEOME EXTRACTION KIT	Protein purification	Merck KGaA, Darmstadt, Germany
SYBR SELECT MASTER MIX	qPCR	Applied Biosystems, Foster City, USA

1.8. CONSUMABLES

The following plastics and consumables have been employed (Table 12).

Table 12: Plastics and consumables.

DEVICE	COMPANY
4 - 12% NUPAGE BIS-TRIS MINI GELS	Invitrogen, Carlsbad, USA
CORNING® CRYOGENIC VIALS, EXTERNAL THREAD, 2.0 ML	Merck KGaA, Darmstadt, Germany
EPPENDORF SAFE-LOCK TUBES, 1.5 ML	Eppendorf AG., Wesseling-Berzdorf, Germany
FALCON® 6 WELL CLEAR FLAT BOTTOM NOT TREATED CELL MULTIWELL CULTURE P/ 9.6 CM²	Becton Dickinson, Schaffhausen, Switzerland
FALCON® 35 MM TC-TREATED EASY-GRIP STYLE CELL CULTURE	Becton Dickinson, Schaffhausen, Switzerland
FALCON® 25 CM² RECTANGULAR CANTED NECK CELL CULTURE FLASK WITH VENTED CAP	Becton Dickinson, Schaffhausen, Switzerland
FALCON® 75 CM² RECTANGULAR CANTED NECK CELL CULTURE FLASK WITH VENTED CAP	Becton Dickinson, Schaffhausen, Switzerland
FALCON® 50 ML HIGH CLARITY PP CENTRIFUGE TUBE, CONICAL BOTTOM	Becton Dickinson, Schaffhausen, Switzerland
KODAK X-RAY FILM	Eastman Kodak Company, New York, USA
MICROSPIN COLUMNS	GE Healthcare, Freiburg, Germany
NEUBAUER COUNTING CHAMBER	LO Laboroptik, Lancing, UK
NUCLEOSPIN GEL AND PCR CLEAN-UP	Machery-Nagel, Düren, Germany
PVDF MEMBRANE	Invitrogen, Carlsbad, USA
S-MONOVETTE® 1.2 ML K2E	SARSTEDT AG & Co. KG, Nümbrecht, Germany
S-MONOVETTE® 1.1 ML Z-GEL	SARSTEDT AG & Co. KG, Nümbrecht, Germany

1.9. TECHNICAL DEVICES

The standard and specific technical devices in Table 13 were used in this study.

Table 13: Technical devices.

DEVICE	APPLICATION	COMPANY
ACCULAB EC-2100 DIGITAL LAB SCALE	Scale	Sartorius Group, Göttingen, Germany
AUTOCLAVE SYSTEC VX-95	Autoclave	Systec, Wettenberg, Germany
BIOPHOTOMETER	Photometer	Eppendorf, Hamburg, Germany
CB 150 CO_2 INCUBATOR	Cell Incubator	Binder, Tuttlingen, Germany

DEVICE	APPLICATION	COMPANY
CENTRIFUGE 5418	Centrifuge	Eppendorf, Hamburg, Germany
CENTRIFUGE HERAEUS BIOFUGE STRATOS	Centrifuge	Kendro Laboratory Products, Osterode, Germany
CHRONOS 400 LIQUID NITROGEN TANK	Liquid nitrogen tank	Messer Griesheim, Sulzbach, Germany
COMBI-SPIN COMBINED CENTRIFUGE FVL-2400	Centrifuge	PEQLAB, Erlangen, Germany
CURIX 60 DEVELOPER	SDS-PAGE	Agfa, Cologne, Germany
GEL DOC 2000	Agarose gel electrophoresis	BioRad, Munich, Germany
GENIOS MICROPLATE READER	Protein quantitation	Tecan Group Ltd., Männedorf, Switzerland
HAAKE B3 WATERBATH	Water bath	Thermo, Karlsruhe, Germany
HERAEUS HERASAFE HS-12 LAMINAR FLOW	Laminar Flow	Kendro Laboratory Products, Osterode, Germany
IKAMAG REO MAGNETIC STIRRER	Stirring plate	IKA, Staufen, Germany
INFINITE 200 PRO	ELISA	Tecan Group Ltd., Männedorf, Switzerland
LTQ ORBITRAPXL MASS SPECTROMETER	Mass spectrometry	Thermo Fisher Scientific, Bonn, Germany
MINISHAKER MS1	Vortex mixer	IKA, Staufen, Germany
MX4000 MULTIPLEX QUANTITATIVE PCR SYSTEM	Real-time quantitative PCR system	Stratagene, San Diego, California
PH 538 PH/ MV-METER PH-METER	pH meter	WTW, Weilheim, Germany
POWER SUPPLY POWER PAC 300	Electrophoresis power supply	BioRad, Munich, Germany
POWER SUPPLY POWER PAC BASIC	Electrophoresis power supply	BioRad, Munich, Germany
PROBOT LIQUID HANDLING SYSTEM	Mass spectrometry	Dionex, Idstein, Germany
PTC-220 PELTIER THERMAL CYCLER DYAD DNA ENGINE	Thermal cycler	MJ Research, St. Bruno, Canada
RMO 76 MAGNETIC STIRRER	Stirring plate	Gerhardt, Königswinter, Germany
ROTATOR MULTI BIO RS-24 MULTIFUNCTION MIXER	Rotator	PEQLAB, Erlangen, Germany
SW20 SHAKING WATER BATH	Water Bath	JULABO, Seelbach, Germany
THERMOMIXER COMFORT	Thermomixer	Eppendorf, Hamburg, Germany

DEVICE	APPLICATION	COMPANY
ULTIMATE 3000 NANO-LC	Mass spectrometry	Dionex, Idstein, Germany
UNIVERSAL 16A LABORATORY CENTRIFUGE	Centrifuge	Hettich, Tuttlingen, Germany
VIDEO COPY PROCESSOR P67E	Printer	Mitsubishi, Tokyo, Japan
WIDE MINI-SUB CELL GT CELL	SDS-PAGE	Biorad, Munich, Germany
WILOVERT S INVERSE MICROSCOPE	Microscope	Helmut Hund GmbH, Wetzlar, Germany
XCELL SURELOCK MINI-CELL	SDS-PAGE	Life Technologies, Carlsbad, USA

2. METHODS

2.1. Molecular Biology

2.1.1. Molecular Cloning

Previously produced clones were re-generated by following the protocol described in the QuikChange II XL Site-Directed Mutagenesis Kit. For clonogenic selection, 10 ng of clone-buffer solution containing the desired OLFML2B cDNA variant within the pcDNA3.0 vector was incubated with XL1-Blue Competent Cells according to the manufacturer's instructions subsequently followed by blue-white colour screening. After the desired white clones were transferred to 5 ml LB-medium (lysogeny broth: 1% (w/v) tryptone, 1% (w/v) sodium chloride, 0.5% (w/v) yeast extract) containing 5 µl ampicillin, the solution was incubated at 37°C under constant agitation overnight for growing purposes. 800 µl of the bacterial solution were transferred to a cryovial and gently mixed with 200 µl of 50% (v/v) sterile glycerol for storage at -80°C. To check for the integration of the plasmid, a control PCR (polymerase chain reaction) was conducted adding 10 µl of each sample to the following master mix (Table 14).

Table 14: Master mix for control PCR.

	MASTERMIX X1
10X TAQ BUFFER	5 µl
DNTP MIX 2 MM	5 µl
$MGCL_2$ 25 MM	3 µl
FORWARD PRIMER 20 µM	0,5 µl
REVERSE PRIMER 20 µM	0,5 µl
TAQ POL 5U/µL	0,25 µl
H_2O	25,75 µl
TOTAL	40 µl

The sequencing reaction was performed by a thermo cycler including the running conditions specified in Table 15.

Table 15: Cycling conditions of control PCR.

TEMPERATURE	TIME	STEPS
95°C	5 min	Initial denaturation
95°C	30 s*	Short denaturation
60°C	30 s*	Primer annealing
72°C	1 min*	Elongation
72°C	10 min	Final elongation

*Steps two to four were carried out 40 times.

The integration of the plasmid was verified by agarose gel electrophoresis, separating DNA fragments by size. For generation of a 1.5% agarose gel, 1.2 g agarose, 80 ml ddH_2O and 0.8 µl ethidium bromide were used. The completed solution was poured in the gel tray and the comb was inserted. After one hour of solidification, the gel was transferred to an electrophoresis chamber filled with TBE buffer (89 mM Tris, 89 mM boric acid, 2 mM EDTA) and the comb was removed. 15 µl of each DNA sample was treated with 3 µl loading buffer (6x: 0.25% bromphenol blue, 40% (w/v) sucrose) and loaded onto the gel including an appropriate ladder, e.g. GeneRuler 100 bp (1 µl loading buffer and 4 µl ddH_2O was added to 1 µl ladder). The gel run was performed with 120 V and terminated as soon as the bromphenol front arrived at the end of the gel. The DNA bands on the gel were revealed by exposing the whole gel to ultraviolet radiation. The QIAquick Gel Extraction Kit was used to extract the desired DNA from the appropriate gel band as described by the manufacturer.

If the integration of the plasmid had been confirmed by blue-white colour screening, 2 ml bacterial suspension was mixed with 200 ml LB-medium as well as 200 µl ampicillin and stored overnight at 37°C under constant agitation. The following plasmid purification with the QIAfilter Plasmid Midi Kit or the EndoFree Plasmid Maxi Kit was performed according to the manufacturer`s instructions. After determining the optical densitometry with a BioPhotometer, the samples were diluted to a concentration of either 1 µg/µl for transient transfections or 100 ng/µl for sequencing reactions and stored at -20°C.

2.1.2. RNA Isolation, Purification and Reverse Transcription including qPCR

Total RNA isolation from HEK293 cells was performed using TRIzol™ Reagent according to the manufacturer's protocol. If the optical density (OD) showed a low 260/280 value afterwards, the RNA was purified with TURBO™ DNase according to the manufacturer's instructions. Once the value was sufficient, the manufacturer's protocol of SuperScript III Reverse Transcriptase was used for reverse transcription of 3 µg/µl of RNA to a final volume of 10 µl. Reverse transcriptase-polymerase chain reactions were performed to control both

the integration of the plasmid and of the variant. The cycling conditions for reverse transcription are described in Table 16.

Table 16: Cycling conditions of reverse transcriptase-polymerase chain reaction.

TEMPERATURE	TIME	STEPS
95°C	5 min	Initial denaturation
95°C	1 min*	Short denaturation
59/ 60°C	30 s*	Primer annealing
72°C	30 s*	Elongation
72°C	10 min	Final elongation

*Steps two to four were carried out 40 times.

The samples were subsequently transferred to a 1.5% agarose gel and the cDNA fractionated according to size by electrophoresis.

Accurate quantitation of RNA transcripts was obtained by using 1 µl of the reverse transcription reaction and the SYBR Select Master Mix for qPCR (quantitative PCR). During this kinetic reaction, the amplification products are continuously quantitated by monitoring the fluorescence. All reactions were conducted involving no template controls as well as endogenous controls (GAPDH) for relative quantitation. The standard running temperatures are listed in Table 17.

Table 17: Running conditions for qPCR.

TEMPERATURE	TIME	STEPS
50°C	2 min	UDG activation
95°C	2 min	Activation of polymerase
95°C	15 s*	Denaturation
60°C	60 s*	Annealing/extension

*Steps three to four were carried out 40 times.

The results were analysed by using the Mx4000 software and adjusting baseline and threshold values to determine the cycle threshold for the amplification curve.

2.2. Cell Culture

2.2.1. Growth and Maintenance of HEK293 Cells

Generally, HEK293 cells were grown in cell culture dishes or bottles at 37°C with 5% CO_2 in a cell culture incubator with growth medium DMEM containing 10% FBS, 100 units or µg/ml penicillin and streptomycin as well as 2 mM l-glutamine. To reach the ideal cell number per ml according to Table 18, cells were split about two times a week.

Table 18: Ideal cell number per container.

CULTURE FORMAT	MEDIUM ADDED TO THE CELLS [ML]	NUMBER OF CELLS [CELLS PER ML]
6-WELL	2	$10x10^5$
T25	5	$25x10^5$
T75	15	$75x10^5$

Depending on the size of the initial container, the required volumes according to Table 19 were applied.

Table 19: Splitting cells of different container sizes.

CULTURE FORMAT	PBS [ML]	TRYPSIN/EDTA [ML]	DMEM FOR STOPPING THE REACTION [ML]	DMEM FOR RESUSPENSION [ML]
T25	3	1.5	1.5	3
T75	10	5	5	10

The old medium was removed and the reagents DMEM, Trypsin and PBS were heated in a 37°C water bath for 20 min before use. The cells were washed once with PBS and 0.05% Trypsin/EDTA was added for 2 min at 37°C so the cells would dissolve from the container. By adding DMEM and transferring the solution to a 15 ml Falcon tube, the reaction was stopped. The cells were centrifuged at 1,000 U/min for 3 min at room temperature, the supernatant extracted by suction and the cell pellet resuspended in DMEM.

To count the cells, 1 drop of cell solution was placed in a 1.5 ml tube while the rest of the cells were stored in the incubator. 20 µl of cell suspension was mixed with 80 µl of trypan blue and put it in a Neubauer counting chamber. After incubation for one minute, the cells in four squares were counted using a light microscope and the correct cell number per ml calculated by using the equation "average x5 (dilution factor) $x10^4$". Then, the remaining cells in the incubator were split accordingly (Table 18).

In most cases, a dilution of 1:10 was sufficient.

2.2.2. Transient Transfection and Lysis of HEK293 Cells

After transient transfection of HEK293 cells with either one of 23 mutant or wildtype OLFML2B clones by Lipofectamine® LTX & PLUS™ Reagent according to the manufacturer's instructions and volumes listed in Table 20, the cells were incubated for 24 hours at 37°C.

Table 20: Reagents and volumes used for transient transfection with different cell culture formats.

CULTURE FORMAT	DNA [MG]	PLUS™ [ML]	LIPOFECTAMINE® LTX [µL]	GROWTH MEDIUM DMEM [ML]	MEDIUM ADDED TO THE CELLS [ML]
6-WELL	2.5	2.5	7.5	500	2
T25	6.25	6.25	18.75	500	5
T75	22.43	22.43	39	750	15

Instead of the suggested Opti-MEM we used pure DMEM supplemented with l-glutamine, FBS and penicillin-streptomycin. Following confluency, the medium was exchanged for the above without FBS in order to starve the cells, a stress that causes them to produce increased amounts of recombinant OLFML2B protein within the next 48 hours.

To assess stability and structure of the protein and to optimize the standard cell culture protocol, modifications of cell culture treatment included:

- Applying of various concentrations of $CaCl_2$ and $MgCl_2$ at different times during cell culture and the following processes
- Variation of cultivation temperature by setting the incubator to 30°C and 41°C in addition to 37°C
- Adjustment of pH value to 6.8, 7.2, 7.9 or 8.5
- Testing various buffers: MES, TBS, HEPES, PBS

2.2.3. Cryo-stocks

To generate cryo stocks for long term storage, HEK293 cells were solubilized and resuspended in 1 ml of 95% DMEM and 5% DMSO before they were transferred into liquid nitrogen.

If the stored cryo stocks needed to be used again, cryo vials were heated in a water bath set to 37°C. After 5 ml of DMEM was added, the cells were centrifuged at 1,000 U/min for 3 min at room temperature and the supernatant was discarded. The cells were then resuspended in the ideal DMEM amount according to Table 19.

2.3. Protein Preparation

2.3.1. Isolation of Protein from HEK293 Cells

After 48 hours of starving the cultivated cells, the supernatant was collected and centrifuged at 20,000 g for 10 min at 4°C. Simultaneously, the cells were washed with PBS and solubilized with 250 µl lysis buffer (1 ml 10x TBS, 200 µl PhosSTOP, 200 µl protease inhibitor c0mplete Tablets EASYpack, 50 µl NP-40, 8.55 ml H_2O) per well, based on a six well dish. The cells were scraped off, incubated for 30 min at 4°C under rotation and centrifuged at 20,000 g for 20 min at 4°C. Then the pellet was discarded and the cell supernatant and lysate were either processed further or quick-frozen in liquid nitrogen and stored at -80°C.

2.3.2. Isolation of Protein from Human Heart Tissue

For detection of OLFML2B protein in human heart tissue, the tissue was grinded and added to lysis buffer (50 mM HEPES, 154 mM sodium chloride, 25 mM sodium hydroxide, 2.5 mM EDTA, 0.5% NP-40, 5% Glycerol, PhosSTOP, protease inhibitor c0mplete Tablets EASYpack) in a ratio of 1:10. After 30 min incubation on ice, the mixture was sonicated six times for 10 s with an amplitude of 50% and then centrifuged at 4°C for 10 min at 13,000 g. The pellet was

discarded and the protein concentration of the supernatant containing the cell lysate as well as the desired protein was measured by BCA and then analysed by Western blot.

Alternatively, the cardiac protein was isolated by using the ProteoExtract® Subcellular Proteome Extraction Kit according to the manufacturer's instructions.

2.3.3. Isolation of Protein from Human Whole Blood

To detect OLFML2B protein in human whole blood, blood serum and plasma were treated differently: whole blood from S-Monovette® 1.1 ml Z-Gel was carefully mixed and incubated for 30 min at room temperature. After centrifugation at 2,500 rpm for 20 min, the serum supernatant was analysed by Western blot. For analysis of plasma, the whole blood from S-Monovette® 1.2 ml K2E was centrifuged shortly immediately after the sampling at 2,500 rpm and the plasma supernatant analysed by Western blot.

2.3.4. Protein Purification by FLAG Tag

For purification purposes, all OLFML2B variant and wildtype clones had previously been fused with the FLAG sequence. By binding to the anti-Flag-M2 antibody and washing the protein complex on a micro-spin column, all other components were eliminated. After separation of the complex by competition with FLAG Peptide, only the purified protein was eluted into the tube.

The Flag-M2-sepharose beads were washed for purification in different ways depending on the substance:

- Cell supernatant: 10 µl Flag-M2-sepharose beads were washed with 50 µl 1x TBS and centrifuged at 500 g for 30 s at room temperature. The supernatant was discarded and 50 µl fresh 1x TBS were added. 60 µl of the washed beads were then combined with the cell supernatant.
- Cell lysate: 5 µl beads were washed with 25 µl 1x TBS and centrifuged at 500 g for 30 s at room temperature. The supernatant was discarded and 25 µl of fresh 1x TBS were added. 30 µl of the washed beads were then combined with the cell lysate.

The mixture was incubated for at least 4 hours so proper binding of the FLAG tagged protein and the anti-Flag-M2 antibody was able to develop. The protein complex was centrifuged at 500 g for 10 min at 4°C, the supernatant discarded and the beads were transferred onto micro-spin columns. The beads were first washed with 500 µl washing buffer (1x TBS + 0.1% NP-40) and then two times with 500 µl TBS. The protein complexes were eluted using 100 µl FLAG elution buffer consisting of 200 µg/ml FLAG peptide and 1x TBS. After incubation of 10 min at 4°C under gentle agitation, the column was put in a tube and centrifuged for 2 min at 10,000 g and 4°C.

2.3.5. Protein Purification by Protein G Conjugated Sepharose Beads

After protein isolation from e.g. human heart tissue, antibody/antigen complexes were purified by immunoprecipitation (IP) using Protein G conjugated Sepharose beads according to the manufacturer's instructions.

2.3.6. Protein Purification by Compat-Able™ Protein Assay

Prior to total protein quantitation by BCA (*III. Material and Methods, chapter 2.3.7 PROTEIN QUANTITATION BY BCA*), the proteins were pre-treated with Compat-Able™ Protein Assay Preparation Reagent Set to remove interfering substances according to the manufacturer's instruction.

2.3.7. Protein Quantitation by BCA

Determination of protein concentration by BCA (bicinchoninic acid) method is based on the biuret reaction, where peptide bonds reduce Cu^{2+} to Cu^{+} in alkaline solutions causing BCA to form mauve-coloured complexes with the reduced copper ions. The amount of protein in solution directly correlates with the intensity of the colorimetric reaction and can be measured at a wavelength of 562 nm. A series of dilution of a common protein such as BSA with known concentrations was processed alongside the protein sample with unknown concentration according to the standard protocol for microplate procedure of the provider. Protein quantitation was done according to the BSA standard curve.

2.4. PROTEIN ANALYSIS

2.4.1. Sodium Dodecyl Sulphate-polyacrylamide Gel Electrophoresis

After preparing the running buffers and adding LDS Sample Buffer and Reducing Agent (10x) to the samples according to the manufacturer's instructions, the wells of the 4-12% Bis-Tris gel were filled with MagicMark™ XP Western Protein Standard or samples. During the following Sodium Dodecyl Sulphate-polyacrylamide gel electrophoresis (SDS-PAGE), the proteins were separated according to their molecular weight using a XCell SureLock™ Mini-Cell and transferred to a PVDF (polyvinylidene difluoride) membrane. To verify the transfer of proteins, the PVDF membrane was stained with Ponceau S solution and subsequently destained with ddH_2O for further processing.

If necessary, the PVDF membrane was stripped to remove all antibodies according to the Instructions of the manufacturer.

2.4.2. Western Blot Analysis

If the protein transfer had been successfully confirmed, the membrane was blocked with 5% skim milk powder in TBST (tris-buffered saline with Tween20) pH 7.4 for one hour at room temperature. Then, the membrane was incubated overnight at 4°C in 5% milk powder in TBST pH 7.4 with a combination of two custom-made rat anti-human OLFML2B monoclonal primary antibodies (OLF1 clone 7C4 (IgG2a) and OLF2 clone 7B9 (IgG2c)), which were raised

against OLFML2B aa 28-48 and aa 197-214 (Dr. Elisabeth Kremmer, HMGU), in a dilution of 1:10. After washing with TBST pH 7.4 the membrane was incubated with the secondary antibody goat anti-rat HRP (horse radish peroxidase) conjugated and TBST pH 7.4 in a dilution of 1:20,000 for one hour at room temperature. Before detection with Amersham ECL (enhanced chemiluminescence) Prime according to the manufacturer's instructions, the membrane was washed again with TBST pH 7.4. The chemiluminescent signals were detected by Kodak X-Ray films, which were incubated on the PVDF membrane for 15 s and developed by the Curix 60.

Densitometrical analysis for quantitation of Western blot images was carried out by using the Image Studio™ Lite software (LI-COR Biosciences GmbH, Bad Homburg vor der Höhe, Germany).

2.4.3. Colloidal Coomassie Staining

The Colloidal Coomassie staining was used to prepare the purified and pre-fractioned proteins for LC-MSMS (liquid chromatography combined with tandem mass spectrometry) analysis. After SDS-PAGE, the gels were incubated three times for 10 min in fixation solution (20% (v/v) methanol, 10% (v/v) phosphoric acid, ddH_2O) while shaking, washed three times for 20 min in 10% (v/v) phosphoric acid and equilibrated once for 30 min in 20 ml equilibration solution (10% (v/v) phosphoric acid, 20% (v/v) methanol and 10% (w/v) ammonium sulphate, ddH_2O). For a 2% (v/v) Coomassie solution, 2 g of Coomassie brilliant blue G-250 was mixed with warm ddH_2O up to 100 ml and run through a fluted filter. 240 µl of the 2% (v/v) Coomassie solution was added to the equilibration solution and incubated shaking overnight. After rinsing the gel in dH_2O, the gel was digitalized by a scanner and the desired bands were cut out.

2.4.4. Mass Spectrometry

In this study, label-free LC-MSMS-based comparative proteomics was performed to identify the antibody binding site as well as potential protein interaction partners of OLFML2B and to determine which parts of the wildtype/ mutant protein are secreted into the supernatant or are retained within the cell, respectively.

For this purpose, HEK293 cells were transiently transfected with FLAG-tagged OLFML2B wildtype. Un-transfected HEK293 cells were prepared alongside as negative controls. OLFML2B protein was isolated from cell lysate and supernatant, purified with Flag-M2-sepharose beads and sub-fractioned by SDS-PAGE. The gel was stained by Colloidal Coomassie for visualization of the protein bands, which were excised and submitted to the Core Facility Proteomics, HMGU, for analysis. Samples for identification of potential PPI partners were prepared without sub-fractioning and submitted to the Core Facility Proteomics, HMGU, directly after FLAG purification. All samples were digested with trypsin and the resulting peptides loaded and separated on a high-performance liquid chromatography (HPLC) system directly coupled to an LTQ OrbitrapXL mass spectrometer

recording the peptide masses. By MSMS ion search with engine Mascot connected to database Ensembl, the aligned peptide profiles resulted in identification of the proteins. Scaffold software was used to analyse the result files from Mascot.

2.5. IMMUNOASSAYS

2.5.1. Dot Blot Analysis

Prior to using antibodies, the binding capability of individual monoclonal antibodies was screened by dot blot analysis carried out at room temperature. For marking the area of the PVDF membrane, that 2-3 µl of the antigen (wildtype OLFML2B collected from the supernatant of transiently transfected HEK293 cells) was applied to, a circle has been drawn with a pencil. Afterwards, the membrane was air dried for one hour and washed with PBS three times for 5 min. Blocking of the membrane was done with 2% FBS in PBS for one hour under rotation. Since each spot was treated with different antibodies, the membrane has been cut according to the marked circles and each spot transferred in one well of a cell culture plate, where 30 µl of the primary antibody were added to each well and incubated for one hour under agitation. After three more washing steps with PBS for 5 min, 30 µl of the secondary subclass-specific antibody was applied in a dilution of 1:1,000 and the plate was incubated for one hour under agitation before the wells were washed again five times with PBS for 5 min. The membrane was then incubated with 30 µl of the substrate TMB (3,3',5,5'-Tetramethylbenzidin) for 40 min and digitalized. For stopping the reaction, ddH_2O was rinsed over the membrane. After air drying, the membrane was photographed again.

2.5.2. Enzyme-linked Immunosorbent Assay

For generation of a biomarker, that can be used to quantify circulating OLFML2B protein in plasma or serum of affected patients, a sandwich enzyme-linked immunosorbent assay (ELISA) was developed and the following protocol established: 96-well microtiter plates were coated with 5 µg/ml purified capture antibody diluted in carbon buffer and incubated overnight at room temperature. After washing with PBS, the wells were incubated for 20 min with 2% FBS in PBS to block unspecific antibody binding and washed with PBS again. For validation purposes, the supernatant of un-starved HEK293 cells transiently transfected with OLFML2B wildtype was used as antigen in a series of dilution starting with application of 100 µl in the first row, which has been diluted 1:10 in 5% skim milk powder in PBS. After thorough resuspension, 50 µl of the solution were transferred to the next column already containing 50 µl of 5% skim milk powder in PBS. This procedure was applied until the end of the microtiter plate, where 50 µl were discarded from all wells of the last row. Before washing with PBS, the antigen needed to be incubated for 20 min. Adding the biotinylated detection antibody in a dilution of 1:1,000 was followed by 20 min incubation at room temperature, one more washing step with PBS and treatment with avidin in a dilution of 1:4,000. After application of 50 µl TMB per well serving as substrate, the colorimetric enzymatic reaction began and the wells started changing their colour into blue. For stopping

the reaction as soon as the negative control turned blue, 50 µl 2 M sulfuric acid was added to each well. Turning the colour into yellow, the absorbance was measured at 450 nm and the OD was read for each well with a microplate reader. The best antibody combinations for the sandwich ELISAs detecting OLFML2B are shown Table 26.

IV. RESULTS

1. CHARACTERIZATION OF THE OLFML2B PROTEIN

1.1. VALIDATION OF MONOCLONAL ANTIBODIES

To detect OLFML2B protein, specific Hybridoma cell line antibodies (*III. Material and Methods, chapter 1.5. Antibodies*) were validated for different areas of use (Western blot analysis or immunoassay). For this purpose, HEK293 cells were transiently transfected with OLFML2B and cultivated at 37°C followed by purification of the protein, SDS-PAGE and Western blot analysis (Figure 10).

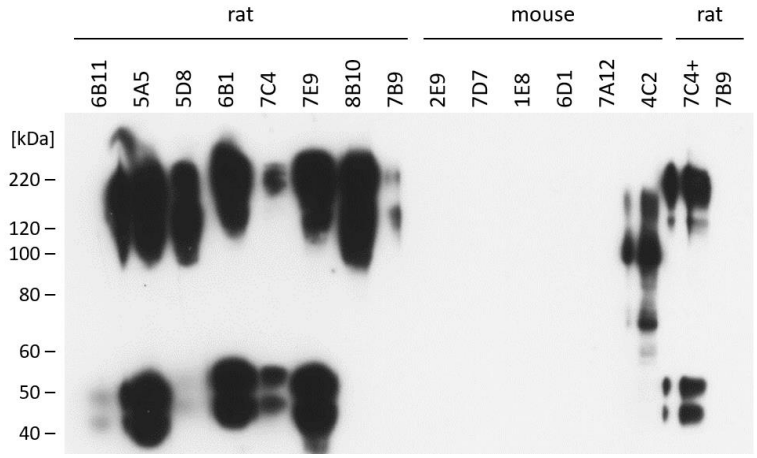

Figure 10: Validation of different primary antibodies from Hybridoma cell lines for detection of recombinant OLFML2B protein expression by Western blot analysis.

The best results for Western blot analysis were achieved by combination of the two custom-made rat anti-human OLFML2B monoclonal primary antibodies 7C4 (IgG2a) against peptide OLF1 (aa 28 to 48) and 7B9 (IgG2c) against peptide OLF2 (aa 197 to 214), which were both raised against the n-terminus of OLFML2B, followed by treatment with the commercial secondary antibody goat anti-rat HRP conjugated (Figure 10, lane 15).

The exemplary Western blot above was generated using extracellular OLFML2B protein gained from cell supernatant as described in *III. Material and Methods, chapter 2.3.1 ISOLATION OF PROTEIN FROM HEK293 CELLS*. Within this blot, the band at 120 kDa presumably represents the glycosylated monomer of OLFML2B with a mass gain of 36 kDa due to glycosylation compared to the unglycosylated monomer of 84 kDa (https://www.genecards.org/cgi-bin/carddisp.pl?gene=OLFML2B&keywords=olfml2b website accessed on April 25th, 2020), while the signal at 220 kDa probably shows the incompletely glycosylated dimer, changing the protein's structure by building disulphide bonds like other members of the OLF protein family. Another lane at around 40 kDa and 50 kDa points to cleaved fragments; the protein product at 50 kDa was later identified as n-terminal part of the OLFML2B protein by LC-MSMS (*IV. Results, chapter 3. Proteomics of OLFML2B by LC-MSMS*).

1.2. Intracellular Presence of Wildtype and 23 Mutant Proteins

After investigating several patient cohorts for potentially pathogenic *OLFML2B* variants, 23 missense variants were chosen in addition to the wildtype for functional characterization (Table 21).

Table 21: 23 analysed *OLFML2B* variants and wildtype showing source, patient's disease and predicted phenotype according to MutationTaster (Schwarz et al., 2010) and SIFT (Sim et al., 2012).

PROTEIN VARIANT			ORIGIN FROM PATIENT WITH	MUTATIONTASTER	SIFT
PROTEIN	CDNA	GENOME (HG19)			
Wildtype		-	Common	-	-
A12S	c.34C>A	1-161993187-C-A	DCM	Polymorphism	Tolerated
V15G	c.44T>G	1-161993177-A-C	AF	Polymorphism	Damaging
R86W	c.256C>T	1-161989891-G-A	LQT	Disease causing	Damaging
S113L	c.338C>T	1-161989809-G-A	LQT	Polymorphism	Damaging
T149A	c.445A>G	1-161987291-T-C	LQT	Disease causing	Tolerated
L269P	c.806T>C	1-161970046-A-G	Common	Polymorphism	Tolerated
P289L	c.866C>T	1-161969986-G-A	Common	Polymorphism	Tolerated
R347W	c.1039G>A	1-161968050-G-A	LQT	Polymorphism	Damaging
R353H	c.1058G>A	1-161968031-C-T	LQT	Polymorphism	Tolerated
R367W	c.1099C>T	1-161967990-G-A	AF	Polymorphism	Damaging
S379L	c.1136C>T	1-161967953-G-A	DCM	Polymorphism	Damaging
S384R	c.1152C>G	1-161967937-G-C	LQT	Polymorphism	Damaging
A436S	c.1306G>T	1-161967783-C-A	AF	Polymorphism	Tolerated
T456I	c.1367C>T	1-161967722-G-A	DCM	Polymorphism	Damaging
W470R	c.1408T>C	1-161967681-A-G	Common	Polymorphism	Tolerated
P504L	c.1512G>T	1-161954734-G-A	SIDS	Disease causing	Damaging
G515E	c.1544G>A	1-161954701-C-T	SIDS	Disease causing	Damaging
R527Q	c.1580G>A	1-161954665-C-T	LQT	Disease causing	Damaging
G536S	c.1606G>A	1-161954639-C-T	SIDS	Disease causing	Damaging
Y557H	c.1669T>C	1-161954049-A-G	SIDS	Disease causing	Tolerated
V604M	c.1810G>A	1-161953908-C-T	DCM	Disease causing	Damaging
G674D	c.2021G>A	1-161953697-C-T	SIDS	Disease causing	Damaging
N690S	c.2069A>G	1-161953649-T-C	AF	Disease causing	Tolerated

Out of these, 20 variants had been selected due to their in-silico prediction to negatively affect protein structure and function (MutationTaster, SIFT) and three variants for their high frequency at the population level as controls in addition to the wildtype.

All variants were tested for their intracellular presence by overexpression of recombinant OLFML2B protein in HEK293 cells and visualized by SDS-PAGE and Western blotting. The results showed equal levels of cytosolic OLFML2B protein for all investigated variants. An exemplary Western blot is included as Figure 11 showing wildtype (Wt) and variants c.1512G>T (P504L), c.1544G>A (G515E), c.1669T>C (Y557H), c.1580G>A (R527Q).

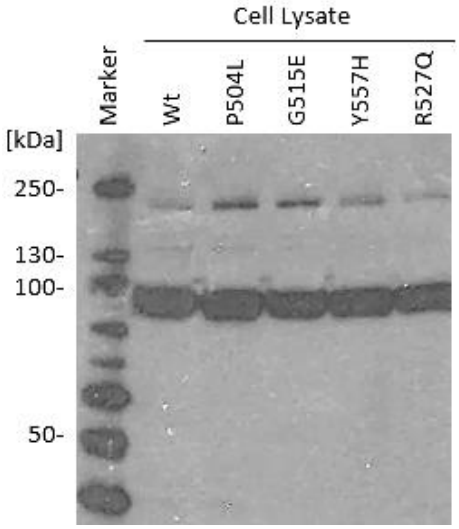

Figure 11: Intracellular levels of OLFML2B protein after transient transfection of HEK293 cells with Wt and variants c.1512G>T (P504L), c.1544G>A (G515E), c.1669T>C (Y557H), c.1580G>A (R527Q).

1.3. In-silico Modelling of the Structure

To predict the structure of the olfactomedin domain (aa 493 to aa 750) within the c-terminal region of OLFML2B, the amino acid sequence was modelled by Swissmodel and complemented with the investigated SIDS variants c.1512G>T (P504L), c.1544G>A (G515E), c.1606G>A (G536S), c.1669T>C (Y557H) and c.2021G>A (G674D) as shown in Figure 12. This model predicts a 5-bladed beta propeller structure for the c-terminus based on the structure of Olfactomedin 1 and a negatively charged patch at the centre, which suggests the presence of a calcium binding site in the core of the protein.

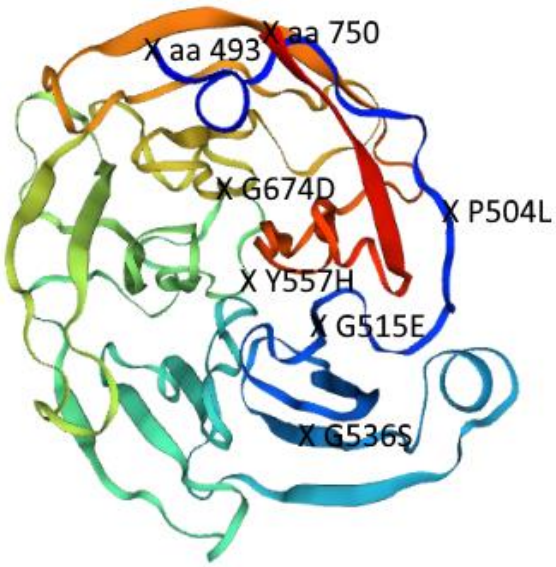

Figure 12: Modelling of OLFML2B c-terminal region (https://swissmodel.expasy.org/interactive/SQLUpV/models/ website accessed on March 10th, 2019) from aa 493 (n-terminal region of c-terminus) to aa 750 (c-terminal region of c-terminus) including SIDS variants.

1.4. Structural Changes

To test this prediction, varying concentrations of magnesium chloride ($MgCl_2$) or calcium chloride ($CaCl_2$) were added during different cell culture steps and signs indicative of structural changes of the OLFML2B protein were recorded. While $MgCl_2$ seemed to have no or only very moderate effects on the wildtype OLFML2B protein, the addition of $CaCl_2$ to the cell lysate shifted the visualized bands on the Western blot to a higher molecular weight of around 220 kDa (Figure 13).

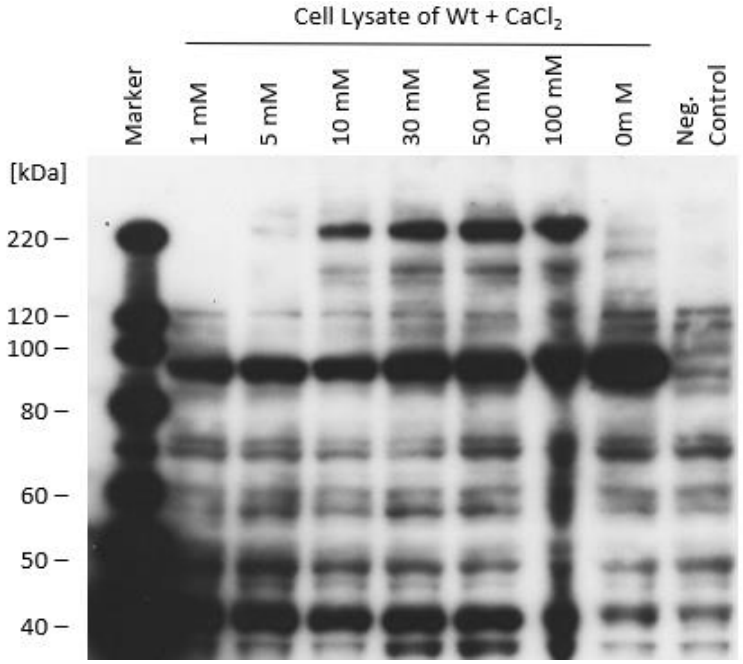

Figure 13: Western blot analysis visualizing the effect of adding $CaCl_2$ to the cell lysate of HEK293 cells transfected with Wt OLFML2B.

The lane at 220 kDa probably represents the incompletely glycosylated dimer of the OLFML2B protein, suggesting an oligomerization of the intracellular protein from a molarity of 3 mM on. Furthermore, a second band at around 38 kDa appeared to be thicker with increasing $CaCl_2$ concentrations, pointing to a potential secondary product of the protein cleaving and re-bonding.

This effect was also tested on mutant OLFML2B protein, which led to similar results. Even variants typically showing no secretion at all like c.1544G>A (G515E) were able to form higher intracellular oligomers under the influence of $CaCl_2$ (Figure 14).

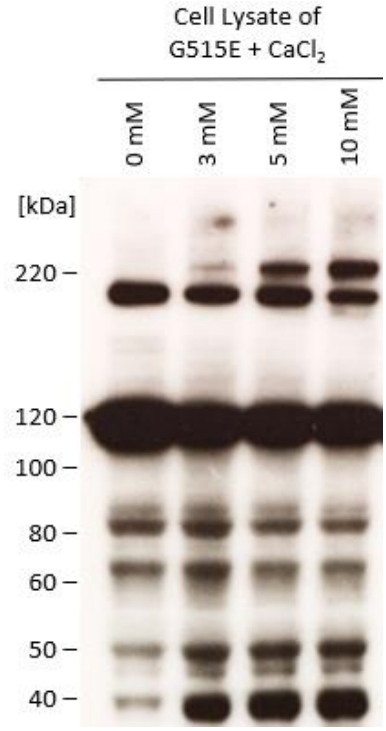

Figure 14: Western blot analysis visualizing the effect of adding $CaCl_2$ to the cell lysate of HEK293 cells transfected with mutant OLFML2B c.1544G>A (G515E).

1.5. Secretional Behaviour

When comparing the intracellular to the extracellular signal of the OLFML2B protein, a shift of the protein size is observed. While the intracellular protein appears at sizes of 84 kDa and 220 kDa, the extracellular protein shows bands at 50 kDa corresponding to the n-terminal fragment and at 120 kDa probably representing the glycosylated monomer as discussed in *IV. Results, chapter 1. Characterization of the OLFML2B Protein*.

While cytosolic protein levels were indistinguishable, signals of secreted OLFML2B varied strongly by protein variant. The secretion ranged between increased levels of secretion compared to the wildtype, a secretion similar to the wildtype, a mild reduction up to a complete absence of secretion. An exemplary Western blot is included as Figure 15.

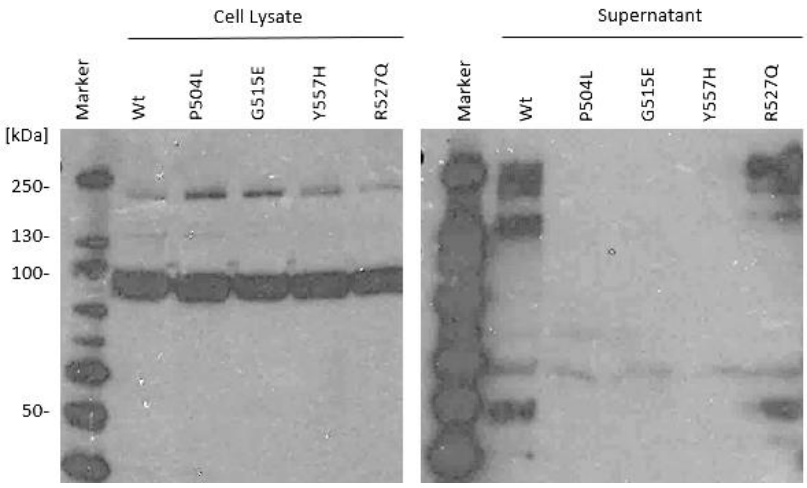

Figure 15: Secretion of Wt and mutant OLFML2B variants c.1512G>T (P504L), c.1544G>A (G515E), c.1669T>C (Y557H) and c.1580G>A (R527Q).

In Western blot analysis, the three common variants c.806T>C (L269P, minor allele frequency (MAF) 1.0%), c.866C>T (P289L, MAF 3.5%) and c.1408T>C (W470R, MAF 34%) showed a secretional behaviour that was only marginally different from the wildtype. Five rare variants from SIDS patients c.1512G>T (P504L), c.1544G>A (G515E), c.1606G>A (G536S), c.1669T>C (Y557H) and c.2021G>A (G674D) led to the secretion of none or only very little protein (≤10% of the wildtype) into the extracellular space. The variant c.1810G>A (V604M) seen in a patient with DCM on the other hand showed a secretion twice as high as the wildtype. A detailed overview about the different secretional behaviour of all investigated variants is given in Table 22.

Table 22: 23 analysed OLFML2B variants and Wt showing source, patient's disease and amount of secretion at 37°C.

PROTEIN VARIANT			ORIGIN FROM PATIENT WITH	SECRETION COMPARED TO WT AT 37°C
PROTEIN	CDNA	GENOME (HG19)		
Wildtype		-	Common	1.00
A12S	c.34C>A	1-161993187-C-A	DCM	0.32
V15G	c.44T>G	1-161993177-A-C	AF	0.86
R86W	c.256C>T	1-161989891-G-A	LQT	0.78
S113L	c.338C>T	1-161989809-G-A	LQT	0.63
T149A	c.445A>G	1-161987291-T-C	LQT	0.49
L269P	c.806T>C	1-161970046-A-G	Common	0.38
P289L	c.866C>T	1-161969986-G-A	Common	0.66
R347W	c.1039G>A	1-161968050-G-A	LQT	0.85
R353H	c.1058G>A	1-161968031-C-T	LQT	1.01
R367W	c.1099C>T	1-161967990-G-A	AF	1.03

PROTEIN VARIANT			ORIGIN FROM PATIENT WITH	SECRETION COMPARED TO WT AT 37°C
PROTEIN	**CDNA**	**GENOME (HG19)**		
S379L	c.1136C>T	1-161967953-G-A	DCM	0.69
S384R	c.1152C>G	1-161967937-G-C	LQT	0.36
A436S	c.1306G>T	1-161967783-C-A	AF	0.83
T456I	c.1367C>T	1-161967722-G-A	DCM	0.54
W470R	c.1408T>C	1-161967681-A-G	Common	0.58
P504L	c.1512G>T	1-161954734-G-A	SIDS	0.01
G515E	c.1544G>A	1-161954701-C-T	SIDS	0.02
R527Q	c.1580G>A	1-161954665-C-T	LQT	0.75
G536S	c.1606G>A	1-161954639-C-T	SIDS	0.00
Y557H	c.1669T>C	1-161954049-A-G	SIDS	0.10
V604M	c.1810G>A	1-161953908-C-T	DCM	2.03
G674D	c.2021G>A	1-161953697-C-T	SIDS	0.00
N690S	c.2069A>G	1-161953649-T-C	AF	0.37

1.6. Dominant Effect

By definition, dominant disease-causing mutations produce protein variants that interfere with the function of the wildtype counterpart, exerting a dominant-negative effect impeding normal protein function and as such defining the functional phenotype (Strachan and Read, 2011). To mimic the heterozygous situation, in which the cell has one mutant and one normally functioning allele complying with the prerequisite for any dominant effect, HEK293 cells were transiently transfected with both wildtype and mutant OLFML2B plasmids at the same time in several different ratios. As seen before, the intracellular levels of OLFML2B protein appear similar while the secreted protein levels differ. When focussing on the combined expression of wildtype and mutant protein, the Western blot of the supernatant solely shows the phenotype of the mutant OLFML2B protein demonstrating the dominant effect of the mutant protein on the wildtype.

For this effect to occur, the secretional nature of the variant seems to be irrelevant as both the only observed over-secreter protein c.1810G>A (V604M) as well as non-secreter protein c.1544G>A (G515E) impose their specific impact on the wildtype protein. Instead of a codominant phenotype showing an intermediate secretion of the protein, secretion is completely suppressed when combining 0.5 µg wildtype plasmid with 0.25 µg plasmid of variant c.1544G>A (G515E) in one cell. The inverse applies for mixing 0.5 µg wildtype plasmid with 0.25 µg plasmid of variant c.1810G>A (V604M), showing a signal as high as in cells only transfected with 0.5 µg c.1810G>A (V604M) plasmid. Taken together, the mutant protein's

signal not only covers the wildtype's signal at equal amounts of plasmid but also when adding twice as much wildtype plasmid to the cells (Figure 16) indicating a dominant-positive (V604M) or a dominant-negative effect (G515E) of the investigated mutant proteins on the wildtype.

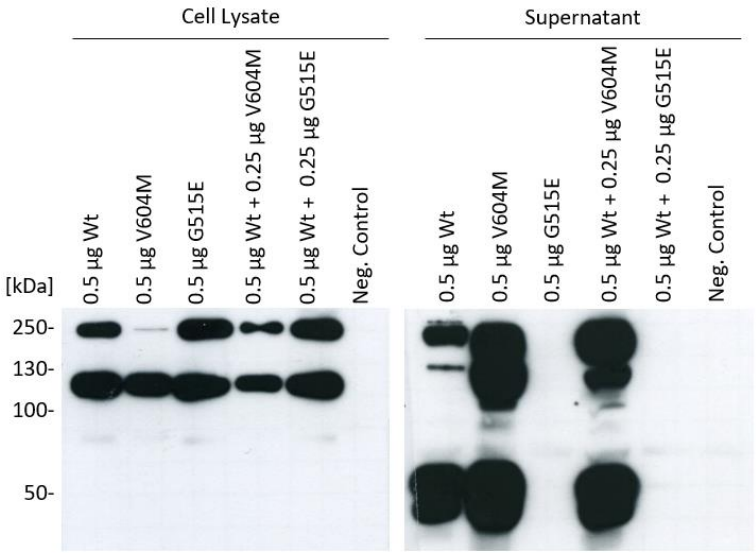

Figure 16: Dominant-positive and dominant-negative effect caused by different concentrations of mutant OLFML2B proteins c.1810G>A (V604M) and c.1544G>A (G515E) on secretion of the Wt into the extracellular space.

1.7. Temperature-Dependent Secretion

Protein secretion of the wildtype and all variants is strongly temperature dependent. As expected for the wildtype as well as for most of the secreted variants, protein secretion was strongest at 30°C followed by 37°C and by 41°C (Figure 17).

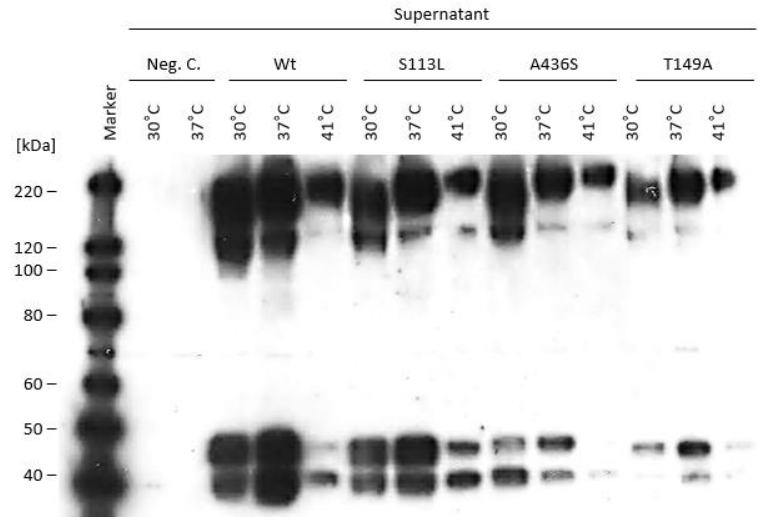

Figure 17: Western blot of temperature-dependent secretion showing the Wt as reference, un-transfected HEK293 cells as negative control and variants with wildtype-like phenotype: c.338C>T (S113L), c.1306G>T (A436S) and c.445A>G (T149A).

However, some variants deviated from the expected pattern (Figure 18).

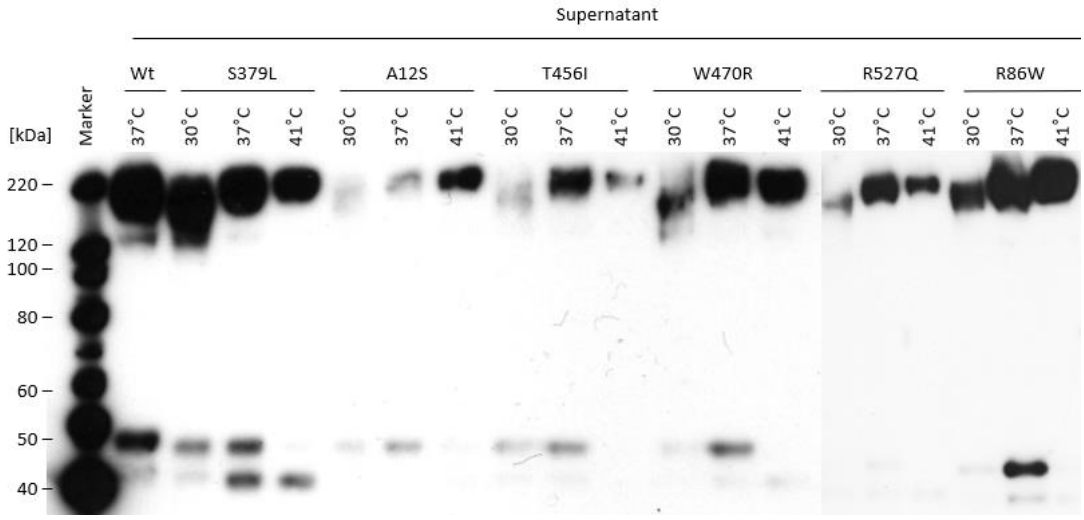

Figure 18: Western blot of temperature-dependent secretion showing the Wt at 37°C plus the wildtype-like secreter c.1136C>T (S379L) as reference and variants with unlikely phenotype: c.34C>A (A12S), c.1367C>T (T456I), c.1408T>C (W470R), c.1580G>A (R527Q) and c.256C>T (R86W).

The six variants c.1152C>G (S384R), c.1367C>T (T456I), c.1408T>C (W470R), c.1580G>A (R527Q), c.1810G>A (V604M) and c.2069A>G (N690S) showed the strongest degree of secretion at 37°C and the two variants c.34C>A (A12S) and c.256C>T (R86W) even at 41°C. The degree of temperature dependent deviation of secretion from the reference at 37°C varied from average values in the wildtype (30°C: +12%, 41°C: -33%) to very low values as observed e.g. with c.1058G>A (R353H, 30°C: +2%, 41°C: -7%) and high values as especially seen at lowly secreted variants e.g. c.1669T>C (Y557H, 30°C: +200%, 41°C: no secretion).

The four rare variants c.1512G>T (P504L), c.1544G>A (G515E), c.1606G>A (G536S) and c.2021G>A (G674D), with MAFs between 0% and 0.02% at the population level were all from SIDS patients and secreted no or only very little protein (≤1% of the wildtype at 37°C) into the extracellular space (Figure 19).

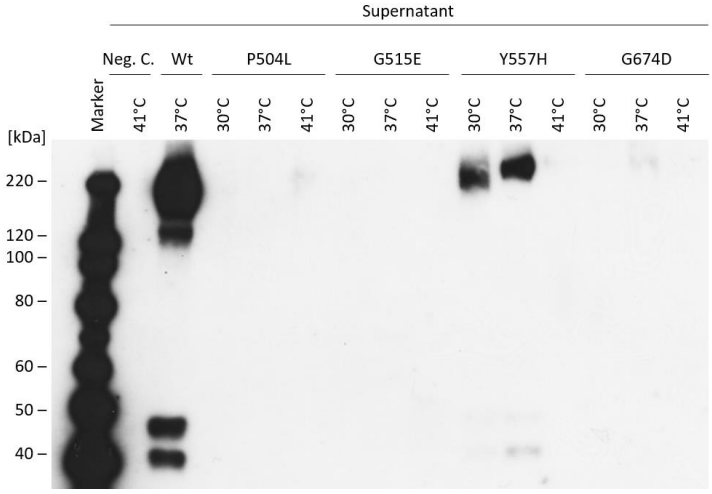

Figure 19: Western blot of temperature-dependent secretion showing the Wt at 37°C as reference, un-transfected HEK293 cells as negative control and variants with low or no secretion: c.1512G>T (P504L), c.1544G>A (G515E), c.1669T>C (Y557H) and c.2021G>A (G674D).

A detailed overview showing the secretional behaviour of all investigated variants as well as allele numbers and frequencies is given in Table 23.

Table 23: 23 analysed OLFML2B variants and Wt showing source, patient's disease, amount of secretion at different temperatures as well as allele numbers and frequencies according to gnomAD (https://gnomad.broadinstitute.org/gene/ENSG00000162745 website accessed on April 20th, 2019).

PROTEIN VARIANT			ORIGIN FROM PATIENT WITH	SECRETION COMPARED TO WT AT 37°C			GNOMAD			
CDNA	PROTEIN	GENOME (HG19)		30°C	37°C	41°C	TOTAL ALLELE NUMBER	VARIANT ALLELE COUNT	HOMO-ZYGOTES	VARIANT ALLELE FREQUENCY
Wildtype		-	Common	1.12	1.00	0.67	-	-	-	-
A12S	c.34C>A	1-161993187-C-A	DCM	0.05	0.32	0.44	269,664	69	0	0.0256 %
V15G	c.44T>G	1-161993177-A-C	AF	1.00	0.86	0.69	243,952	2	0	0.0008 %
R86W	c.256C>T	1-161989891-G-A	LQT	0.61	0.78	0.98	282,860	377	1	0.1333 %
S113L	c.338C>T	1-161989809-G-A	LQT	0.65	0.63	0.45	282,880	33	0	0.0117 %
T149A	c.445A>G	1-161987291-T-C	LQT	0.76	0.49	0.11	277,902	193	0	0.0695 %
L269P	c.806T>C	1-161970046-A-G	Common	0.49	0.38	0.28	282,808	2,785	47	0.9848 %
P289L	c.866C>T	1-161969986-G-A	Common	0.76	0.66	0.35	282,090	9,737	248	3.4520 %
R347W	c.1039G>A	1-161968050-G-A	LQT	0.95	0.85	0.35	250,460	1	0	0.0004 %
R353H	c.1058G>A	1-161968031-C-T	LQT	1.03	1.01	0.94	282,446	22	0	0.0078 %
R367W	c.1099C>T	1-161967990-G-A	AF	1.08	1.03	0.42	282,762	492	6	0.1740 %
S379L	c.1136C>T	1-161967953-G-A	DCM	0.94	0.69	0.47	282,828	48	0	0.0170 %
S384R	c.1152C>G	1-161967937-G-C	LQT	0.22	0.36	0.33	282,802	715	11	0.2528 %
A436S	c.1306G>T	1-161967783-C-A	AF	0.97	0.83	0.73	251,350	1	0	0.0004 %
T456I	c.1367C>T	1-161967722-G-A	DCM	0.32	0.54	0.18	282,872	117	1	0.0414 %
W470R	c.1408T>C	1-161967681-A-G	Common	0.42	0.58	0.52	282,612	186,479	61,811	65.98 %
P504L	c.1512G>T	1-161954734-G-A	SIDS	0.03	0.01	0.01	250,558	30	0	0.0120 %
G515E	c.1544G>A	1-161954701-C-T	SIDS	0.03	0.02	0.00	251,458	0	0	0 %
R527Q	c.1580G>A	1-161954665-C-T	LQT	0.40	0.75	0.21	251,462	8	0	0.0032 %
G536S	c.1606G>A	1-161954639-C-T	SIDS	0.00	0.00	0.00	282,700	42	0	0.0149 %
Y557H	c.1669T>C	1-161954049-A-G	SIDS	0.30	0.10	0.00	204,916	150	1	0.0732 %
V604M	c.1810G>A	1-161953908-C-T	DCM	1.65	2.03	1.81	248,176	1	0	0.0004 %
G674D	c.2021G>A	1-161953697-C-T	SIDS	0.00	0.00	0.00	251,480	0	0	0 %
N690S	c.2069A>G	1-161953649-T-C	AF	0.30	0.37	0.27	251,494	3	0	0.0012 %

The degree of secretion of wildtype or mutant OLFML2B protein correlates strongly with the corresponding variant allele frequency of these variants at the population level. Rarer

variants tend to have a highly impaired secretion while common variants had only moderately decreased secretion patterns or behaved similar to the wildtype. A visual depiction of the correlation between the variant's allele frequency and their protein secretion is given in Figure 20.

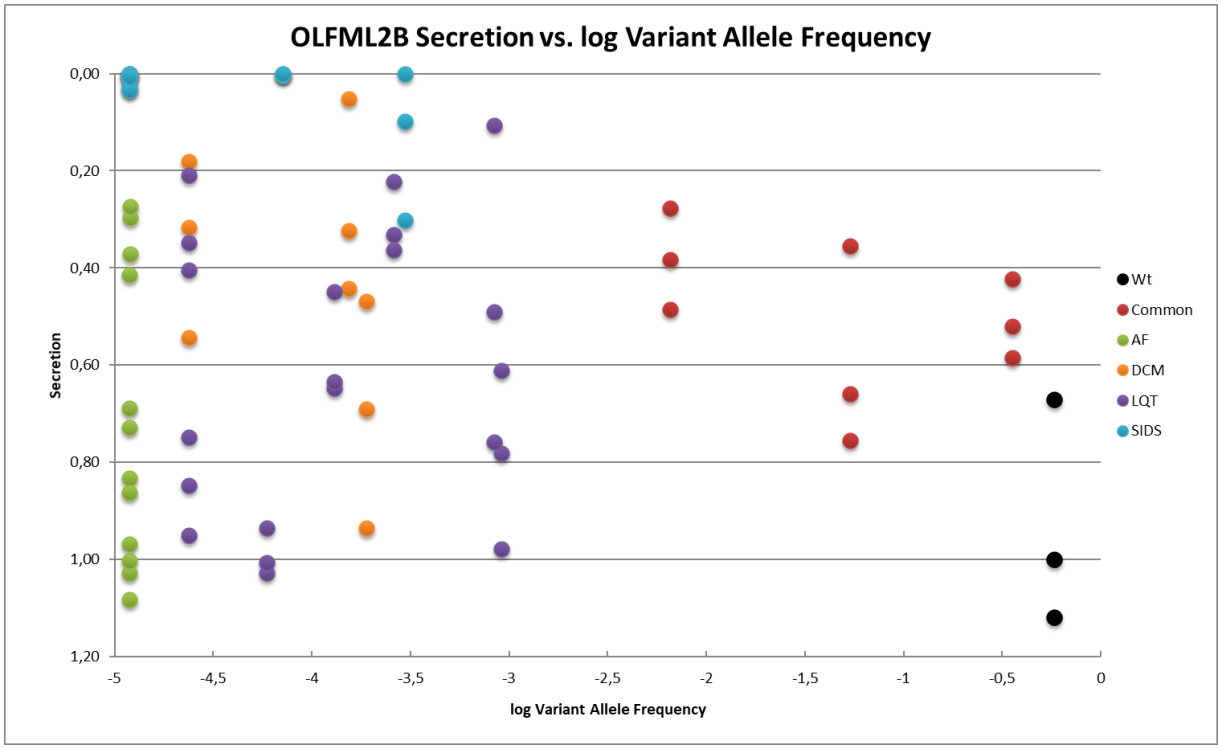

Figure 20: Plot of secretion vs. variant allele frequency (logarithmized) for the temperatures 30°C, 37°C and 41°C showing the correlated diseases atrial fibrillation (AF), dilated cardiomyopathy (DCM), long-QT syndrome (LQT) and sudden infant death syndrome (SIDS) as well as wildtype (Wt) and common variants. The plot reveals the correlation of effect size with allele frequency and especially the absence of common variants showing poor secretion within the general population.

Furthermore, secretion of any disease relevant mutation was highly correlated with the disease severity from which it originated (wildtype > DCM & AF > LQT > SIDS). All of the five variants identified in children with SIDS c.1512G>T (P504L), c.1544G>A (G515E), c.1606G>A (G536S) and c.2021G>A (G674D) were among the lowest secreted variants (≤3% of wildtype secretion at any investigated temperature) with the only exception of c.1669T>C (Y557H), which was also the most common of the five at the population level showing a secretion of 30% of the wildtype at 30°C and 10% of the wildtype at 37°C.

2. Detection of OLFML2B in Human Heart Tissue

To test the cardiac expression of native OLFML2B protein, human heart tissue from the left ventricle was grinded, lysed and visualized by Western blot. Compared to lysate of HEK293 cells transfected with OLFML2B wildtype and detected with different primary antibodies, each of the samples shows clear lanes of OLFML2B protein (Figure 21).

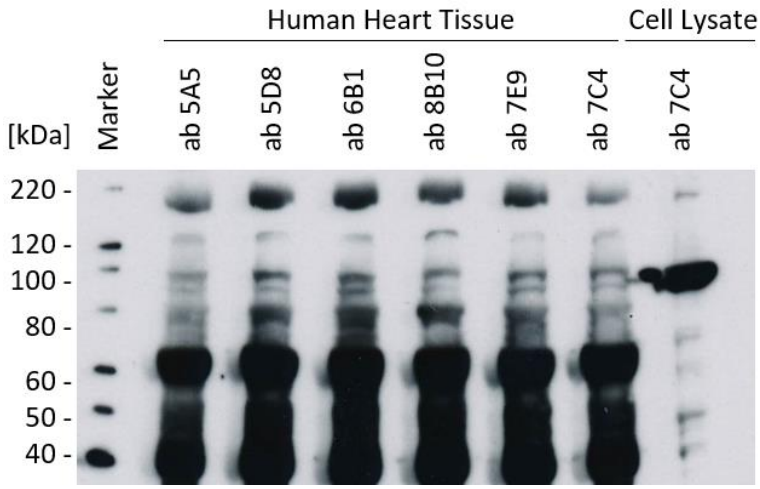

Figure 21: Western blot showing human heart tissue and lysate of HEK293 cells transfected with OLFML2B Wt analysed with different primary abs.

While the lanes at 220 kDa presumably represent the incompletely glycosylated dimer of the OLFML2B protein and are strongly visible in the samples of human heart tissue, the band appears weaker in the cell lysate. In contrast, there is more glycosylated monomer at 120 kDa in the cell lysate suggesting that the endogenous OLFML2B protein exists rather in dimerized conformity or is bound to other proteins. Protein signals below the 84 kDa monomer are most likely produced by cleaving with different states of glycosylation and length. This pattern of cardiac OLFML2B protein resembles the appearance of the secreted OLFML2B protein, indicating that endogenous OLFML2B protein presumably remains mostly in the extracellular space.

3. Proteomics of OLFML2B by LC-MSMS

Label-free LC-MSMS-based comparative proteomics was performed to validate the monoclonal antibodies for their specific binding to the OLFML2B protein, to map the epitopes and to identify which parts of the wildtype or mutant protein are secreted into the supernatant or are retained within the cell, respectively. Analysis of HEK293 cells transiently transfected with the wildtype and un-transfected HEK293 cells serving as controls allowed to ascertain the binding of all applied primary antibodies to the n-terminal region of the OLFML2B protein.

LC-MSMS also identified the cleaved 50 kDa fragment in the supernatant visible by Western blotting as n-terminal part of the OLFML2B protein.

In addition, analysis of the wildtype plus variants c.1580G>A (R257Q), c.1058G>A (R353H), c.1544G>A (G515E), c.1669T>C (Y557H) and c.1810G>A (V604M) by LC-MSMS enabled the identification of more than 300 possible protein-protein interaction (PPI) partners of the OLFML2B protein. After cleaning up the potential interaction partners by excluding proteins with ≤1 peptide identified, proteins known to be contaminants (Keller et al., 2008; Hodge et al., 2013) and proteins showing high abundance in the control sample (un-transfected HEK293 cells), the remaining candidates were functionally analysed by using the website

GeneCards (https://www.genecards.org/ website accessed on Dec 25th, 2019) and summarized in Table 24 (intracellular PPI partners) and Table 25 (extracellular PPI partners).

Table 24: Most likely protein-protein interaction partners in the cell lysate.

SYMBOL	UNIPROTKB	PROTEIN NAME	PROTEIN FUNCTION
FAF2	Q96CS3	Fas associated factor family member 2	Endoplasmic reticulum-associated degradation
RPS21	P63220	Ribosomal protein S21	Ribosomal protein
DNAJB11	Q9UBS4	DnaJ (Hsp40) homolog, subfamily B, member 11	Co-chaperone for HSPA5, required for proper folding, trafficking or degradation of proteins
BAG2	O95816	BCL2-associated athanogene 2	Nucleotide-exchange factor promoting the release of ADP from the HSP70 and HSC70 proteins
TNC	P24821	Tenascin C	ECM-protein; guidance of migrating neurons as well as axons during development, synaptic plasticity, and neuronal regeneration

Table 25: Most likely protein-protein interaction partners in the supernatant.

SYMBOL	UNIPROTKB	PROTEIN NAME	PROTEIN FUNCTION
NANS	Q9NR45	N-acetylneuraminic acid synthase	Biosynthetic pathway of sialic acid
CLU	P10909	Clusterin	Secreted chaperone
MFAP2	P55001	Microfibrillar-associated protein 2	Component of the elastin-associated microfibrils
TNC	P24821	Tenascin C	ECM-protein; guidance of migrating neurons as well as axons during development, synaptic plasticity, and neuronal regeneration

Within this pool, the extracellular matrix glycoprotein Tenascin C (TNC, NM_002160.4) stood out as likely PPI partner since it was not only identified in previous experiments (Schäfer, 2012) but also confirmed in every run of this study including wildtype and mutant OLFML2B supernatant. In addition, TNC is the only protein identified in the extracellular space with a confidence score and peptide count higher than OLFML2B itself in each experiment. The TNC protein reaches a normalized abundance, that is 164.87 times higher in HEK293 cells transfected with the wildtype than in un-transfected cells. As results of proteomics point to Tenascin C as most probable interaction partner of OLFML2B, its role was further investigated in confirmatory experiments.

4. Tenascin C as Interaction Partner of OLFML2B

To investigate the concurrent presence and colocalization of OLFML2B and TNC proteins in the human heart, the method of immunoprecipitation (IP) was employed. A Western blot was generated from human cardiac tissue samples as well as commercial purified TNC as positive control. Both anti-OLFML2B and anti-TNC antibodies were used to capture protein from the tissue sample preparation and to detect it in the Western blot (Figure 22).

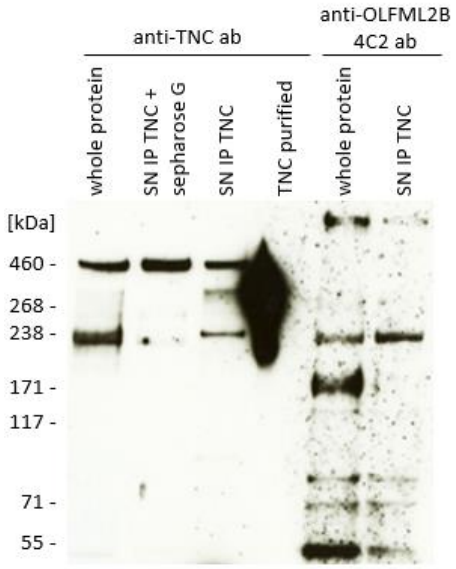

Figure 22: Western blot showing human heart tissue whole protein, supernatant (SN) IP TNC plus Protein G conjugated Sepharose beads, SN IP TNC and purified TNC as positive control, all treated with rabbit anti-TNC and goat anti-rabbit ab; in addition, whole protein and SN IP TNC were visualized by the mouse anti-OLFML2B ab 4C2 and rat anti-mouse HRP ab.

The most convincing results indicating protein-protein interaction between OLFML2B and Tenascin C were obtained, when human heart supernatant was purified using anti-TNC antibody, the purified fraction submitted to SDS-PAGE followed by detection of a 241 kDa band using the anti-OLFML2B antibody 4C2 (Figure 22, lane 6). This molecular mass matches the TNC monomer of 241 kDa (https://www.genecards.org/cgi-bin/carddisp.pl?gene= TNC& keywords=tnc website accessed on April 25th, 2020), confirming the interaction between OLFML2B and TNC in human heart tissue.

A second, similar Western blot was generated, the PVDF membrane stripped and visualized with mouse anti-TNC E-9 ab and rat anti-mouse HRP ab (Figure 23).

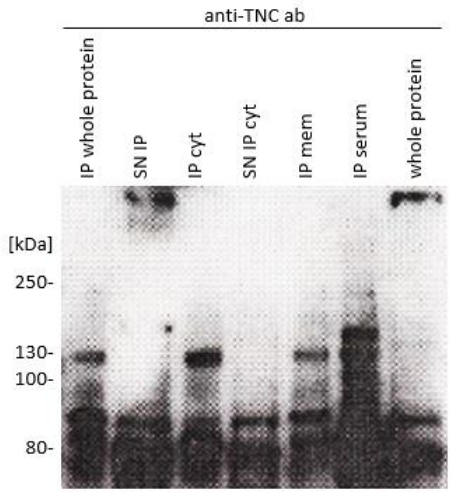

Figure 23: Western blot showing human heart tissue IP whole protein, SN IP, cytosolic fraction (IP cyt) and the respective SN (SN IP cyt), membrane/ organelle protein fraction (IP mem), IP of human serum (IP serum) and whole protein; the signal was visualized by the mouse anti-OLFML2B ab 4C2 and rat anti-mouse IgG2b HRP ab, stripped and incubated with mouse anti-TNC E-9 ab and rat anti-mouse HRP ab.

Figure 23 shows two signals, that are visible in both Western blots, the initial blot incubated with an anti-OLFML2B antibody and the stripped blot, where an anti-Tenascin C antibody was applied: the two lanes with the highest molecular weight around 500 kDa within the SN IP whole protein and the whole protein. Signals of this size could indicate protein complexes formed by the incompletely glycosylated dimer of OLFML2B (220 kDa) and the monomer of TNC (241 kDa).

5. Establishment of two Sandwich ELISAs for Soluble OLFML2B

Prior to establishing the sandwich ELISAs, the best binding capabilities of primary antibody conjugates to the desired antigen OLFML2B were evaluated by dot blot analysis. While some antibodies showed no binding at all and others nonspecific signals across the whole membrane, the monoclonal antibody 7C4 stood out giving a specific and strong signal exclusively at the spot, where the antigen was applied to (Figure 24).

Figure 24: Dot blot analysis of monoclonal hybridoma cell line antibody 7C4 from rat.

Afterwards, all antibodies were tested for their best capture/ detection antibody combinations, which not only relied on specificity and sensitivity but also on the condition that the antibodies recognize two different non-overlapping epitopes. Two of the resulting matched pairs showed robust and strong signals when tested with the cell supernatant containing wildtype OLFML2B (Table 26).

Table 26: Best antibody combinations for sandwich ELISAs detecting OLFML2B protein.

CAPTURE ANTIBODY				**DETECTION ANTIBODY**				**HRP ANTIBODY**
2E9	Mouse, monoclonal	IgG1	Fusion Peptide	**8B10 50% biotinylated**	Rat, monoclonal	IgG2a	cDNA	**Avidin**
4C2	Mouse, monoclonal	IgG2b	Fusion Peptide	**5D8 50% biotinylated**	Rat, monoclonal	IgG2a	cDNA	**Avidin**

As soon as validation with the cell supernatant was successfully completed, human serum of healthy controls was tested showing similar results.

V. DISCUSSION

1. CHARACTERIZATION OF THE OLFML2B PROTEIN

For more than a decade, Genome-wide association studies (GWAS) have been used to detect associations between genetic variants and traits. Although these associations are not directly informative regarding the causal gene(s) or the mechanism by which the variant is linked with the respective phenotype(s), the experimental design of GWAS has proven itself as a powerful tool (Visscher et al., 2017). After GWAS results pointed to both *NOS1AP* and *OLFML2B* as potential regulators of the QT interval, this study investigated the contribution of the OLFML2B protein to cardiac repolarization by functional characterization and pathophysiological evaluation of the *Olfactomedin-like 2B* gene.

First, the general potential of OLFML2B being relevant regarding cardiac physiology had to be confirmed; therefore, OLFML2B expression in the human heart was demonstrated at the protein level through visualization of OLFML2B protein by Western blot analysis.

Modelling the protein's structure predicted a five-bladed beta propeller formation, known to function as hydrolase, transferase or ligand binding protein (Chen et al., 2011), of the c-terminal olfactomedin domain and a negatively charged patch at the centre. This is in accordance with the findings among other members of the olfactomedin family, who share the olfactomedin domain. Donegan et al. (2012) for example showed that the olfactomedin domain of myocilin binds calcium in the centre of the propeller, while Han and Kursula (2015) revealed the five-bladed beta propeller structure of gliomedin, and Jackson et al. (2015) demonstrated that the olfactomedin-like domain of Latrophilin also forms a five-bladed beta propeller, recommending this structure as well as metal-binding sites for several olfactomedin domain containing proteins such as myocilin, olfactomedin-like 2A, olfactomedin-like 2B and noelins.

Investigating this model, the addition of calcium chloride ($CaCl_2$) to HEK293 cell lysate transfected with wildtype OLFML2B showed a shift of the visualized bands on the Western blot to a higher molecular weight suggesting that binding of $CaCl_2$ triggers a change into the functional conformation enabling the stabilization and oligomerization of the intracellular protein. This agrees with the observation of Maurer et al. (1996) that calcium ions may induce a profound conformational change by binding to a protein. Han and Kursula (2015) illustrated that oligomerization via neighbouring domains or disulphide bridges is a general feature of olfactomedin domains referring to the coiled-coil dimerization of myocilin and emphasizing the importance for the biological activity. It seems likely that this assumption applies to OLFML2B, a protein with a c-terminal olfactomedin domain and an n-terminal coiled-coil domain, that is known to build homo- and oligomers by disulphide-bonds (Furutani et al., 2005). If the protein changes its structure by binding calcium, the coiled-coil domain may become accessible so the protein is able to oligomerize.

As protein function is controlled by shape and charge (Clapham, 2007), point mutations within this crucial highly conserved calcium binding region could cause misfolding of OLFML2B, preventing the protein from executing its function and thereby causing diseases. The importance of variants modulating cation binding is exemplified in fibrillin, where mutations inhibiting the binding of calcium to the protein induce Marfan syndrome (Dietz and Pyeritz, 1995), or in the dwarfing condition pseudoachondroplasia provoked by variation within the calcium binding region of the cartilage oligomeric matrix protein (Hecht et al., 1995).

When looking at the investigated variants, this hypothesis appears even more plausible. All of the OLFML2B mutations from individuals with sudden infant death syndrome (SIDS), the most lethal evaluated phenotype, are located within the olfactomedin domain. Moreover, adding $CaCl_2$ to the cell lysate starting at a molarity of 3 mM facilitated the oligomerization not only of wildtype but also of mutant olfactomedin protein including variants associated with more severe disease phenotypes. On the other hand, the observed changes of the protein's degree of oligomerization were only observed in cell lysate, i.e. intracellularly, where calcium is not as abundantly available as in the extracellular space. With a ca. 20,000-fold concentration gradient between interstitium and cytosol, calcium is highly downregulated at concentrations of about 100 nM free calcium inside the cell (Clapham, 2007). Due to its various responsibilities in the extracellular space including cell-cell, cell-matrix and matrix-matrix contacts (Maurer and Hohenester, 1997), calcium reaches concentrations in the mM range in the interstitial space. This indicates a specific effect, where the protein either functions intracellularly activated by calcium triggering the conformational change and initiating the oligomerization, or where the protein is stabilized for the transport into the extracellular space, the location it is known to interact with the extracellular matrix (ECM) components heparin and chondroitin sulphate-E (Furutani et al., 2005).

However, since variant c.1544G>A (G515E) has already been shown to bind $CaCl_2$ and changing its molecular mass as a consequence, the hypothesis that mutations at the core of the 5-bladed beta propeller structure of the olfactomedin domain abolish its ability to bind cations could not be verified. A more subtle influence of such mutations on the ion-affinity of the olfactomedin domain can't be ruled out entirely though.

By comparing the disease-causing mechanisms of other members of the olfactomedin family, the similarities of OLFML2B to myocilin stand out. Myocilin is a protein, in which dominant-negative mutations have been shown to cause primary open angle glaucoma (POAG) by suppression of protein secretion (Jacobson et al., 2001). Similar secretion experiments of OLFML2B performed in this study demonstrated that wildtype and mutant proteins were detectable in cytosolic fractions at equal concentrations implicating that missense mutations do not prevent the protein from being synthesized all together as required for a dominant-negative mechanism. However, while wildtype and common variants were represented in the extracellular space, other mutants showed increased or

reduced levels of secretion up to a complete absence in the supernatant. With identical intracellular amounts of protein, the difference in the extracellular space could be caused by either different amounts of protein being transported out of the cell, or a protein formation that is stable to a greater or lesser extent in general.

The 23 investigated variants were distributed across the whole OLFML2B protein to cover most regions and domains. Given this evenly distributed and systematic evaluation of the protein, the observation stands out, that mutations having the most extreme secretional phenotype all cluster within the olfactomedin domain ranging from amino acid 493 to 750. This includes the over-secreter mutation c.1810G>A (V604M) showing a secretion twice as high as the wildtype, as well as the highly reduced secreter or non-secreter mutations c.1512G>T (P504L), c.1544G>A (G515E), c.1606G>A (G536S), c.1669T>C (Y557H) and c.2021G>A (G674D). Since the olfactomedin domain is highly conserved and harbours an internal calcium binding site as shown before, it is not surprising that mutations within this domain have such high effect sizes. As mentioned before, point mutations within calcium binding sites of ECM proteins are already known to be responsible for diseases such as Marfan syndrome, pseudoachondroplasia and haemophilia B (Winship and Dragon, 1991). Lowered or non-secretion of sufficiently misfolded proteins may be due to quality control within the endoplasmic reticulum (ER), which prevents misfolded proteins from being secreted into the extracellular space (Dobson, 2004). Processes like secretion are by now known to depend directly on folding and unfolding of the protein (Radford and Dobson, 1999) with a severe impact on living systems and seem to be the cause of many human diseases (Thomas et al., 1995; Dobson, 2001). Taken together, the susceptibility to misfolding of the OLFML2B protein could determine the pathogenicity of each variant (Dobson, 2003).

In the heterozygous state with one impaired allele due to a point mutation, the wildtype allele might still enable transportation of half the wildtype or further reduced amounts of the OLFML2B protein into the extracellular space, the protein's putative functional site. To resemble this heterozygous situation, co-expression of wildtype and mutant constructs revealed that the mutant protein determines the extracellular phenotype, irrespective of the variant's associated disease or secretional phenotype. Assuming the protein's functional site is located within the ECM, a dominant-negative effect is equivalent to a loss-of-function (LOF) phenotype for all variants suppressing protein secretion significantly, namely c.1512G>T (P504L), c.1544G>A (G515E), c.1606G>A (G536S), c.1669T>C (Y557H) and c.2021G>A (G674D). Presumably depending on a certain amount of OLFML2B protein to be functional, all other 17 variants showing reduced secretion would cause a LOF phenotype as well. As previously stated, this dominant-negative effect has also been shown for myocilin, where the LOF is supposed to cause POAG (Jacobson et al., 2001). On the other hand, variants inducing a reduced secretion could provoke an intermediate phenotype, where some of the protein reaches its functional site and the overall effect is not lost but diminished leading to an incomplete LOF. At this time, it is not possible to say which amount

of OLFML2B or any other given olfactomedin protein in the ECM is required to comply its functional task. Consequently, it is also unknown, if quantitative reduction causes LOF right away, or if a threshold model applies, where mutations causing slighter diminution above the threshold have no pathophysiological effect. This dominant effect indicates why the investigated mutations – which were all originally identified in patients with cardiac arrhythmias, cardiomyopathies or SIDS – have the potential to cause severe cardiac conditions by an autosomal-dominant mechanism as all of them have been observed in a heterozygous (monoallelic) state in these patients.

Despite of the applicable process, it could be shown that the nature of protein secretion has no effect on the amount of protein inside the cell considering the uniform and indistinguishable intracellular pattern of all studied mutants, leading to the assumption that the protein is misfolded but doesn't accumulate in the cell. This is not surprising as degradation of misfolded or damaged and therefore potentially toxic proteins by the proteasome is a common mechanism of eukaryotic cells protecting themselves against e.g. extreme temperatures (Goldberg, 2003).

These extreme cellular temperatures were imitated by repeating all secretional experiments at two additional temperatures: 30°C simulating mild hypothermia and 41°C mimicking a fever-like condition. Cell culture at overall three different temperatures showed a clear temperature dependent modification of the protein´s secretional behaviour, while the intracellular protein production did not seem to be sensitive to the temperature changes.

In the case of mutations potentially predisposing to arrhythmias and sudden infant death this is an especially interesting finding, as hyperthermia is a well-known risk factor for both diseases in the general population (Stanton, 1984). In addition, bed-sharing, another established risk factor for SIDS, is known to be not only caused by suffocation through overlaying but also by overheating (Scragg et al., 1993).

With cultivation at 30°C, the extracellular protein secretion signal generally increased up to twice or more for secreted variants compared to the signal at 37°C. At high temperatures like 41°C on the opposite, amino acid bonds are destabilized which led to an excessive decrease of protein secretion. The majority of the investigated protein species (n=11) including the wildtype and variants displayed this expected secretional pattern (Table 23). Exceptions from this general rule were the two variants c.34C>A (A12S) and c.256C>T (R86W), notably both at the n-terminal end of the protein, which had their highest secretion at 41°C; the six variants c.1152C>G (S384R), c.1367C>T (T456I), c.1408T>C (W470R), c.1580G>A (R527Q), c.1810G>A (V604M) and c.2069A>G (N690S) had their highest level of secretion at 37°C, all of them located rather in the middle of the protein; the four variants c.1512G>T (P504L), c.1544G>A (G515E), c.1606G>A (G536S) and c.2021G>A (G674D), all within the OLF domain and associated with SIDS, were not secreted at any temperature. These observations are in line with established assumptions of the facilitation of protein folding and processing when cultured with mild hypothermia (Kjaer and Ibanez, 2003; Kumar

et al., 2008; Vergara et al., 2013). They suggest that also for OLFML2B, temperature changes have a low impact on protein synthesis but a strong effect on protein folding and secretion. As these results show that increased temperature augments the effect of OLFML2B hypo- or non-secretion with the majority of the variants and especially the rare and potentially pathogenic mutants, this might offer a mechanism by which fever may precipitate cardiac arrhythmias.

Among the mutations identified in SIDS, c.1669T>C (Y557H) was the one with the highest population allele frequency (MAF 0.073%). While not being secreted at 41°C (0%) and only marginally at 37°C (10%) it showed by far the most significant rescue of secretion (30%) of any of the mutations from SIDS at 30°C. This may be the most likely explanation, why c.1669T>C (Y557H) is able to maintain a relatively high allele frequency despite its potential pathological phenotypic effects, and a reason for future genetic studies being warranted. While the cardiac observations for this female patient were mostly negative by showing a normal cardiac weight and no signs of pericarditis or myocarditis, her head was completely covered by the blanket when she was found, which is not only a clear sign for overheating or suffocation but also two of the most established risk factors for SIDS. If this initial link between variant c.1669T>C (Y557H) and hyperthermia could be confirmed, it would be the first example of a gene - environment interaction (GxE) in SIDS with the involvement of a rare rather than a common variant.

Interestingly, the secretional behaviour of OLFML2B protein variants ranging from mild impairment to no secretion at any temperature was found to be correlated with frequency of the variants at the population level and the disease severity of the patients in whom the respective mutations were identified. This striking relation indicates a mechanism of purifying selection acting on the *OLFML2B* variants over evolutionary periods, which is highly suggestive for a functional role of the pathogenic variants being selected against. In addition to this correlation, Figure 20 indicates that rare variants with large effects also hold the highest pathogenicity. This applies especially for all rare potentially pathogenic variants, which were seen in patients either exclusively or with a much lower allele frequency than in the general population.

Many researchers have observed that common variants identified by GWAS generally contribute only a relatively small amount of effect size to the associated phenotype. This has inspired them to investigate the so called “missing heritability”, the perceived gap between often high heritabilities of certain traits but only low fractions of this heritability explained by GWAS. The fact that the identification of common regulatory variants in the *OLFML2B-NOS1AP* region modifying cardiac phenotypes led us to identify rare coding variants in *OLFML2B* with strong phenotypic effects pinpoints to one of the possible strategies, namely to close the missing heritability gap by looking at both common and rare variants in a pathophysiological relevant region. This correlation is paradigmatic for population genetic results where complex genetic inheritance is explained by polygenic and oligogenic alleles, which have historically been termed leading factors (Wright, 1968).

Regarding the connection between the cellular and the clinical phenotype, a low or absent secretion of the protein plus a low or absent allele frequency of a variant in the general population both appear strongly associated with the severity of the repolarization disturbance i.e. the disease of the affected individual. As SIDS is a disease with an earlier onset than LQTS, a stronger pathophysiological impact of the respective mutation on the protein is evident.

If temperature dependent secretion of the OLFML2B wildtype protein will turn out to be pathophysiologically important even at the population level, these findings may introduce an innovative concept and novel line of research in clinical and cellular electrophysiology. This could lead to a better understanding and possibly improved future prevention of fever-induced arrhythmias.

On the other hand, the examination of the secretional status has some limitations, which are either due to the design of the study or due to the findings obtained. One limitation is that it is impossible to determine whether the correlation between the degree of non-secretion and pathogenicity of a mutant is the main pathogenic effect i.e. the extracellular absence is the main pathogenic factor, or if other potential structural effects of the protein may play an additional role. Even a secreted OLFML2B protein can be highly relevant to the disease if the mutation changes its structure enough to prevent potential ECM interaction partners from binding.

Another limitation is that by design this study can't explain the common variant – common effects observation from the initial GWAS as is mainly focused on rare nonsynonymous coding variants of *OLFML2B*. GWAS have to this date identified multiple independent regional genetic variants to modify QT interval. However, all identified variants are common (MAF>10%) and correspondingly all their effect size estimators are small (+1 to +2.5 ms QT interval length). The variants interact in a codominant (logarithmic additive) model, their mode of action is likely gene regulatory as they are located in the 50 kb intergenic region between the genes OLFML2B and NOS1AP, and as it is well established for intergenic GWAS findings, they do not allow any of the two genes to be singled out as the causal one in a pathophysiological sense.

2. Interaction Partners of the OLFML2B Protein

The search for protein-protein interaction (PPI) partners of OLFML2B by mass spectrometric analysis of the intracellular fraction identified the proteins FAF2, RPS21, DNAJB11 and BAG2 that are involved in trafficking, folding and misfolding processes within the ER. As secreted glycoprotein, OLFML2B is known to be processed by the ER so that interactions with chaperons and other proteins within this cell organelle are not unexpected. In addition, 13 peptides of Tenascin C (TNC) were identified in each experiment.

The extracellular space however showed a higher variety regarding the function of some PPI partners, e.g. NANS, which regulates the half-life of glycoproteins by synthesizing sialic acid

(Weigel and Yik, 2002), secreted ECM-proteins (CLU and MFAP2) as well as high amounts of TNC.

Out of the more than 300 proteins identified, all evidence points to Tenascin C as most likely interaction partner (*IV. Results, chapter 3. Proteomics of OLFML2B by LC-MSMS* and chapter *4. Tenascin C as Interaction Partner of OLFML2B*). With 2201 amino acids and a molecular mass of 241 kDa as monomer (https://www.genecards.org/cgi-bin/carddisp.pl?gene=TNC&keywords=tnc website accessed on April 25th, 2020), the large ECM glycoprotein TNC binds to many extracellular proteins such as soluble factors, cell surface proteins, matrix components and pathogens revealing the protein's diverse range of functions (Giblin and Midwood, 2015). The protein is widely spread throughout embryonic development but shows limited distribution in adult tissues (Midwood et al., 2016). However, Chiquet-Ehrismann and Chiquet (2003) illustrated that TNC protein expression is upregulated in adults in a spatiotemporally restricted manner during mechanical stress such as wound healing or in pathological conditions. This applies for cancer (Yoshida et al., 2015) or inflammation (Patel et al., 2011) as well as for cardiac diseases like dilated cardiomyopathy (Tamura et al., 1996; Aso et al., 2004), myocarditis (Imanaka-Yoshida et al., 2002; Morimoto et al., 2005), myocardial infarction (Imanaka-Yoshida et al., 2001; Sato et al., 2006) and myocardial hibernation (Frangogiannis et al., 2002). Even though it remains unknown if overexpression of Tenascin C represents the cause or a consequence of this cardiac remodelling (Park et al., 2017), the correlation of TNC and cardiac injuries was reproduced enough times for the protein to be recommended as reliable biomarker predicting the risk for severe heart failure and sudden death (Niebroj-Dobosz, 2012). Additionally, TNC was demonstrated to bind to neuronal voltage-gated sodium channels (Srinivasan et al., 1998). Mutations within *SCN5A* affect the alpha-subunit of sodium channels, lead to impairment of inactivation and trigger inherited long-QT syndrome type 3 (Table 1; Wang et al., 1995), progressive cardiac conduction disorder (Schott et al., 1999), Brugada syndrome (Probst et al., 2009) and sudden infant death syndrome (Wedekind et al., 2001). Consequently, if TNC would be proven to bind to cardiac sodium channels, the protein would be linked with SCD and SIDS. Taking into account that the moments of TNC expression match the phenotypes associated with OLFML2B (e.g. SIDS), the connection of both proteins and thereby the possibility of interaction becomes even more apparent. Further experiments will be necessary to establish the entire network of OLFML2B interaction partners within the ECM.

In addition to mass spectrometric analysis, the proteins OLFML2B and TNC both occurred within a sample of the same human heart, namely cardiac tissue showing arrhythmogenic right ventricular dysplasia, as visualized in the Western blot of Figure 22. While it is not surprising to find Tenascin C in an injured heart, there appears to be a direct correlation of not only locating both proteins in the same area in general but also simultaneously.

This correlation is even more emphasized in Figure 23, where both proteins have been detected two times successively in the same lane of the Western blot, suggesting a protein

complex formed by the monomer of TNC (241 kDa) and the incompletely glycosylated dimer of OLFML2B (220 kDa), which is the conformity of OLFML2B that was already proven to primarily occur in human heart tissue as seen in *IV. Results, chapter 2. Detection of OLFML2B in Human Heart Tissue*.

While the relation between those proteins seems logical regarding state-of-the-art knowledge, it so far has never been established. When searching through STRING, a database of known and predicted protein-protein interactions, most of the proposed interaction partners in Figure 25 origin from automated text mining (green lines) or from co-expression (black lines) and only three have been experimentally determined (pink lines).

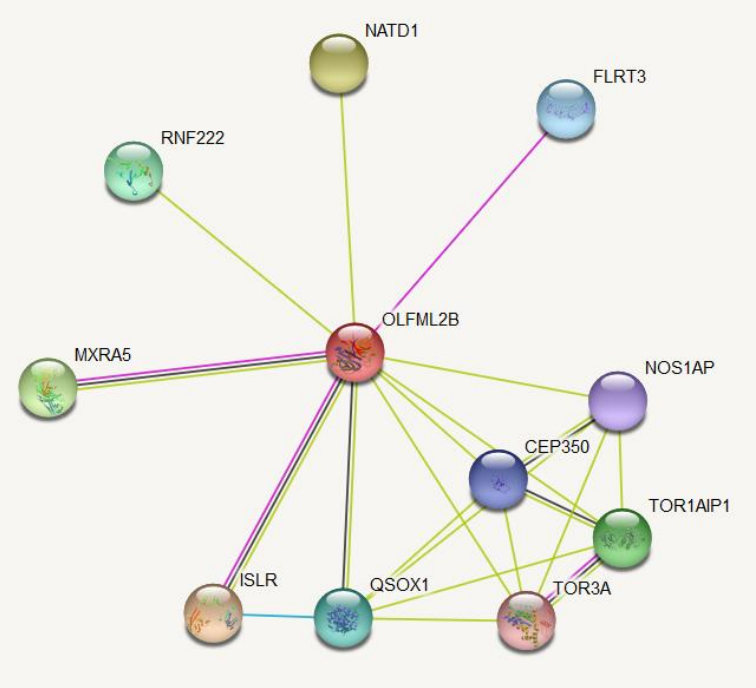

Figure 25: Predicted protein-protein interactions based on STRING (https://string-db.org/cgi/network.pl?taskId=E5mft6kaAeDh website accessed on May 26th, 2020).

These data support the hypothesis of a specific signal transduction from the cell secreting OLFML2B, which then interacts with TNC generating a complex, that executes its function on the myocardium. If the OLFML2B protein carries a missense mutation that prevents most of the protein from being secreted or changing the protein's conformation in a way that inhibits the bond with TNC, the potential signal cascade may be interrupted and the function of TNC impaired. Keeping in mind that Tenascin C is only upregulated during cardiac stress, LOF in this critical situation may be fatal.

3. Generation of a Biomarker Assay to Detect Circulating OLFML2B Protein

Current data of the World Health Organization (WHO) state that heart diseases have been the leading cause of human death in the year 2000 globally (Figure 26) and are still emerging as displayed in data from 2016 (Figure 27).

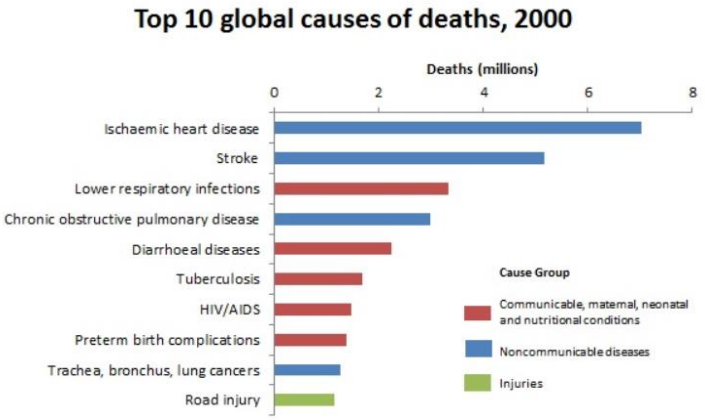

Figure 26: The top 10 causes of death in 2000 according to the WHO (https://www.who.int/news-room/fact-sheets/detail/the-top-10-causes-of-death website accessed on May 26th, 2020).

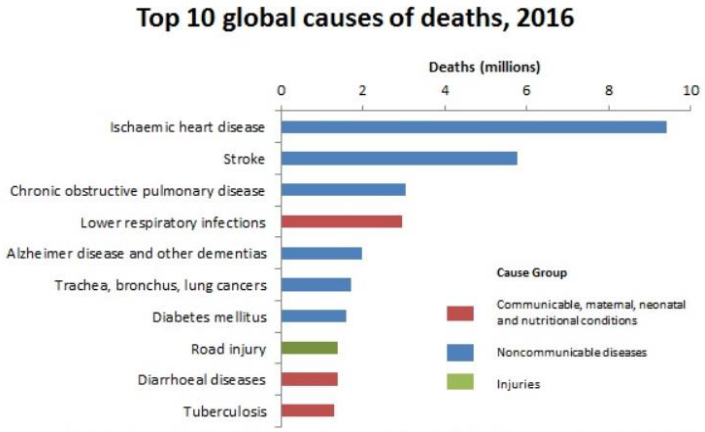

Figure 27: The top 10 causes of death in 2016 according to the WHO (https://www.who.int/news-room/fact-sheets/detail/the-top-10-causes-of-death website accessed on May 26th, 2020).

This trend becomes even more apparent when the data included in the graph are narrowed down to high-income countries like Germany, where causes of death can be determined more thoroughly (Figure 28).

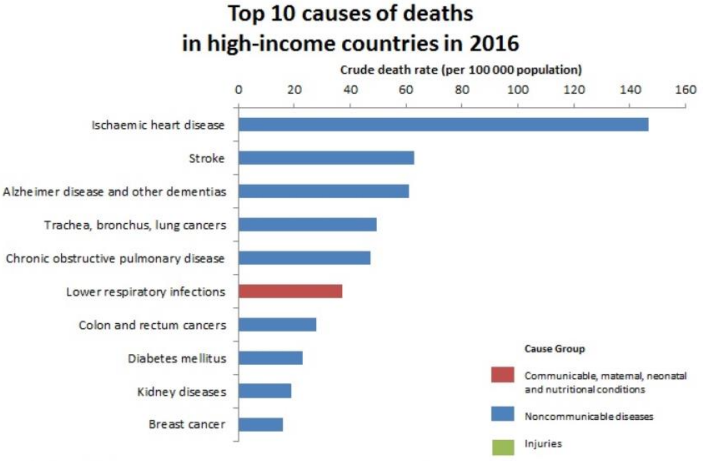

Figure 28: The top 10 causes of death in high-income countries in 2016 according to the WHO (https://www.who.int/news-room/fact-sheets/detail/the-top-10-causes-of-death website accessed on May 26th, 2020).

Though there has been a lot of progress in prevention, treatment and health care of cardiac diseases, myocardial infarction and stroke still hold about 39.7% of all deaths in Germany and are therefore the most frequent causes of death according to data collected and summarized in 2015 by the Robert Koch Institut (https://www.rki.de/EN/Content/HealthMonitoring/Health_Reporting/HealthInGermany/health_germany_node.html website accessed on May 26th, 2020).

To counteract on this major public health problem, a biomarker predicting a predisposition to cardiac arrhythmia in advance is urgently needed. Testing may not only offer a definite diagnosis to the patient, which would especially help patients with inconclusive clinical data, but also support personalized medical treatment and management.

In this thesis, the protein OLFML2B was identified as potential prognostic marker and for the first time, two sandwich ELISAs detecting the protein in cells and human serum were established. Ideally, these detection systems will be validated in whole blood not only of healthy individuals but also of patients suffering from heart disease.

While Tenascin C has been recommended by several studies as a prognostic marker for cancer (Jahkola et al., 1998; Emoto et al., 2001; Brunner et al., 2004; Ishiwata et al., 2005; Yoshida et al., 2015) or cardiac disease (Morimoto et al., 2005; Sato et al., 2006; Tsukada et al., 2009; Golledge et al., 2011; Kitaoka et al., 2012; Yao et al., 2013; Ozmen et al., 2017), the suitability of the protein for this task has also been controversially discussed (Schenk et al., 1995; Brellier et al., 2012). According to Kemp et al. (2004), the following criteria should be matched for a good cardiac biomarker:

Table 27: Characteristics of the ideal cardiac biomarker (adapted from Kemp et al., 2004).

HIGH SENSITIVITY	Abundant in cardiac tissue
HIGH SPECIFICITY	Absent from non-myocardial tissue Not detectable in blood from non-diseased subjects
RELEASE	Rapid release for early diagnosis Long half-life in blood for late diagnosis
ANALYTICAL	Cost effective Short turnaround time Precise Accurate
CLINICAL	Ability to influence therapy and so improve patient outcome Validated by clinical studies

Due to the fact that TNC has many functions, its contribution to cardiac injuries is still unknown, and the protein is represented in a great variety of tissues, the accuracy of such prediction is in question.

However, even though the expression of OLFML2B is poorly restricted (Figure 9), the protein has been repeatedly located in cardiac tissue. By now, OLFML2B is detectable in human

serum and hopefully will be in human whole blood. As the procedure is set up currently, it takes until the next day for the test results to be reported but time can be greatly shortened by preparing the ELISA microtiter plates up front. If OLFML2B turns out to be a better choice for detecting cardiac diseases must be awaited.

4. Conclusion

Taken together, this functional proteomic investigation suggests a high impact of the OLFML2B protein on myocardial repolarization. While the observations of this study provide first indications of a pathophysiological mechanism, further details will have to be evaluated.

The initial assumptions of this thesis, which were based on the characteristics of dominant-negative myocilin mutations in POAG could be extended to OLFML2B by the functional investigation and supported the hypothesis that cellular phenotypes of OLFML2B, i.e. hyper-, hypo- or non-secretional mutations, were associated with both human disease severity and population allele frequency of the mutations. Co-expression of wildtype and mutant protein showed dominant effects on the OLFML2B protein regardless of the ratios of mutant and wildtype protein concentrations. This indicates possible molecular and evolutionary mechanisms, by which the OLFML2B protein may be affected and disturbed in its function: If wildtype and mutant OLFML2B proteins are prevented from secretion into the extracellular space, the putative function of the protein is inhibited resulting in a loss-of-function phenotype.

Additionally, detection of OLFML2B in the human heart opened the possibility of cardiac tissue operating as effect site. The identification of Tenascin C as probable interaction partner, an ECM protein that is highly correlated with injuries of the human heart and was demonstrated to lead to impairment of inactivating sodium channels, emphasizes the initial hypothesis and elucidates a plausible pathological mechanism, by which OLFML2B is able to influence the QT interval.

The generated data indicate a functional role for rare OLFML2B mutations in multifactorial and complex diseases such as sudden infant death syndrome (SIDS) and repolarization disturbances (AF, DCM, LQTS) in particular and potentially even a more general part of OLFML2B in fever induced arrhythmias.

By using the generated biomarkers for OLFML2B, serum of affected patients can now be tested for identification of more *OLFML2B* mutations, gaining deeper insights into the overall mechanism and explaining a higher percentage of QT interval variance.

VI. REFERENCES

Aarnoudse, A.-J. L. H. J., Newton-Cheh, C., de Bakker, P. I. W., Straus, S. M. J. M., Kors, J. A., Hofman, A., Uitterlinden, A. G., Witteman, J. C. M. and Stricker, B. H. C. (2007) Common *NOS1AP* Variants Are Associated With a Prolonged QTc Interval in the Rotterdam Study. Circ., 116, 10-16.

Abhilash, S. P. and Namboodiri, N. (2014) Sudden cardiac death - Historical perspectives. Indian Heart J., 66, 4-9.

Adam, M. F., Belmouden, A., Binisti, P., Brézin, A. P., Valtot, F., Béchetoille, A., Dascotte, J. C., Copin, B., Gomez, L., Chaventré, A., Bach, J.-F. and Garchon H.-J. (1997) Recurrent mutations in a single exon encoding the evolutionarily conserved olfactomedin-homology domain of TIGR in familial open-angle glaucoma. Hum. Mol. Gen., 6 (12), 2091–2097.

Al-Khatib, S. M., LaPointe, N. M. A., Kramer, J. M. and Califf, R. M. (2003) What Clinicians Should Know About the QT interval. JAMA, 289, 2120-2127.

Alders, M., Bikker, H. and Christiaans, I. (2003, updated 2018) Long QT Syndrome. GeneReviews® [Internet]. Seattle (WA): University of Washington, Seattle; 1993-2020.

American Academy of Pediatrics, Task Force on Sudden Infant Death Syndrome (2005, updated 2011, updated 2016) SIDS and Other Sleep-Related Infant Deaths: Updated 2016 Recommendations for a Safe Infant Sleeping Environment. Ped., 138 (5), 1-12.

Amor, V., Feinberg, K., Eshed-Eisenbach, Y., Vainshtein, A., Frechter, S., Grumet, M., Rosenbluth, J. and Peles, E. (2014) Long-Term Maintenance of Na+ Channels at Nodes of Ranvier Depends on Glial Contact Mediated by Gliomedin and NrCAM. The J. of Neurosc., 34 (15), 5089-5098.

Anholt, R. R. H. (2014) Olfactomedin proteins: central players in development and disease. Front. Cell Dev. Biol., 2 (6), 1-10.

Anholt, R. R., Peetro, A. E. and Rivers A. M. (1990) Identification of a group of novel membrane proteins unique to chemosensory cilia of olfactory receptor cells. Biochem., 29, 3366-3373.

Arking, D. E., Pfeufer, A., Post, W., Kao, W. H. L., Newton-Cheh, C., Ikeda, M., West, K., Kashuk, C., Akyol, M., Perz, S., Jalilzadeh, S., Illig, T., Gieger, C., Guo, C.-Y., Larson, M. G., Wichmann, H. E., Marbán, E., O'Donnell, C. J., Hirschhorn, J. N., Kääb, S., Spooner, P. M.,

Meitinger, T. and Chakravarti, A. (2006) A common genetic variant in the NOS1 regulator *NOS1AP* modulates cardiac repolarization. Nat. Genet., 38, 644-651.

Arking, D. E. and Sotoodehnia, N. (2012) The Genetics of Sudden Cardiac Death. Annu. Rev. Genom. Hum. Genet., 13, 223-239.

Aso, N., Tamura, A. and Nasu, M. (2004) Circulating tenascin-C levels in patients with idiopathic dilated cardiomyopathy. Am. J. Cardiol., 94, 1468-1470.

Atanasovska, B., Kumar, V., Fu, J., Wijmenga, C. and Hofker, M. H. (2015) GWAS as a Driver of Gene Discovery in Cardiometabolic Diseases. Trends Endocrinol. Metab., 26 (12), 722-732.

Behr, E. R., Dalageorgou, C., Christiansen, M., Syrris, P., Hughes, S., Esteban, M. T. T., Rowland, E., Jeffery, S., and McKenna, W. J. (2008) Sudden arrhythmic death syndrome: familial evaluation identifies inheritable heart disease in the majority of families. Eur. Heart J., 29, 1670-80.

Benito, B., Brugada, J., Brugada R. and Brugada P. (2009) Brugada Syndrome. Rev. Esp. Cardiol., 62 (11), 1297-1315.

Border, W. L. and Benson, D. W. (2007) Sudden infant death syndrome and long QT syndrome: The Zealots versus the Naysayers. Heart Rhythm, 4 (2), 167-169.

Brellier, F., Martina, E., Degen, M., Heuzé-Vourc'h, N., Petit, A., Kryza, T., Courty, Y., Terracciano, L., Ruiz, C. and Chiquet-Ehrismann, R. (2012) Tenascin-W is a better cancer biomarker than tenascin-C for most human solid tumors. BMC Clin. Pathol., 12 (14), 1-10.

Brunner, A., Mayerl, C., Tzankov, A., Verdorfer, I., Tschörner, I., Rogatsch, H. and Mikuz, G. (2004) Prognostic significance of tenascin-C expression in superficial and invasive bladder cancer. J. Clin. Pathol., 57, 927-931.

Burge, C. and Karlin, S. (1997) Prediction of Complete Gene Structures in Human Genomic DNA. J. Mol. Biol., 268, 78-94.

Chen, C. K., Chan, N. L., and Wang, A. H. (2011) The many blades of the β-propeller proteins: conserved but versatile. Trends Biochem. Sci., 36, 553-561.

Chiquet-Ehrismann, R. and Chiquet, M. (2003) Tenascins: regulation and putative functions during pathological stress. J. Pathol. 200, 488-499.

Chugh, S. S., Kelly, K. L. and Titus, J. L. (2000) Sudden cardiac death with apparently normal heart. Circ., 102, 649-654.

Chugh, S. S., Reinier, K., Teodorescu, C., Evanado, A., Kehr, E., Al Samara, M., Mariani, R., Gunson, K. and Jui, J. (2008) Epidemiology of Sudden Cardiac Death: Clinical and Research Implications. Prog. Cardiovasc. Dis., 51 (3), 213-28.

Clapham, D. E. (2007) Calcium Signaling. Cell, 131, 1047-1058.

Dekker, J. M., Crow, R. S., Hannan, P. J., Schouten, E. G., Folsom, A. R. and ARIC Study Group (2004) Heart rate-corrected QT interval prolongation predicts risk of coronary heart disease in black and white middle-aged men and women: the ARIC study. J. Am. Coll. Cardiol., 43 (4), 565-571.

Dietz, H.C. and Pyeritz, R.E. (1995) Mutations in the human gene for fibrillin-1 (FBN1) in the Marfan syndrome and related disorders. Hum. Mol. Genet. 4, 1799-1809.

Dobson, C. M. (2001) The structural basis of protein folding and its links with human disease. Phil. Trans. R. Soc. Lond. B., 56, 133-145.

Dobson, C. M. (2003) Protein folding and misfolding. Nat., 426, 884-890.

Dobson, C. M. (2004) Principles of protein folding, misfolding and aggregation. Seminars in Cell & Dev. Biol., 15, 3-16.

Donegan, R. K., Hill, S. E., Turnage, K. C., Orwig, S. D. and Lieberman, R. L. (2012) The glaucoma-associated olfactomedin domain of myocilin is a novel calcium-binding protein. J. Biol. Chem., 287, 43370–43377.

Emoto, K., Yamada, Y., Sawada, H., Fujimoto, H., Ueno, M., Takayama, T., Kamada, K., Naito, A., Hirao, S. and Nakajima, Y. (2001) Annexin II Overexpression Correlates With Stromal tenascin-C Overexpression: A Prognostic Marker in Colorectal Carcinoma. Am. Cancer Society, 92 (6), 1419-1426.

Eshed, Y., Feinberg, K., Carey, D. J. and Peles, E. (2007) Secreted gliomedin is a perinodal matrix component of peripheral nerves. J. of Cell Biol., 177, 551-562. CrossRef Medline.

Eshed-Eisenbach, Y. and Peles, E. (2013) The making of a node: a co-production of neurons and glia. Curr. Opin. Neurobiol., 23, 1049-1056.

Feinberg, K., Eshed-Eisenbach, Y., Frechter, S., Amor, V., Salomon, D., Sabanay, H., Dupree, J. L., Grumet, M., Brophy, P. J., Shrager, P. and Peles, E. (2010) A glial signal consisting of gliomedin and NrCAM clusters axonal Na^+ channels during the formation of nodes of Ranvier. Neuron, 65 (4), 490-502.

Frangogiannis, N. G., Shimoni, S., Chang, S. M., Ren, G., Dewald, O., Gersch, C., Shan, K., Aggeli, C., Reardon, M., Letsou, G. V., Espada, R., Ramchandani, M., Entman, M. L. and Zoghbi, W. A. (2002) Active interstitial remodeling: an important process in the hibernating human myocardium. J. Am. Coll. Cardiol., 39, 1468-1474.

Funayama, T., Mashima, Y., Ohtake, Y., Ishikawa, K., Fuse, N., Yasuda, N., Fukuchi, T., Murakami, A., Hotta, Y. and Shimada, N. (2006) SNPs and interaction analyses of noelin 2, myocilin, and optineurin genes in Japanese patients with open-angle glaucoma. Invest. Ophthalmol. Vis. Sci., 47, 5368–5375.

Furutani, Y., Manabe, R.-I., Tsutsui, K., Yamada, T., Sugimoto, N., Fukuda, S., Kawai, J., Sugiura, N., Kimata, K., Hayashizaki, Y. and Sekiguchi, K. (2005) Identification and characterization of photomedins: novel olfactomedin-domain-containing proteins with chondroitin sulphate-E-binding activity. Biochem. J., 389, 675-684.

Garcia-Elias, A. and Benito, B. (2018) Ion Channel Disorders and Sudden Cardiac Death. Int. J. Mol. Sci., 19 (3), 692.

Gelfer, P. and Tatum, M. (2014) Sudden Infant Death Syndrome. J. of Ped. Health Care, 28 (5), 470-474.

Giblin, S. and Midwood, K. S. (2015) Tenascin-C: Form versus function. Cell Adhesion & Migration, 9 (1-2), 48-82.

Goldberg, A. L. (2003) Protein degradation and protection against misfolded or damaged proteins. Nat., 426, 895-899.

Golledge, J., Clancy, P., Maguire, J., Lincz, L. and Koblar, S. (2011) The role of tenascin C in cardiovascular disease. Cardiovasc. Res., 92, 19-28.

Han, H. and Kursula, P. (2015) The Olfactomedin Domain from Gliomedin Is a β-Propeller with Unique Structural Properties. J. of Biol. Chem., 290 (6), 3612-3621.

Hauck, F. R., Moore, C. M., Herman, S. M., Donovan, M., Kalelkar, M., Christoffel, K. K., Hoffman, D. J. and Rowley, D. (2002) The Contribution of Prone Sleeping Position to the

Racial Disparity in Sudden Infant Death Syndrome: The Chicago Infant Mortality Study. Ped., 110 (4), 772-780.

Hauck, F. R., Omojokun, O. O. and Siadaty, M. S. (2005) Do Pacifiers Reduce the Risk of Sudden Infant Death Syndrome? A Meta-analysis. Ped., 116 (5), e716-e723.

Hauck, F. R., Thompson, J. M. D., Tanabe, K. O., Moon, R. Y. and Vennemann, M. M. (2011) Breastfeeding and Reduced Risk of Sudden Infant Death Syndrome: A Meta-analysis. Ped., 128 (1), 103-110.

Hecht, J. T., Nelson, L. D., Crowder, E., Wang, Y., Elder, F. F., Harrison, W. R., Francomano, C. A., Prange, C. K., Lennon, G. G., Deere, M. and Lawler, J. (1995) Mutations in exon 17B of cartilage oligomeric matrix protein (COMP) cause pseudoachondroplasia. Nat. Genet., 10, 325-329.

Hodge, K., Have, S. T., Hutton, L. and Lamond, A. I. (2013) Cleaning up the masses: Exclusion lists to reduce contamination with HPLC-MS/MS. J. of Prot., 88, 92-103.

Horsley, T., Clifford, T., Barrowman, N., Bennett, S., Yazdi, F., Sampson, M., Moher, D., Dingwall, O., Schachter, H. and Côté, A. (2007) Benefits and harms associated with the practice of bed sharing: a systematic review. Arch. Ped. Adolesc. Med., 161 (3), 237-245.

Huikuri, H. V., Castellanos, A. and Myerburg, R. J. (2001) Sudden death due to cardiac arrhythmias. N. Engl. J. of Med., 345 (20), 1473-1482.

Hunt, C. E. and Hauck, F. R. (2006) Sudden infant death syndrome. Canadian Med. Ass. J., 174 (13), 1861-1869.

Imanaka-Yoshida, K., Hiroe, M., Nishikawa, T., Ishiyama, S., Shimojo, T., Ohta, Y., Sakakura, T. and Yoshida, T. (2001) Tenascin-C Modulates Adhesion of Cardiomyocytes to Extracellular Matrix during Tissue Remodeling after Myocardial Infarction. Lab. Invest., 81 (7), 1015-1024.

Imanaka-Yoshida, K., Hiroe, M., Yasutomi, Y., Toyazaki, T., Tsuchiya, T., Noda, N., Maki, T., Nishikawa, T., Sakakura, T. and Yoshida, T. (2002) Tenascin-C is a useful marker for disease activity in myocarditis. J. Pathol., 197, 388-394.

Ishiwata, T., Takahashi, K., Shimanuki, Y., Ohashi, R., Cui, R., Takahashi, F., Shimizu, K., Miura, K. and Fukuchi, Y. (2005) Serum Tenascin-C as a Potential Predictive Marker of Angiogenesis in Non-small Cell Lung Cancer. Anticancer Res., 25, 489-496.

Jackson, V. A., del Toro, D., Carrasquero, M., Roversi, P., Harlos, K., Klein, R., and Seiradake, E. (2015) Structural Basis of Latrophilin-FLRT Interaction. Cell Press, Structure, 23, 1-8.

Jacobson, N., Andrews, M., Shepard, A. R., Nishimura, D., Searby, C., Fingert, J. H., Hageman, G., Mullins, R., Davidson, B. L., Kwon, Y. H., Alward, W. L. M., Stone, E. M., Clark, A. F. and Sheffield, V. C. (2001) Non-secretion of mutant proteins of the glaucoma gene *myocilin* in cultured trabecular meshwork cells and in aqueous humor. Hum. Mol. Genet., 10 (2), 117-125.

Jahkola, T., Toivonen, T., Virtanen, I., von Smitten, K., Nordling, S., von Boguslawski, K., Haglund, C., Nevanlinna, H. and Blomqvist, C. (1998) Tenascin-C expression in invasion border of early breast cancer: a predictor of local and distant recurrence. Br. J. of Cancer, 78 (11), 1507-1513.

Kanetake, J., Aoki, Y. and Funayama, M. (2003) Evaluation of rebreathing potential on bedding for infant use. Ped. Internat., 45 (3), 284-289.

Kapoor, A., Sekar, R. B., Hansen, N. F., Fox-Talbot, K., Morley, M., Pihur, V., Chatterjee, S., Brandimarto, J., Moravec, C. S., Pulit, S. L., QT Interval-International GWAS Consortium, Pfeufer, A., Mullikin, J., Ross, M., Green, E. D., Bentley, D., Newton-Cheh, C., Boerwinkle, E., Tomaselli, G. F., Cappola, T. P., Arking, D. E., Halushka, M. K. and Chakravarti, A. (2014) An Enhancer Polymorphism at the Cardiomyocyte Intercalated Disc Protein NOS1AP Locus Is a Major Regulator of the QT Interval. The Am. J. of Hum. Genet., 94, 854-869.

Karavanich, C. A. and Anholt, R. R. H. (1998) Molecular Evolution of Olfactomedin. Mol. Biol. Evol., 15 (6), 718-726.

Keller, B. O., Sui, J., Young, A. B. and Whittal, R. M. (2008) Interferences and contaminants encountered in modern mass spectrometry. Anal. Chim. Acta, 627 (1), 71-81.

Kemp, M., Donovan, J., Higham, H. and Hooper, J. (2004) Biochemical markers of myocardial injury. Br. J. of Anaesthesia, 93 (1), 63-73.

Kitaoka, H., Kubo, T., Baba, Y., Yamasaki, N., Matsumura, Y., Furuno, T. and Doi, Y. L. (2012) Serum tenascin-C levels as a prognostic biomarker of heart failure events in patients with hypertrophic cardiomyopathy. J. of Cardiol., 59, 209-214.

Kjaer, S. and Ibanez, C. F. (2003) Intrinsic susceptibility to misfolding of a hot-spot for Hirschsprung disease mutations in the ectodomain of RET. Hum. Mol. Genet., 12 (17), 2133-2144.

Kobayashi, D., Koshida, S., Moriai, R., Tsuji, N. and Watanabe, N. (2007) Olfactomedin 4 promotes S-phase transition in proliferation of pancreatic cancer cells. Cancer Sci., 98 (3), 334-340.

Koshida, S., Kobayashi, D., Moriai, R., Tsuji, N. and Watanabe, N. (2007) Specific overexpression of OLFM4$^{GW112/hGC-1}$ mRNA in colon, breast and lung cancer tissues detected using quantitative analysis. Cancer Sci., 98 (3), 315-320.

Kumar, N., Gammell, P., Meleady, P., Henry, M. and Clynes, M. (2008) Differential protein expression following low temperature culture of suspension CHO-K1 cells. BMC Biotech., 8 (42), 1-13.

Lek, M., Karczewski, K. J., Minikel, E. V., Samocha, K. E., Banks, E., Fennell, T., O'Donnell-Luria, A. H., Ware, J. S., Hill, A. J., Cummings, B. B., Tukiainen, T., Birnbaum, D. P., Kosmicki, J. A., Duncan, L. E., Estrada, K., Zhao, F., Zou, J., Pierce-Hoffman, E., Berghout, J., Cooper, D. N., Deflaux, N., DePristo, M., Do, R., Flannick, J., Fromer, M., Gauthier, L., Goldstein, J., Gupta, N., Howrigan, D., Kiezun, A., Kurki, M. I., Moonshine, A. L., Natarajan, P., Orozco, L., Peloso, G. M., Poplin, R., Rivas, M. A., Ruano-Rubio, V., Rose, S. A., Ruderfer, D. M., Shakir, K., Stenson, P. D., Stevens, C., Thomas, B. P., Tiao, G., Tusie-Luna, M. T., Weisburd, B., Won, H. H., Yu, D., Altshuler, D. M., Ardissino, D., Boehnke, M., Danesh, J., Donnelly, S., Elosua, R., Florez, J. C., Gabriel, S. B., Getz, G., Glatt, S. J., Hultman, C. M., Kathiresan, S., Laakso, M., McCarroll, S., McCarthy, M. I., McGovern, D., McPherson, R., Neale, B. M., Palotie, A., Purcell, S. M., Saleheen, D., Scharf, J. M., Sklar, P., Sullivan, P. F., Tuomilehto, J., Tsuang, M. T., Watkins, H. C., Wilson, J. G., Daly, M. J. and MacArthur, D. G. (2016) Analysis of protein-coding genetic variation in 60,706 humans. Nat., 536, 285-291 (Exome aggregation consortium, Boston, MA).

MacArthur, J., Bowler, E., Cerezo, M., Gil, L., Hall, P., Hastings, E., Junkins, H., McMahon, A., Milano, A., Morales, J., Pendlington, Z. M., Welter, D., Burdett, T., Hindorff, L., Flicek, P., Cunningham, F. and Parkinson, H. (2017) The new NHGRI-EBI Catalog of published genome-wide association studies (GWAS Catalog). Nucleic Acids Res., 45, 896-901.

Manolio, T. A., Brooks, L. D. and Collins, F. S. (2008) A HapMap harvest of insights into the genetics of common disease. J. Clin. Invest., 118 (5), 1590-1605.

Manolio, T. A., and Collins, F. S. (2009) The HapMap and Genome-Wide Association Studies in Diagnosis and Therapy. Annu. Rev. Med., 60, 443-456.

Maurer, P., Hohenester, E. and Engel, J. (1996) Extracellular calcium-binding proteins. Curr. Opin. Cell Biol., 8 (5), 609-617.

Maurer, P. and Hohenester, E. (1997) Structural and Functional Aspects of Calcium Binding in Extracellular Matrix Proteins. Matrix Biol., 15, 569-580.

Midwood, K. S., Chiquet, M., Tucker, R. P. and Orend, G. (2016) Tenascin-C at a glance. The Company of Biologists Ltd, J. of Cell Sci., 129, 4321-4327.

Miljkovic-Licina, M., Hammel, P., Garrido-Urbani, S., Lee, B. P.-L., Meguenani, M., Chaabane, C., Bochaton-Piallat, M.-L. and Imhof, B. A. (2012) Targeting Olfactomedin-like 3 Inhibits Tumor Growth by Impairing Angiogenesis and Pericyte Coverage. Mol. Cancer Ther., 11 (12), 2588-2599.

Mitchell, E. A., Stewart, A. W., Clements, M. and Ford, R. P. K., (1995) Immunisation and the sudden infant death syndrome. New Zealand Cot Death Study Group. Arch. Dis. Child., 73 (6), 498-501.

Morimoto, S.-I., Imanaka-Yoshida, K., Hiramitsu, S., Kato, S., Ohtsuki, M., Uemura, A., Kato, Y., Nishikawa, T., Toyozaki, T., Hishida, H., Yoshida, T. and Hiroe, M. (2005) Diagnostic Utility of tenascin-C for Evaluation of the Activity of Human Acute Myocarditis. The J. of Pathol., 205 (4), 460-467.

Newton-Cheh, C., Eijgelsheim, M., Rice, K. M., de Bakker, P. I. W., Yin, X., Estrada, K., Bis, J. C., Marciante, K., Rivadeneira, F., Noseworthy, P. A., Sotoodehnia, N., Smith, N. L., Rotter, J. I., Kors, J. A., Witteman, J. C. M., Hofman, A., Heckbert, S. R., O'Donnell, C. J., Uitterlinden, A. G., Psaty, B. M., Lumley, T., Larson, M. G. and Stricker, B. H. C. (2009) Common variants at ten loci influence QT interval duration in the QTGEN Study. Nat. Genet., 41 (4), 399-406.

Niebroj-Dobosz, I. (2012) Tenascin-C in human cardiac pathology. Clin. Chim. Acta., 413, 1516-1518.

Otagiri, T., Kijima, K., Osawa, M., Ishii, K., Makita, M., Matoba, R., Umetsu, K. and Hayasaka, K. (2008) Cardiac Ion Channel Gene Mutations in Sudden Infant Death Syndrome. Ped. Res., 64 (5), 482-487.

Oue, N., Sentani, K., Noguchi, T., Ohara, S., Sakamoto, N., Hayashi, T., Anami, K., Motoshita, J., Ito, M., Tanaka, S., Yoshida, K. and Yasui, W. (2009) Serum olfactomedin 4 (GW112, hGC-1) in combination with Reg IV is a highly sensitive biomarker for gastric cancer patients. Int. J. Cancer, 125, 2383-2392.

Ozmen, C., Deniz, A., Deveci, O. S., Cagliyan, C. E., Celik, A. I., Yildiz, I., Yildiz, P. Ö., Demir, M. and Kanadasi, M. (2017) Association among tenascin-C and NT-proBNP levels and arrhythmia prevalence in heart failure. Clin. Invest. Med., 40 (6), E219-E227.

Panoutsopoulou, K., Tachmazidou, I. and Zeggini, E. (2013) In search of low-frequency and rare variants affecting complex traits. Hum. Mol. Gen., 22 (R1), 16-21.

Parakh, N. (2015) Sudden Cardiac Death. J. of the Pract. of Cardiovasc. Sci., 1 (2), 113-119.

Park, W. J., Jeong, D. and Oh, J. G. (2017) Tenascin-C in Cardiac Hypertrophy and Fibrosis - Friend or Foe? J. Am. Coll. Cardiol., 70 (13), 1616-1617.

Patel, A. L., Harris, K. and Thach, B. T. (2001) Inspired CO_2 and O_2 in sleeping infants rebreathing from bedding: relevance for sudden infant death syndrome. J. Appl. Physiol., 91 (6), 2537-2545.

Patel, L., Sun, W., Glasson, S. S., Morris, E. A., Flannery, C. R. and Chockalingam, P. S. (2011) Tenascin-C induces inflammatory mediators and matrix degradation in osteoarthritic cartilage. BMC Musculoskeletal Disorders, 12 (164), 1-14.

Pattaro, C., Marroni, F., Riegler, A., Mascalzoni, D., Pichler, I., Volpato, C. B., Cero, U. D., De Grandi, A., Egger, C., Eisendle, A., Fuchsberger, C., Gögele, M., Pedrotti, S., Pinggera, G. K., Stefanov, S. A., Vogl, F. D., Wiedermann, C. J., Meitinger, T. and Pramstaller, P. P. (2007) The genetic study of three population microisolates in South Tyrol (MICROS): study design and epidemiological perspectives. BMC Med. Genet., 8 (29), 1-15.

Pfeufer, A., Sanna, S., Arking, D. E., Müller, M., Gateva, V., Fuchsberger, C., Ehret, G. B., Orrú, M., Pattaro, C., Köttgen, A., Perz, S., Usala, G., Barbalic, M., Li, M., Pütz, B., Scuteri, A., Prineas, R. J., Sinner, M. F., Gieger, C., Najjar, S. S., Kao, W. H. L., Mühleisen, T. W., Dei, M., Happle, C., Möhlenkamp, S., Crisponi, L., Erbel, R., Jöckel, K.-H., Naitza, S., Steinbeck, G., Marroni, F., Hicks, A. A., Lakatta, E., Müller-Myhsok, B., Pramstaller, P. P., Wichmann, H.-E., Schlessinger, D., Boerwinkle, E., Meitinger, T., Uda, M., Coresh, J., Kääb, S., Abecasis, G. R. and Chakravarti, A. (2009) Common variants at ten loci modulate the QT interval duration in the QTSCD Study. Nat. Genet., 41 (4), 407-414.

Pilia, G., Chen, W.-M., Scuteri, A., Orru´, M., Albai, G., Dei, M., Lai, S., Usala, G., Lai, M., Loi, P., Mameli, C., Vacca, L., Deiana, M., Olla, N., Masala, M., Cao, A., Najjar, S. S., Terracciano, A., Nedorezov, T., Sharov, A., Zonderman, A. B., Abecasis, G. R., Costa, P., Lakatta, E. and Schlessinger, D. (2006) Heritability of cardiovascular and personality traits in 6,148 Sardinians. PLoS Genet., 2 (8), e132, 1207-1223.

Ponsonby, A.-L., Dwyer, T., Gibbons, L. E., Cochrane, J. A., Jones, M. E. and McCall, M. J. (1992) Thermal environment and sudden infant death syndrome: case-control study. BMJ., 304 (6822), 277-282.

Post, W., Shen, H., Damcott, C., Arking, D. E., Kao, W. H. L., Sack, P. A., Ryan, K. A., Chakravarti, A., Mitchell, B. D. and Shuldiner, A. R. (2007) Associations between genetic variants in the *NOS1AP* (CAPON) gene and cardiac repolarization in the old order Amish. Hum. Hered., 64, 214-219.

Priori, S. G., Bloise, R. and Crotti, L. (2001) The long QT syndrome. Europace, 3, 16-27.

Probst, V., Wilde, A. A. M., Barc, J., Sacher, F., Babuty, D., Mabo, P., Mansourati, J., Le Scouarnec, S., Kyndt, F., Le Caignec, C., Guicheney, P., Gouas, L., Albuisson, J., Meregalli, P. G., Le Marec, H., Tan, H. L. and Schott, J.-J. (2009) SCN5A Mutations and the Role of Genetic Background in the Pathophysiology of Brugada Syndrome. Circ. Cardiovasc. Genet., 2 (6), 552-557.

Radford, S. E. and Dobson, C. M. (1999) From computer simulations to human disease: emerging themes in protein folding. Cell, 97 (3), 291-298.

Roden, D. M. (2008) Long-QT Syndrome. Clinical practice. N. Engl. J. Med., 358 (2), 169-176.

Sato, A., Aonuma, K., Imanaka-Yoshida, K., Yoshida, T., Isobe, M., Kawase, D., Kinoshita, N., Yazaki, Y. and Hiroe, M. (2006) Serum Tenascin-C Might Be a Novel Predictor of Left Ventricular Remodeling and Prognosis After Acute Myocardial Infarction. J. Am. Coll. Cardiol., 47 (11), 2319-2325.

Schäfer, Z. S. (2012) Genetic Variation and Functional Analysis of the Cardiomedin Gene, (Dissertation), Technische Universität München.

Schenk, S., Muser, J., Vollmer, G. and Chiquet-Ehrismann, R. (1995) Tenascin-C in serum: A questionable tumor marker. Internat. J. of cancer, 61 (4), 443-449.

Schmermund, A., Möhlenkamp, S., Stang, A., Grönemeyer, D., Seibel, R., Hirche, H., Mann, K., Siffert, W., Lauterbach, K., Siegrist, J., Jöckel, K.-H. and Erbel, R. (2002) Assessment of clinically silent atherosclerotic disease and established and novel risk factors for predicting myocardial infarction and cardiac death in healthy middle-aged subjects: rationale and design of the Heinz Nixdorf Recall Study. Am. Heart J., 144 (2), 212–218.

Schott, J.-J., Alshinawi, C., Kyndt, F., Probst, V., Hoorntje, T. M., Hulsbeek, M., Wilde, A. A. M., Escande, D., Mannens, M. M. A. M. and Le Marec, H. (1999) Cardiac conduction defects associate with mutations in SCN5A. Nat. Genet., 23 (1), 20-21.

Schwartz, P. J., Stramba-Badiale, M., Segantini, A., Austoni, P., Bosi, G., Giorgetti, R., Grancini, F., Marni, E. D., Perticone, F., Rosti, D. and Salice, P. (1998) Prolongation of the QT interval and the sudden infant death syndrome. N. Engl. J. Med., 338 (24), 1709-1714.

Schwartz, J., Priori, S. G., Bloise, R., Napolitano, C., Ronchetti, E., Piccinini, A., Goj, C., Breithardt, G., Schulze-Bahr, E., Wedekind, H. and Nastoli, J. (2001) Molecular diagnosis in a child with sudden infant death syndrome. Lancet, 358 (9290), 1342-1343.

Schwartz, P. J., Stramba-Badiale, M., Crotti, L., Pedrazzini, M., Besana, A., Bosi, G., Gabbarini, F., Goulene, K., Insolia, R., Mannarino, S., Mosca, F., Nespoli, L., Rimini, A., Rosati, E., Salice, P. and Spazzolini, C. (2009) Prevalence of the Congenital Long-QT Syndrome. Circ., 120, 1761-1767.

Schwarz, J. M., Rödelsperger, C., Schuelke, M. and Seelow, D. (2010) MutationTaster evaluates disease-causing potential of sequence alterations. Nat. Methods, 7 (8), 575-576.

Schwartz, P. J., Crotti, L. and Insolia, R. (2012) Long-QT Syndrome: From Genetics to Management. Circ. Arrhythm. Electrophysiol., 5, 868-877.

Scragg, R., Mitchell, E. A., Taylor, B. J., Stewart, A. W., Ford, R. P., Thompson, J. M., Allen, E. M. and Becroft, D. M. (1993) Bed sharing, smoking, and alcohol in the sudden infant death syndrome. New Zealand Cot Death Study Group. BMJ, 307 (6915), 1312-1318.

Sim, N.-L., Kumar, P., Hu, J., Henikoff, S., Schneider, G. and Ng, P. C. (2012) SIFT web server: predicting effects of amino acid substitutions on proteins, Nucleic Acids Res., 40, 452–457.

Skinner, J. R. (2005) Is there a relation between SIDS and long QT syndrome? Arch. Dis. Child., 90, 445-449.

Snyder, D. A., Rivers, A. M., Yokoe, H., Menco, B. P., and Anholt, R. R. H. (1991) Olfactomedin: purification, characterization and localization of a novel olfactory glycoprotein. Biochem., 30 (38), 9143-9153.

Spears, D. A. and Gollob, M. H. (2015) Genetics of inherited primary arrhythmia disorders. The Appl. of Clin. Gen., 8, 215-233.

Srinivasan, J., Schachner, M., and Catterall, W. A. (1998) Interaction of voltage-gated sodium channels with the extracellular matrix molecules tenascin-C and tenascin-R. Proc. Natl. Acad. Sci. USA, 95, 15753-15757.

Stanton, A. N. (1984) Sudden infant death. Overheating and cot death. Lancet, 2 (8413), 1199-1201.

Stewart, A. J., Williams, S. M., Mitchell, E. A., Taylor, B. J., Ford, R. P. and Allen, E. M. (1995) Antenatal and intrapartum factors associated with sudden infant death syndrome in the New Zealand Cot Death Study. J. Paediatr. Child Health, 31 (5), 473-478.

Stone, E. M., Fingert, J. H., Alward, W. L., Nguyen, T. D., Polansky, J. R., Sunden, S. L., Nishimura, D., Clark, A. F., Nystuen, A. Nichols, B. E., Mackey, D. A., Ritch, R., Kalenak, J. W., Craven, E. R. and Sheffield, V. C. (1997) Identification of a gene that causes primary open angle glaucoma. Sci., 275 (5300), 668-670.

Strachan, T. and Read, A. (2011) Human Molecular Genetics, 4th edn., Garland Science, New York.

Susuki, K. (2013) Node of Ranvier disruption as a cause of neurological diseases. Am. Soc. for Neurochem., 5 (3), 209-219.

Tamura, A., Kusachi, S., Nogami, K., Yamanishi, A., Kajikawa, Y., Hirohata, S. and Tsuji, T. (1996) Tenascin expression in endomyocardial biopsy specimens in patients with dilated cardiomyopathy: distribution along margin of fibrotic lesions. Heart, 75, 291-294.

Tester, D. J. and Ackerman, M. J. (2005) Sudden infant death syndrome: how significant are the cardiac channelopathies? Cardiovasc. Res., 67, 388-396.

Tester, D.J. and Ackerman, M.J. (2011) Genetic testing for potentially lethal, highly treatable inherited cardiomyopathies/channelopathies in clinical practice. Circ., 123 (9), 1021-1037.

Tester, D. J., Wong, L. C. H., Chanana, P., Jaye, A., Evans, J. M., FitzPatrick, D. R., Evans, M. J., Fleming, P., Jeffrey, I., Cohen, M. C., Tfelt-Hansen, J., Simpson, M. A., Behr, E. R. and Ackerman, M. J. (2018) Cardiac Genetic Predisposition in Sudden Infant Death Syndrome. J. Am. Coll. Cardiol., 71 (11), 1217-1227.

Thomas, P. J., Qu, B. H. and Pedersen, P. L. (1995) Defective protein folding as a basis of human disease. Trends Biochem. Sci., 20 (11), 456-459.

Tobin, M. D., Kähönen, M., Braund, P., Nieminen, T., Hajat, C., Tomaszewski, M., Viik, J., Lehtinen, R., Ng, G. A., Macfarlane, P. W., Burton, P. R., Lehtimäki, T. and Samani, N. J. (2008) Gender and effects of a common genetic variant in the NOS1 regulator *NOS1AP* on cardiac repolarization in 3761 individuals from two independent populations. Int. J. Epidemiol., 37, 1132-1141.

Trachtenberg, F. L., Haas, E. A., Kinney, H. C., Stanley, C. and Krous, H. F. (2012) Risk Factor Changes for Sudden Infant Death Syndrome After Initiation of Back-to-Sleep Campaign. Ped., 129 (4), 630-638.

Tsukada, B., Terasaki, F., Shimomura, H., Otsuka, Ko., Otsuka, Ka., Katashima, T., Fujita, S., Imanaka-Yoshida, K., Yoshida, T., Hiroe, M. and Kitaura, Y. (2009) High prevalence of chronic myocarditis in dilated cardiomyopathy referred for left ventriculoplasty: expression of tenascin C as a possible marker for inflammation. Hum. Pathol., 40 (7), 1015-1022.

Vergara, M., Becerra, S., Berrios, J., Reyes, J., Acevedo, C., Gonzalez, R., Osses, N. and Altamirano, C. (2013) Protein folding and glycosylation process are influenced by mild hypothermia in batch culture and by specific growth rate in continuous cultures of CHO cells producing rht-PA. BMC Proceedings, 7 (6), 1-4.

Visscher, P. M., Brown, M. A., McCarthy, M. I. and Yang, J. (2012) Five Years of GWAS Discovery. Am. J. Hum. Genet., 90, 7-24.

Visscher, P. M., Wray, N. R., Zhang, Q., Sklar, P., McCarthy, M. I., Brown, M. A. and Yang, J. (2017) 10 Years of GWAS Discovery: Biology, Function, and Translation. Am. J. Hum. Genet., 101, 5-22.

Wallace, E., Howard, L., Liu, M., O'Brien, T., Ward, D., Shen, S. and Prendiville, T. (2019) Long QT Syndrome: Genetics and Future Perspective. Ped. Cardiol., 40, 1419-1430.

Wang, Q., Shen, J., Splawski, I., Atkinson, D., Li, Z., Robinson, J. L., Moss, A. J., Towbin, J. A. and Keating, M. T. (1995) *SCN5A* Mutations Associated with an Inherited Cardiac Arrhythmia, Long QT Syndrome. Cell, 80 (5), 805-811.

Wedekind, H., Smits, J. P., Schulze-Bahr, E., Arnold, R., Veldkamp, M. W., Bajanowski, T., Borggrefe, M., Brinkmann, B., Warnecke, I., Funke, H., Bhuiyan, Z. A., Wilde, A. A. M., Breithardt, G. and Haverkamp, W. (2001) De novo mutation in the *SCN5A* gene associated with early onset of sudden infant death. Circ., 104 (10), 1158-1164.

Weigel, P. H. and Yik, J. H. N. (2002) Glycans as endocytosis signals: the cases of the asialoglycoprotein and hyaluronan/chondroitin sulphate receptors. Biochim. Biophys. Acta, 1572 (2-3), 341-363.

Welter, D., MacArthur, J., Morales, J., Burdett, T., Hall, P., Junkins, H., Klemm, A., Flicek, P., Manolio, T., Hindorff, L. and Parkinson, H. (2014) The NHGRI GWAS Catalog, a curated resource of SNP-trait associations. Nucleic Acids Res., 42, 1001-1006.

Wever, E. F. D. and de Medina, E. O. R. (2004) Sudden Death in Patients Without Structural Heart Disease. J. Am. Coll. Cardiol., 43 (7) 1137-1144.

Wichmann, H.-E., Gieger, C., Illig, T. and MONICA/KORA Study Group (2005) KORA-gen-resource for population genetics, controls and a broad spectrum of disease phenotypes. Gesundheitswesen, 67, 26-30.

Willinger, M., James, L. S., and Catz, C. (1991) Defining the sudden infant death syndrome (SIDS): Deliberations of an expert panel convened by the national Institute of Child health and Human Development. Ped. Pathol., 11 (5), 677-684.

Winship, P. R., and Dragon, A. C. (1991) Identification of haemophilia B patients with mutations in the two calcium binding domains of factor IX: importance of a β-OH Asp 64→Asn change. Br. J. Haematol., 77 (1), 102-109.

Wright, S. (1968) Evolution and the Genetics of Populations, Vol. 1. University of Chicago Press, Chicago.

Wu, L., Chang, W., Zhao, J., Yu, Y., Tan, X., Su, T., Zhao, L., Huang, S., Liu, S. and Cao, G. (2010) Development of Autoantibody Signatures as Novel Diagnostic Biomarkers of Non–Small Cell Lung Cancer. Clin. Cancer Res., 16 (14), 3760–3768.

Yao, H.-C., Han, Q.-F., Zhao, A.-P., Yao, D.-K. and Wang, L-X. (2013) Prognostic Values of Serum Tenascin-C in Patients with Ischaemic Heart Disease and Heart Failure. Heart, Lung and Circ., 22 (3), 184-187.

Yoshida, T., Akatsuka, T. and Imanaka-Yoshida, K. (2015) Tenascin-C and integrins in cancer. Cell Adhesion & Migration, 9 (1-2), 96-104.

Zeng, L.-C., Han, Z.-G., and Ma, W.-J. (2005) Elucidation of subfamily segregation and intramolecular coevolution of the olfactomedin-like proteins by comprehensive phylogenetic analysis and gene expression pattern assessment. Fed. of Eur. Biochem. Soc. Lett., 579 (25), 5443-5453.

Zipes, D. P. and Wellens, H. J. J. (1998) Sudden cardiac death. Circ., 98, 2334-2351.

VII. LIST OF FIGURES

Figure 1: Schematic ECG showing extended QT interval in red. 11

Figure 2: Triple-Risk Hypothesis for SIDS (Tester et al., 2018). 14

Figure 3: The interactive GWAS diagram visualizes all SNP-trait associations with P < 5.0 x 10^{-8}, mapped to the SNP's cytogenetic band (https://www.ebi.ac.uk/gwas website accessed on May 17th, 2020). 16

Figure 4: GWAS of QT interval showing the three-stage study design (Arking et al., 2006). .. 17

Figure 5: Fine mapping of *NOS1AP* showing LD between SNPs. Each value in the diamonds corresponds to pairwise correlation signals between SNPs, also represented in the shading of the fields. Fields without a number represent a signal of 1. *NOS1AP* exons 1 and 2 are shown in orange (Arking et al., 2006). 18

Figure 6: Manhattan Plot of genome-wide association analyses. The threshold for genome-wide significance is marked by the blue dotted line (5×10^{-8}). SNPs within loci exceeding this threshold are highlighted in green (Pfeufer et al., 2009). 18

Figure 7: Association results at locus 1q23.3 spanning ± 600 kb around each SNP. The SNPs are coloured according to their LD; the leading variant is highlighted with a blue square, while SNPs representing independent signals from the leading variant are highlighted with a purple diamond. Gene transcripts are annotated in the lower box indicating the direction of transcription by '+' or '-'(Pfeufer et al., 2009). 19

Figure 8: Schematic domain structure showing photomedin-1 (OLFML2A) and photomedin-2 (OLFML2B). Signal sequences (labelled 'Pre') and Ser/Thr-rich regions are shaded dark and light grey respectively; regions containing CXC motifs including $CXCXCX_9C$ motifs are indicated by white boxes, coiled-coil domains by hatched boxes, and olfactomedin domains by black boxes displaying the sequence homologies between photomedin-1 and photomedin-2 below (Furutani et al., 2005). 20

Figure 9: Gene expression of OLFML2B in human tissue (https://gtexportal.org/home/gene/OLFML2B website accessed on May 3rd, 2020). 21

Figure 10: Validation of different primary antibodies from Hybridoma cell lines for detection of recombinant OLFML2B protein expression by Western blot analysis. 43

Figure 11: Intracellular levels of OLFML2B protein after transient transfection of HEK293 cells with Wt and variants c.1512G>T (P504L), c.1544G>A (G515E), c.1669T>C (Y557H), c.1580G>A (R527Q). 45

Figure 12: Modelling of OLFML2B c-terminal region (https://swissmodel.expasy.org/interactive/SQLUpV/models/ website accessed on March 10th, 2019) from aa 493 (n-terminal region of c-terminus) to aa 750 (c-terminal region of c-terminus) including SIDS variants. ... 46

Figure 13: Western blot analysis visualizing the effect of adding $CaCl_2$ to the cell lysate of HEK293 cells transfected with Wt OLFML2B. 46

Figure 14: Western blot analysis visualizing the effect of adding $CaCl_2$ to the cell lysate of HEK293 cells transfected with mutant OLFML2B c.1544G>A (G515E). 47

Figure 15: Secretion of Wt and mutant OLFML2B variants c.1512G>T (P504L), c.1544G>A (G515E), c.1669T>C (Y557H) and c.1580G>A (R527Q). 48

Figure 16: Dominant-positive and dominant-negative effect caused by different concentrations of mutant OLFML2B proteins c.1810G>A (V604M) and c.1544G>A (G515E) on secretion of the Wt into the extracellular space. 50

Figure 17: Western blot of temperature-dependent secretion showing the Wt as reference, un-transfected HEK293 cells as negative control and variants with wildtype-like phenotype: c.338C>T (S113L), c.1306G>T (A436S) and c.445A>G (T149A). 50

Figure 18: Western blot of temperature-dependent secretion showing the Wt at 37°C plus the wildtype-like secreter c.1136C>T (S379L) as reference and variants with unlikely phenotype: c.34C>A (A12S), c.1367C>T (T456I), c.1408T>C (W470R), c.1580G>A (R527Q) and c.256C>T (R86W). 51

Figure 19: Western blot of temperature-dependent secretion showing the Wt at 37°C as reference, un-transfected HEK293 cells as negative control and variants with low or no secretion: c.1512G>T (P504L), c.1544G>A (G515E), c.1669T>C (Y557H) and c.2021G>A (G674D). 51

Figure 20: Plot of secretion vs. variant allele frequency (logarithmized) for the temperatures 30°C, 37°C and 41°C showing the correlated diseases atrial fibrillation (AF), dilated cardiomyopathy (DCM), long-QT syndrome (LQT) and sudden infant death syndrome (SIDS) as well as wildtype (Wt) and common variants. The plot reveals the correlation of effect size with allele frequency and especially the absence of common variants showing poor secretion within the general population. 53

Figure 21: Western blot showing human heart tissue and lysate of HEK293 cells transfected with OLFML2B Wt analysed with different primary abs. 54

Figure 22: Western blot showing human heart tissue whole protein, supernatant (SN) IP TNC plus Protein G conjugated Sepharose beads, SN IP TNC and purified TNC as positive control, all treated with rabbit anti-TNC and goat anti-rabbit ab; in addition, whole protein and SN IP TNC were visualized by the mouse anti-OLFML2B ab 4C2 and rat anti-mouse HRP ab. 56

Figure 23: Western blot showing human heart tissue IP whole protein, SN IP, cytosolic fraction (IP cyt) and the respective SN (SN IP cyt), membrane/ organelle protein fraction (IP mem), IP of human serum (IP serum) and whole protein; the signal was visualized by the mouse anti-OLFML2B ab 4C2 and rat anti-mouse IgG2b HRP ab, stripped and incubated with mouse anti-TNC E-9 ab and rat anti-mouse HRP ab. 57

Figure 24: Dot blot analysis of monoclonal hybridoma cell line antibody 7C4 from rat. 57

Figure 25: Predicted protein-protein interactions based on STRING (https://string-db.org/cgi/network.pl?taskId=E5mft6kaAeDh website accessed on May 26th, 2020). 66

Figure 26: The top 10 causes of death in 2000 according to the WHO (https://www.who.int/news-room/fact-sheets/detail/the-top-10-causes-of-death website accessed on May 26th, 2020). 67

Figure 27: The top 10 causes of death in 2016 according to the WHO (https://www.who.int/news-room/fact-sheets/detail/the-top-10-causes-of-death website accessed on May 26th, 2020). 67

Figure 28: The top 10 causes of death in high-income countries in 2016 according to the WHO (https://www.who.int/news-room/fact-sheets/detail/the-top-10-causes-of-death website accessed on May 26th, 2020). 67

VIII. List of Tables

Table 1: Overview about 15 subtypes of congenital LQTS (adapted from Spears and Gollob, 2015)..... 11

Table 2: Overview of olfactomedins and their functions..... 21

Table 3: Patient and control cohorts..... 23

Table 4: Nucleotide sequence of primers..... 23

Table 5: *OLFML2B* cDNA clones (AF: atrial fibrillation, DCM: dilated cardiomyopathy, LQTS: long-QT syndrome, SIDS: sudden infant death syndrome)..... 25

Table 6: Commercial primary antibodies..... 26

Table 7: Peptide sequence of self-generated primary antibodies..... 26

Table 8: Self-generated primary hybridoma cell line antibodies..... 27

Table 9: Secondary antibodies..... 27

Table 10: Chemicals and reagents..... 28

Table 11: Molecular biology kits..... 30

Table 12: Plastics and consumables..... 31

Table 13: Technical devices..... 31

Table 14: Master mix for control PCR..... 33

Table 15: Cycling conditions of control PCR..... 34

Table 16: Cycling conditions of reverse transcriptase-polymerase chain reaction..... 35

Table 17: Running conditions for qPCR..... 35

Table 18: Ideal cell number per container..... 36

Table 19: Splitting cells of different container sizes..... 36

Table 20: Reagents and volumes used for transient transfection with different cell culture formats..... 36

Table 22: 23 analysed *OLFML2B* variants and wildtype showing source, patient's disease and predicted phenotype according to MutationTaster (Schwarz et al., 2010) and SIFT (Sim et al., 2012)..... 44

Table 23: 23 analysed OLFML2B variants and Wt showing source, patient's disease and amount of secretion at 37°C..... 48

Table 24: 23 analysed OLFML2B variants and Wt showing source, patient's disease, amount of secretion at different temperatures as well as allele numbers and frequencies according to gnomAD (https://gnomad.broadinstitute.org/gene/ENSG00000162745 website accessed on April 20th, 2019)..... 52

Table 25: Most likely protein-protein interaction partners in the cell lysate..... 55

Table 26: Most likely protein-protein interaction partners in the supernatant. 55
Table 27: Best antibody combinations for sandwich ELISAs detecting OLFML2B protein. 58
Table 28: Characteristics of the ideal cardiac biomarker (adapted from Kemp et al., 2004). . 68

IX. ACKNOWLEDGEMENTS

First and foremost, I thank Marcel so much for always encouraging me to follow my passion for science, for listening patiently to my long-lasting remarks about scientific problems and for always supporting me whenever I needed it.

A very special thanks goes to my parents and my whole family, who gave me the maximum amount of support at any time, in all phases of my studies, with every conceivable obstacle.

In addition, I thank my friends for their love and help during all this time.

I would especially like to thank Priv.-Doz. Dr. Arne Pfeufer for mentoring my project, for all his ideas, the encouraging discussions and advices and his guidance throughout this project.

I also want to thank my second supervisor Prof. Dr. Hans-Werner Mewes and my mentor Prof. Dr. med. Michael Näbauer for their great support with helpful suggestions and discussions of results and hypotheses.

I am very grateful to Dr. Elisabeth Kremmer and her workgroup at the HMGU, Institute for Molecular Immunology, for their help with the immunological part of this study.

Huge thanks go to all my former colleagues for creating such a friendly atmosphere at work. Particularly, I want to thank Heike Kartmann and Monika Schell for introducing me to the lab, for their constant help and for teaching me the cell and molecular biology techniques.